# Theory and Simulation of Passive Scalar Mixing in the Presence of a Mean Scalar Gradient

Thesis by

Paul O'Gorman

In Partial Fulfillment of the Requirements

for the Degree of

Doctor of Philosophy


California Institute of Technology

Pasadena, California

2004

(Submitted May 27, 2004)

# Acknowledgements

Studying and performing research at Caltech was a rewarding and pleasant experience for me. I would like to thank my advisor, Dale Pullin, for making this possible, and providing the necessary guidance and encouragement. Almost all the work for this thesis was carried out in the Iris lab, and so I thank my friends who worked there for the range of conversation and strange debates that made it easy to come to work each day.

A special mention goes to my housemates at 201 South Michigan, where we stayed for four years, despite heat, cold, and poor cleaning. The last year has been extra fun thanks to Rosie and Cathy.

I would like to thank my parents, Ambrose and Imelda, and my sister Mary. They provided a good perspective on what is important in life, and have supported me well at each turning point.

This work was supported in part by the National Science Foundation under Grant CTS-0227881. Use of the QSC supercomputer was made possible by the Academic Strategic Alliances Program of the Accelerated Strategic Computing Initiative (ASCI/ASAP) under subcontract no. B341492 of DOE contract W-7405-ENG-48.

# Abstract

The turbulent mixing of a passive scalar in the presence of a mean scalar gradient was investigated using theory and simulation. The velocity-scalar cospectrum measures the distribution of the mean scalar flux across scales. An inequality is shown to bound the magnitude of the cospectrum in terms of the shell-summed energy and scalar spectra. At high Schmidt number this bound limits the possible contribution of the sub-Kolmogorov scales to the scalar flux. At low Schmidt number we use an argument of Batchelor, Howells, and Townsend (1959) to derive a new asymptotic result for the cospectrum in the inertial-diffusive range, with a $-11/3$ power law wavenumber dependence. A comparison is made with results from large-eddy simulation at low Schmidt number.

The sparse direct-interaction perturbation (SDIP) was used to calculate the cospectrum for a range of Schmidt numbers. The Kolmogorov type scaling result is recovered in the inertial-convective range, and the constant of proportionality was calculated. At high Schmidt numbers, the cospectrum is found to decay exponentially in the viscous-convective range, and at low Schmidt numbers the $-11/3$ power law is observed in the inertial-diffusive range. The stretched-spiral vortex model was used to calculate the cospectrum, and asymptotic expressions were found for the contribution to the cospectrum from the axial velocity in the vortex structures. Results are reported for the cospectrum from a direct numerical simulation at a Taylor Reynolds number of 265, and a comparison is made of results for the cospectrum from the SDIP, the stretched-spiral vortex model, simulation, and experiment.

The stretched-spiral vortex model was also used to derive expressions for the modal time correlation functions of the velocity and scalar fields. These expressions were evaluated numerically and asymptotically. Winding by the vortex core is shown to lead to an inertial timescale, and movement of the vortex structures by the large scale flow leads to a sweeping timescale. The velocity and scalar modal time correlation

functions were calculated in the direct numerical simulation. They coincide for large enough wavenumber, and are found to collapse to universal forms when a sweeping timescale is used.

# Contents

# List of Figures

# List of Tables

# Chapter 1 Introduction

The problem of turbulent passive scalar mixing shares many of the features of the classical turbulence problem, and has important applications in areas such as turbulent combustion and dispersion in geophysical flows. A passive scalar is a contaminant in a fluid that has no dynamical effect on the fluid itself, for example, temperature in the case of a weakly heated flow. The scalar field evolves under the combined influence of molecular diffusion and advection by the velocity field, according to the advection-diffusion equation. Although this equation is linear in the scalar, predicting the statistics of the scalar field is nonetheless a difficult problem. The canonical problem for passive scalar mixing involves mixing by an incompressible turbulent velocity field in the presence of a uniform mean scalar gradient. The velocity field is assumed to be statistically homogeneous and isotropic, and it can then be shown that the mean scalar gradient is preserved by the evolution of the flow. This problem has been the subject of extensive study because the mean gradient acts as a source of scalar variance, allowing a statistical steady state to be reached, see Overholt and Pope [37]. The mean gradient makes the problem non-isotropic, however, and so a mean scalar flux arises. The statistics of the scalar field show many similarities to that of the velocity field, but the mean scalar gradient also leads to some interesting difference, for example, anisotropy at small scales due to 'ramp-cliff' structures in the scalar field, see the review by Warhaft [48]. Here we will concentrate on two particular statistics; the velocity-scalar cospectrum, and the Eulerian modal time correlation functions. The velocity-scalar cospectrum represents the distribution of the mean scalar flux across scales, and the modal time correlation functions can be used to determine the characteristic timescales for the high wavenumber modes of the velocity and scalar fields.

Firstly we will review what is currently know about the velocity-scalar cospectrum. The shell-summed velocity-scalar cospectrum, $C_{u_1c}(k)$, is defined so that the mean

scalar flux is given by

$$\overline{u_1 c} = \int_0^\infty C_{u_1 c}(k)\, dk, \tag{1.1}$$

where $c$ is the scalar fluctuation, $u_1$ is the component of velocity in the direction of the mean scalar gradient, $k$ is the wavenumber, and the overbar indicates an ensemble average. Thus the velocity-scalar cospectrum gives the distribution of the mean scalar flux across scales, making it relevant, for example, to problems in turbulent heat transfer. A mean scalar flux can only occur as a result of anisotropy, and so it is interesting to know how quickly the cospectrum decays with increasing wavenumber. If, as is thought, the cospectrum decays faster than the scalar or energy spectra, then this is a measure of the approach to isotropy at the smaller scales. In addition, because the total scalar flux represents transport in the scalar advection-diffusion equation, knowledge of the cospectral properties of vortex-models is expected to be useful in their application to the building of subgrid scalar-flux and mixing models for use in large-eddy simulation [38]. Also of interest is the effect of the Schmidt number on the cospectrum, and hence the scalar flux, where the Schmidt number is defined as the ratio of viscosity to the scalar diffusivity. The effect of Schmidt number on the scalar spectrum is still the subject of ongoing research, for example, the experimental work of Miller and Dimotakis [31] at high Reynolds number, and the simulation by Yeung *et al.* [50] at low Reynolds number.

While considering the effect of buoyancy on the energy spectrum, Lumley [28] used a similarity hypothesis to predict the shell-summed cospectrum of the velocity and potential temperature in the inertial-convective range. If the gravitational force is set to zero, then the absolute and potential temperatures are the same, and Lumley's equation (12) for the cospectrum simplifies to

$$C_{u_1 c}(k) \sim \mu\, \epsilon^{1/3}\, k^{-7/3}, \tag{1.2}$$

where $\epsilon$ is the energy dissipation and $\mu$ is the scalar gradient. We are assuming the flow is such that temperature is approximately a passive scalar, and the turbulent velocity field is isotropic. Note that (1.2) follows from dimensional analysis if the

cospectrum depends only on $k$, $\epsilon$ and $\mu$.

Mydlarski and Warhaft [34] studied the velocity-temperature cospectrum in a wind tunnel for Taylor Reynolds numbers, $R_\lambda$, as high as 582. Fluctuations in the passive temperature field were generated by imposing a linear mean temperature gradient across the tunnel. The resulting cospectrum was noisier than the energy or scalar spectra, and this was explained by noting that no mathematical limitation keeps the spectrum either positive or negative. Nonetheless, they found a wavenumber dependence of approximately $k^{-2}$ in the inertial-convective range for $R_\lambda$ of 582, see also [33]. Interestingly this would represent a slower approach to isotropy at the small scales than the Lumley scaling result (1.2). Of course, the experimental exponent may indeed approach $-7/3$ for higher Reynolds number, but the variation in the exponent over the range of $R_\lambda$ reported by Mydlarski and Warhaft [34] seems to asymptote to an exponent closer to $-2$.

Kaimal *et al.* [20] measured the cospectra of velocity and potential temperature in the atmospheric surface layer, see also Wyngaard and Coté [49]. They found that the cospectrum involving the horizontal velocity showed a $k^{-5/2}$ scaling range, and the cospectrum involving the vertical velocity showed a $k^{-7/3}$ scaling range. We mention these results for completeness, although of course the surface layer is significantly different from the simpler mixing case we consider here.

There have been few attempts to calculate the velocity-scalar cospectrum using either theory or simulation. Herr, Wang and Collins [17] performed an EDQNM calculation of the cospectrum, and compared it with direct numerical simulation (DNS) at an $R_\lambda$ of 81, although it should be noted that two constants were chosen in the EDQNM calculation by matching the EDQNM and DNS cospectra.

We turn now from the velocity-scalar cospectrum to two-point, two-time statistics of the velocity and scalar fields. A fundamental, but still disputed property of isotropic, homogeneous turbulence is the characteristic timescale over which the small scales of the velocity field decorrelate in an Eulerian frame of reference. Kolmogorov scaling in the inertial range suggests the inertial eddy-turnover time, $(\epsilon k^2)^{-1/3}$. There is, however, also evidence that the relevant timescale is the 'sweeping' time, $(u_{rms}k)^{-1}$,

where $u_{rms}$ is the root-mean-square (rms) velocity [45, 36, 16, 22, 25]. Knowledge of the correct time scaling would be useful, for example, as an input to the recent functional derivative closure (FDC) [12] for random advection of a passive scalar, and in interpreting the importance of the random sweeping effect [45]. Also of interest is the characteristic timescale of the small scales of a passive scalar mixed by a turbulent velocity field.

The velocity modal time correlations are the time correlations of the Fourier modes of the velocity field, and so are a two-time, two-point statistic. Several attempts have been made to use characteristic time scalings to collapse these correlations to a universal form. The main experimental work is by Comte-Bellot and Corrsin [6] in decaying grid turbulence, and is at a maximum $R_\lambda$ of 72. They achieved a collapse of the modal time correlations using a parallel combination of four different characteristic timescales. DNS studies by Orszag and Patterson [36] at $R_\lambda \sim 16$, Gotoh *et al.* [16] at $R_\lambda \sim 46$, Kaneda *et al.* [22] at $R_\lambda \sim 126$, and Sanada and Shanmugasundaram [45] at $R_\lambda \sim 200$, all found the 'sweeping' timescale to be dominant.

Kraichnan [25] studied the modal time correlation and made a simple linearized estimate, and also an estimate based on the direct interaction approximation (DIA), both of which resulted in the 'sweeping' time being the characteristic timescale. McComb *et al.* [30] studied numerical solutions to the DIA and local energy transfer (LET) theories, and in contrast to Kraichnan's asymptotic prediction for the DIA, found that while neither the 'sweeping' timescale nor the inertial eddy-turnover timescale were completely effective in collapsing the modal time-correlation data, the inertial scaling became more dominant for both theories as $R_\lambda$ was increased. Finally, Gotoh *et al.* [16] studied the modal time correlation using both DNS and DIA at $R_\lambda \sim 35$, and found that the sweeping timescale gave a poor collapse of the correlation data from the DIA relative to the data from the DNS. In contrast to the velocity modal time correlation function, the scalar modal time correlation function has received little attention.

Having described and motivated some features of turbulent passive scalar mixing that we would like to investigate, we now describe the methods that we will use. Our

overall aim is to study the velocity-scalar cospectrum and modal time correlation functions using a combination of theory and direct numerical simulation (DNS). It is of interest to use approaches that have been shown to provide quantitative results for the velocity statistics to problems involving a passive scalar, one example being the recent use of the stretched spiral-vortex model to calculate the scalar spectrum [40] for homogeneous but non-isotropic turbulence. Here we will work with two notable theories that are successful in linking the Navier-Stokes equations and the Kolmogorov phenomenology, namely, the stretched-spiral vortex model introduced by Lundgren [29], and a Lagrangian reformulation of the direct-interaction approximation (DIA) of Kraichnan [25].

The stretched spiral-vortex model of turbulence uses an ensemble of vortex tubes to model the fine scales of turbulence. The vortex tubes do not interact except in that they are stretched on average by the surrounding flow. The vortex tubes are assumed to be straight, with no dependence of the velocity field on the coordinate parallel to the tube axis. In each tube the vorticity is evolved by the Navier Stokes equations and the scalar is evolved by the advection-diffusion equation. The axial vorticity, the axial velocity, and the scalar are each wound up into spirals by the differential rotation of the cores of the vortices. Average flow statistics are calculated by performing an average over time and space. This model gives good results for energy [29] and scalar spectra [40] individually. By also performing an average over vortex orientation the model was used to calculate vorticity and velocity-derivative moments [41], as well as one-dimensional spectra [42]. Here we will use the model to calculate the velocity-scalar cospectrum, as well as modal time correlation functions of the velocity and scalar fields.

In contrast to the stretched-spiral vortex model where an ensemble of local asymptotic solutions to the Navier-Stokes equations are used to model turbulence, the DIA seeks to use a set of statistical assumptions to close the equations for second order statistics that result from the Navier-Stokes equations. Alternatively, the DIA can be derived by truncating a renormalized perturbation expansion of the exact equations for second order statistical quantities, see Leslie [27]. If the DIA is ap-

plied in an Eulerian frame of reference, the resulting equations are not consistent with the Kolmogorov form for the energy spectrum in the inertial range. However, there are several Lagrangian reformulations of the DIA without this property, one example being the sparse direct-interaction perturbation (SDIP), first introduced by Kida and Goto [24] with the name Lagrangian direct-interaction approximation. It is a renormalized closure theory for second-order turbulent statistics that applies a similar procedure to Kraichnan's direct-interaction approximation (DIA) [25] in a Lagrangian framework. The SDIP is simpler than the Lagrangian history DIA of Kraichnan [26], and yields the same integro-differential equations as the Lagrangian renormalized approximation (LRA) of Kaneda [21]. The SDIP has been used to calculate the energy spectrum [24], and the scalar spectrum [14]. Goto and Kida [15] applied the SDIP to a simpler dynamical model to better understand the basis of the approximation. In light of the importance of sparse coupling in the approximation, the name sparse direct-interaction perturbation was then chosen in place of Lagrangian direct-interaction approximation. Here, we will use the SDIP to calculate the velocity-scalar cospectrum. One advantage that the SDIP has over simulation and experiment is the relative ease with which the cospectrum can be calculated for a range of different Schmidt numbers.

To complement the above calculations we performed a DNS of turbulent mixing of a passive scalar with a resolution of $512^3$ gridpoints. There have been a number of numerical passive scalar mixing studies at comparable resolution, see Overholt and Pope [37], or Yeung *et al.* [50]. Comparison with box turbulence simulations at higher resolution but with no passive scalar suggest that at this resolution we can expect to capture the beginning of the inertial range, see Kaneda *et al.* [23]. One advantage of DNS is the ease with which different statistics can be calculated, and here we report results for the velocity-scalar cospectrum, as well as the modal time correlation functions of the velocity and scalar fields.

In Chapter 2 we discuss the velocity-scalar cospectrum. The cospectrum is defined, and an inequality is derived that bounds the magnitude of the cospectrum using the shell-summed energy and scalar spectra. This inequality is an extension of the one-

dimensional cross-spectrum inequality to the three-dimensional shell-summed case, and applied in particular to the velocity-scalar cospectrum. A new asymptotic form for the cospectrum at low Schmidt number is derived, and this is compared with results from large-eddy simulation (LES). Calculations of the cospectrum using the stretched-spiral vortex model, the SDIP, and results from DNS are presented. The SDIP results are for a range of Schmidt numbers, and the SDIP equation is shown to be consistent with the asymptotic form at low Schmidt number derived earlier. Comparison at Schmidt number order unity is made between theory, experiment, and simulation. In Chapter 3 we discuss the Eulerian modal time correlation functions. Results are presented for both the velocity and scalar fields using the stretched-spiral vortex model. DNS results are also presented, and comparison is made with the results from the model. In Chapter 4 the overall results are summarized, conclusions are drawn, and possibilities for future work are discussed.

# Chapter 2 The Velocity-Scalar Cospectrum

Throughout this chapter we will consider a passive scalar mixed by an incompressible, statistically homogeneous and isotropic velocity field, $u_i(\mathbf{x}, t)$. The scalar is assumed to have a mean scalar gradient, $\mu$, in the 1 direction, so that we can decompose the scalar as $\mu\, x_1 + c(\mathbf{x}, t)$. The scalar fluctuation $c(\mathbf{x}, t)$ is statistically homogeneous, and axisymmetric about the $x_1$ axis, but not isotropic. By definition it has zero mean, $\overline{c(\mathbf{x}, t)} = 0$, where the overbar indicates an ensemble average. If we define the velocity-scalar correlation by

$$\mathcal{R}_{u_i c}(\mathbf{r}) = \overline{u_i(\mathbf{x}, t)\, c(\mathbf{x} + \mathbf{r}, t)}, \tag{2.1}$$

then the shell-summed velocity-scalar cospectrum is defined by

$$C_{u_i c}(k) = \frac{1}{(2\pi)^3} \int_S \int_V \mathcal{R}_{u_i c}(\mathbf{r}) e^{-i\,\mathbf{k}\cdot\mathbf{r}} d\mathbf{r}\, dS_k, \tag{2.2}$$

where the $S$ integral is a surface integral over a spherical shell in wavenumber space, and the $V$ integral is a volume integral over all space. The shell-summed cospectrum has no imaginary part, as may be seen by rewriting the shell integral as an integral over a hemisphere,

$$\int_S e^{-i\,\mathbf{k}\cdot\mathbf{r}}\, dS_k = 2 \int_{S^h} \cos(\mathbf{k}\cdot\mathbf{r})\, dS_k^h, \tag{2.3}$$

and it integrates to the scalar flux,

$$\overline{u_i c} = \int_0^\infty C_{u_i c}(k) dk. \tag{2.4}$$

The shell-summed cospectrum is thus a measure of the distribution of the scalar flux across scales.

One-dimensional spectra are often more convenient for experimental measurement, and so we define the one-dimensional velocity-scalar cross spectrum by

$$F_{u_ic}^{1D}(k_3) = \frac{1}{2\pi}\int_{-\infty}^{\infty} \mathcal{R}_{u_ic}(0,0,r_3)e^{-ik_3r_3}dr_3. \tag{2.5}$$

In general the cross spectrum may be complex, and can be split into real and imaginary parts as

$$2\,F_{u_ic}^{1D}(k_3) = C_{u_ic}^{1D}(k_3) - i\,Q_{u_ic}^{1D}(k_3), \tag{2.6}$$

where $C_{u_ic}^{1D}(k_3)$ is the cospectrum and $Q_{u_ic}^{1D}(k_3)$ is the quadrature spectrum [3]. The integral of the one-dimensional cospectrum over all wavenumbers is also equal to the scalar flux,

$$\overline{u_ic} = \int_0^{\infty} C_{u_ic}^{1D}(k_3)dk_3. \tag{2.7}$$

The quadrature spectrum is related to phase differences between the Fourier components of the scalar and the velocity fields. In Appendix A the quadrature spectrum is shown to be zero for the case of isotropic incompressible turbulence and a mean scalar gradient. It is also shown that only the cospectrum of the scalar and the velocity component in the direction of the mean scalar gradient is non-zero, where this holds for both the shell-summed and one-dimensional cospectra.

In this chapter we will investigate the velocity-scalar cospectrum using a combination of theory, simulation, and comparison with experiment. In section 2.1.1 an upper bound is derived for the magnitude of the cospectrum in terms of the energy spectrum and the shell-summed scalar spectrum. This has immediate implications for the contribution of the smallest scales to the scalar flux in high Schmidt number flows. At low Schmidt number we derive an asymptotic expression for the cospectrum in the inertial-diffusive range. This derivation is based on an argument for the scalar spectrum by Batchelor, Howells, and Townsend [2] , and we also show how their result for the scalar spectrum is modified by the presence of a mean scalar gradient. The low

Schmidt number asymptotic forms for the velocity-scalar cospectrum and the scalar spectrum are compared with results from a large-eddy simulation.

In section 2.2 the cospectrum is calculated using the stretched-spiral vortex model. The mean scalar gradient is held fixed, while the isotropic turbulent velocity field is modeled using vortex tubes oriented with equal probability in all directions. For the velocity field provided by the stretched-spiral vortex, the velocity-scalar cospectrum can be divided into two additive components contributed by the velocity components along the vortex axis, and in the plane normal to this axis, respectively. For the axial velocity field, a new exact solution of the scalar advection-diffusion equation is found exhibiting scalar variation in the direction of the vortex tube axis, allowing the scalar evolution to be influenced by the axial velocity. This is important because the scalar and the axial velocity evolve in a similar way, unlike the scalar and a given planar component of the velocity, and leads to an important contribution to the velocity-scalar correlation. An asymptotic expression is found for the cospectrum contributed by this solution and the axial velocity, with the leading order term showing a $k^{-5/3}$ range. This term is produced by the winding of the initial axial velocity field by the axisymmetric vortex core. The next-order term gives a $k^{-7/3}$ range, and arises from the lowest order effect of the non-axisymmetric vorticity on the evolution of the axial velocity. Its coefficient can be of either sign or zero depending on the initial conditions. The contribution to the cospectrum from the velocity in the plane of the vortex is also calculated, but no universal high wavenumber asymptotic form is found. The integrals are evaluated numerically and it is found that the the resulting cospectrum does not remain of one sign. Its form depends on the choice of the vortex core velocity profile and time cutoff in the spectral integrals.

In section 2.3 the sparse direct-interaction approximation of Kida and Goto [24] is used to calculate the cospectrum. In the inertial-convective range the Lumley form $\mu\,\epsilon^{1/3}\,k^{-7/3}$ is recovered, and the constant of proportionality is calculated. The cospectrum is also calculated in the entire universal wavenumber range by numerical solution of an integral equation, and results for a range of Schmidt numbers are presented. The asymptotic form of the SDIP equation for low Schmidt number is

derived, appropriate for wavenumbers in the inertial-diffusive and viscous-diffusive wavenumber ranges. This form agrees with the asymptotic result of section 2.1 in the inertial-diffusive range.

In section 2.4 we describe a DNS of turbulent passive scalar mixing, performed at a Taylor Reynolds number of 265, and a Schmidt number of 0.7. Results are reported for the cospectrum, and these are compared with the bound given by the cospectrum inequality.

Finally, in section 2.5 we make a comparison between the results for the cospectrum from the stretched-spiral vortex model, the SDIP, the experiment of Mydlarski and Warhaft [34], and our DNS.

## 2.1 The cospectrum at small and large Schmidt numbers

Here we consider the effects of Schmidt number on the cospectrum, where the Schmidt number is defined as the ratio of viscosity to diffusivity, $Sc = \nu/D$. In later chapters we will calculate the cospectrum using turbulence theory and DNS, but we can use some simpler analysis to limit the possible behavior of the cospectrum, and in the case of low Schmidt number to predict its asymptotic form. Firstly, in subsection 2.1.1 we find an upper bound for the magnitude of the cospectrum, and this is shown in subsection 2.1.2 to have implications for the form of the cospectrum at high Schmidt number. Then in subsection 2.1.3 we present an argument for the asymptotic form of the cospectrum at low Schmidt number in the inertial-diffusive wavenumber range. This derivation is similar to that used by Batchelor, Howells, and Townsend [2] for the form of the scalar spectrum in the inertial-diffusive range. In subsection 2.1.4 we show how their result for the scalar spectrum is modified for the case of a mean scalar gradient, allowing us to compare the asymptotic result for the cospectrum with the bound given by the cospectrum inequality. Finally, in subsection 2.1.5 we compare the results for the velocity-scalar cospectrum and the scalar spectrum in the

inertial-diffusive range with results from a large-eddy simulation.

### 2.1.1 The cospectrum inequality

Here we will derive an upper bound for the magnitude of the shell-summed velocity-scalar cospectrum in terms of the energy and scalar spectra. This bound has close ties to the one-dimensional cross-spectrum inequality and coherence function, discussed in Bendat and Piersol [3]. In effect, we are extending the one-dimensional cross-spectrum inequality to the three-dimensional shell-summed case, and applying it in particular to the velocity-scalar cospectrum.

It is convenient to use the formulation of the SDIP calculation in section 2.3, where we first work in a periodic box of side $L$, and then take the limit $L \to \infty$. For consistency, we also adopt the convention used in that section for denoting integrals, where the associated infinitesimal is placed beside the integration sign.

The velocity field $u_i(\mathbf{x}, t)$ can be decomposed as

$$u_i(\mathbf{x}, t) = \left(\frac{2\pi}{L}\right)^3 \sum_{\mathbf{k}} \tilde{u}_i(\mathbf{k}, t)\, \exp(i\, \mathbf{k} \cdot \mathbf{x}), \tag{2.8}$$

where $k_i = 2\pi\, n_i / L$, and $n_i \in \mathbb{Z}$. The inverse Fourier transform is given by

$$\tilde{u}_i(\mathbf{k}, t) = \left(\frac{1}{2\pi}\right)^3 \int d^3\mathbf{x}\, u_i(\mathbf{x}, t)\, \exp(-i\, \mathbf{k} \cdot \mathbf{x}), \tag{2.9}$$

and a similar transformation is defined for the scalar fluctuation, $c(\mathbf{x}, t)$. We then define the second order statistical quantities

$$\tilde{V}_{ij}(\mathbf{k}, t, t) = \left(\frac{2\pi}{L}\right)^3 \overline{\tilde{u}_i(\mathbf{k}, t)\, \tilde{u}_j(-\mathbf{k}, t)}, \tag{2.10}$$

$$\tilde{Z}(\mathbf{k}, t, t) = \left(\frac{2\pi}{L}\right)^3 \overline{\tilde{c}(\mathbf{k}, t)\, \tilde{c}(-\mathbf{k}, t)}, \tag{2.11}$$

$$\tilde{W}_i(\mathbf{k}, t, t) = \left(\frac{2\pi}{L}\right)^3 \overline{\tilde{c}(\mathbf{k}, t)\, \tilde{u}_i(-\mathbf{k}, t).} \tag{2.12}$$

The double reference to the time $t$ is included to be consistent with the definition of more complicated Lagrangian quantities in section 2.3.

For a given instance in the ensemble, we have that

$$Re\,(\tilde{c}(\mathbf{k},t)\,\tilde{u}_1(-\mathbf{k},t)) \leq |\tilde{c}(\mathbf{k},t)|\,|\tilde{u}_1(\mathbf{k},t)|, \tag{2.13}$$

where we have used that $\tilde{u}(-\mathbf{k},t) = \tilde{u}(\mathbf{k},t)^*$. Taking an ensemble average we find that

$$Re\left(\overline{\tilde{c}(\mathbf{k},t)\,\tilde{u}_1(-\mathbf{k},t)}\right) \leq \overline{|\,\tilde{c}(\mathbf{k},t)\,|\,|\,\tilde{u}_1(\mathbf{k},t)\,|} \leq \left(\overline{|\,\tilde{c}(\mathbf{k},t)\,|^2}\;\overline{|\,\tilde{u}_1(\mathbf{k},t)\,|^2}\right)^{1/2}. \tag{2.14}$$

The second inequality can be derived by considering the expression

$$\overline{(\,|\,\tilde{c}(\mathbf{k},t)\,| + \xi|\,\tilde{u}_1(\mathbf{k},t)\,|)^2}, \tag{2.15}$$

as a quadratic in the real number $\xi$, and requiring that it be non-negative.

Taking the limit $L \to \infty$ we can relate $\tilde{V}_{ij}(\mathbf{k},t,t)$, $\tilde{Z}(\mathbf{k},t,t)$, and $\tilde{W}_i(\mathbf{k},t,t)$ to power spectral density functions. The shell-summed energy spectrum, $E(k)$, scalar spectrum, $E_c(k)$, and velocity-scalar cospectrum, $C_{u_1c}(k)$, are given by

$$E(k) = \frac{1}{2}\int dS_k\,\tilde{V}_{ii}(\mathbf{k},t,t), \tag{2.16}$$

$$E_c(k) = \int dS_k\,\tilde{Z}(\mathbf{k},t,t), \tag{2.17}$$

$$C_{u_1c}(k) = \int dS_k\,\tilde{W}_1(\mathbf{k},t,t), \tag{2.18}$$

where $\int dS_k$ denotes a surface integral over a shell in wavenumber space, rather than a solid angle integration. We will now use the fact that the shell-summed cospectrum is real. This can be seen from equation (2.18), and the relation $\tilde{W}_1(\mathbf{k},t,t) = \tilde{W}_1(-\mathbf{k},t,t)^*$. Noting that the isotropy of the velocity field implies that $\tilde{V}_{11}(\mathbf{k},t,t) =$

$E(k)/(6\pi k^2)$, we deduce the inequality

$$C_{u_1c}(k) \leq \frac{1}{k}\left(\int dS_k\, \tilde{Z}(\mathbf{k},t,t)^{1/2}\right)\left(\frac{E(k)}{6\pi}\right)^{1/2}. \tag{2.19}$$

Similarly we can show that inequality (2.19) holds for $-C_{u_1c}(k)$, and so it also holds for the magnitude $|C_{u_1c}(k)|$. The scalar spectrum is anisotropic, and so we cannot perform the solid angle integration without further knowledge of $\tilde{Z}(\mathbf{k},t,t)$. Nonetheless, we can find a bound in terms of the shell-summed scalar spectrum. Using the Cauchy-Schwartz inequality we have that

$$\int dS_k\, \tilde{Z}(\mathbf{k},t,t)^{1/2}\, 1^{1/2} \leq \left(\int dS_k\, \tilde{Z}(\mathbf{k},t,t)\right)^{1/2}\left(\int dS_k\right)^{1/2} = \left(4\pi\, k^2\, E_c(k)\right)^{1/2}, \tag{2.20}$$

and so,

$$|C_{u_1c}(k)| \leq \left(\frac{2\, E(k)\, E_c(k)}{3}\right)^{1/2}. \tag{2.21}$$

It should be noted that a tighter bound might be deduced with more detailed knowledge of the scalar anisotropy.

### 2.1.2 Implications of the bound

From (2.21) we see that the magnitude of the cospectrum is bounded by the geometric mean of the scalar and energy spectra multiplied by a constant of order unity. To discuss the implications of this, we first briefly review the phenomenology of the scalar spectrum at different Schmidt numbers.

We assume in what follows that the Reynolds number is sufficiently large for an inertial-convective range to exist. The Schmidt number is defined as the ratio of the viscosity to the diffusivity, $Sc = \nu/D$. We define $k_P$ as the wavenumber at the peak of the energy spectrum or the scalar spectrum, whichever wavenumber is greater. The Kolmogorov wavenumber is defined by $k_K = (\epsilon/\nu^3)^{1/4}$, the Batchelor wavenumber is given by $k_B = (\epsilon/\nu\, D^2)^{1/4} = Sc^{1/2}\, k_K$, and the Obukhov-Corrsin wavenumber is

given by $k_C = (\epsilon/D^3)^{1/4} = Sc^{3/4}\, k_K$. Then for wavenumbers in the inertial-convective range the scalar spectrum has the form

$$E_c(k) \propto \epsilon_c\, \epsilon^{-1/3}\, k^{-5/3}, \qquad k_P \ll k \ll min(k_K, k_C), \tag{2.22}$$

where $\epsilon_c$ is the scalar dissipation, and the constant of proportionality is known as the Obukhov-Corrsin constant, see Tennekes and Lumley [46]. For large Schmidt number a different power law behavior is thought to exist in the viscous-convective range [1],

$$E_c(k) \propto \epsilon_c\, \nu^{1/2}\, \epsilon^{-1/2}\, k^{-1}, \qquad k_K \ll k \ll k_B, Sc \gg 1. \tag{2.23}$$

For very small Schmidt number, in the inertial-diffusive range,

$$E_c(k) \propto \epsilon_c\, D^{-3}\, \epsilon^{2/3}\, k^{-17/3} \left(1 + \frac{2\, D\, \mu^2}{\epsilon_c}\right), \qquad k_C \ll k \ll k_K, Sc \ll 1. \tag{2.24}$$

We show this in subsection 2.1.4 by modifying a result of Batchelor, Howells, and Townsend [2] for the presence of a mean scalar gradient. There are other theoretical predictions for the scalar spectrum in this range, for example, Gibson [11] found a $k^{-3}$ wavenumber dependence. Finally, in the viscous-diffusive range the scalar spectrum decays exponentially.

Now consider the velocity-scalar cospectrum for the case of large Schmidt number in the viscous-convective range. According to (2.23) the scalar spectrum has a $k^{-1}$ wavenumber dependence, whereas the energy spectrum will be decaying exponentially with wavenumber because $k \gg k_K$. Therefore, the bound given by inequality (2.21) will decay exponentially in this range, and we expect that the cospectrum will also decay exponentially. This would imply that the contribution to the mean scalar flux at length scales smaller than the Kolmogorov lengthscale is very small, even if the Schmidt number is very large. It should be noted that if the scaling law given by (2.23) is correct, as the Schmidt number goes to infinity the scalar variance is unbounded, see Dimotakis and Miller [8] for a discussion of this issue. More generally, if the scalar flux has a weak Schmidt number dependence at large Schmidt number, then

this should be apparent in a comparison between the mean scalar profile for mixing layer flows at different Schmidt numbers, see Dimotakis [7] for a review of free shear layer mixing in gases and liquids.

In contrast, for the case of small Schmidt number in the inertial-diffusive range, the scalar spectrum has a wavenumber dependence of $k^{-17/3}$ according to (2.24), the energy spectrum has a $k^{-5/3}$ wavenumber dependence because $k_P \ll k \ll k_K$, and so the bound given by inequality (2.21) has a $k^{-11/3}$ dependence. Therefore, in this wavenumber range we do not necessarily have reason to expect exponential or power law behavior of the cospectrum based on the inequality. However we will be able to derive an asymptotic form for the inertial-diffusive range in subsection 2.1.3.

In subsection 2.3.6 the SDIP is used to solve for the cospectrum at a range of Schmidt numbers, and a comparison is made of the resulting cospectra with the bounds given by (2.21).

### 2.1.3 Asymptotic form in the inertial-diffusive range

We consider the case of low Schmidt number, and wavenumbers in the inertial-diffusive range, $k_C \ll k \ll k_K$. The advection-diffusion equation for the scalar fluctuation is given by

$$\frac{\partial}{\partial t}\, c(\mathbf{x},t) + u_j(\mathbf{x},t)\, \frac{\partial}{\partial x_j}\, c(\mathbf{x},t) = D\, \frac{\partial^2}{\partial x_j \partial x_j}\, c(\mathbf{x},t) - \mu\, u_1(\mathbf{x},t), \tag{2.25}$$

where we note the gradient forcing term. This can be written in Fourier space as

$$\left[\frac{\partial}{\partial t} + D\, k^2\right] \tilde{c}(\mathbf{k},t) = -\mu\, \tilde{u}_1(\mathbf{k},t) - i\, \left(\frac{2\pi}{L}\right)^3 \sum_{\mathbf{q}} q_j\, \tilde{u}_j(\mathbf{k}-\mathbf{q},t)\, \tilde{c}(\mathbf{q},t). \tag{2.26}$$

Following the argument of Batchelor, Howells, and Townsend [2] we note that the convolution sum in equation (2.26) is dominated by wavenumbers $\mathbf{q}$ smaller than $k_C$, that is $|\mathbf{q}| < k_C$. This is justified because the scalar spectrum drops off rapidly for higher wavenumbers. Then assuming that $k \gg k_C$, implies that $|\mathbf{k}-\mathbf{q}| \simeq k$. We now argue that the timescales of $\tilde{u}_j(\mathbf{k}-\mathbf{q},t)$ and $\tilde{c}(\mathbf{q},t)$ are much longer that that of

$\tilde{c}(\mathbf{k},t)$. This can be seen in the case of $\tilde{u}_j(\mathbf{k}-\mathbf{q},t)$ by comparing the inertial timescale $\epsilon^{-1/3}\,k^{-2/3}$ with the diffusive timescale $D^{-1}\,k^{-2}$ and using $k \gg k_C$. Therefore, we can make a stationary balance approximation, and neglect the time derivative in equation (2.26). Multiplying by $u_1(-\mathbf{k},t)$, taking an ensemble average, and using the definition of $\tilde{W}_i(\mathbf{k},t,t)$ (2.12) we find

$$\begin{aligned}\tilde{W}_1(\mathbf{k},t,t) = &-\frac{\mu}{D\,k^2}\left(\frac{2\pi}{L}\right)^3 \overline{\tilde{u}_1(-\mathbf{k},t)\,\tilde{u}_1(\mathbf{k},t)} \\ &-\frac{i}{D\,k^2}\left(\frac{2\pi}{L}\right)^6 \sum_{\mathbf{q}} q_j\,\overline{\tilde{u}_j(\mathbf{k}-\mathbf{q},t)\,\tilde{c}(\mathbf{q},t)\,\tilde{u}_1(-\mathbf{k},t)}.\end{aligned} \tag{2.27}$$

We have already argued that $|\mathbf{q}| \ll |\mathbf{k}-\mathbf{q}| \simeq k$, and so we make the further approximation that $\tilde{c}(\mathbf{q},t)$ is statistically independent of $\tilde{u}_j(\mathbf{k}-\mathbf{q},t)$ and $\tilde{u}_1(-\mathbf{k},t)$. The mean $\overline{\tilde{c}(\mathbf{q},t)}$ is zero, and so

$$\tilde{W}_1(\mathbf{k},t,t) = -\frac{\mu}{D\,k^2}\,\tilde{V}_{11}(\mathbf{k},t,t). \tag{2.28}$$

Taking the limit $L \to \infty$, and using (2.16) and (2.18) to make contact with shell-summed spectra we find

$$C_{u_1 c}(k) = -\frac{2\,\mu}{3\,D\,k^2}\,E(k). \tag{2.29}$$

The wavenumber $k$ is in the inertial range, and so

$$E(k) = K\,\epsilon^{2/3}\,k^{-5/3}, \tag{2.30}$$

where $K$ is the Kolmogorov constant, with the result,

$$C_{u_1 c}(k) = -\frac{2\,\mu\,K}{3\,D}\,k^{-11/3}\,\epsilon^{2/3}. \tag{2.31}$$

Thus the cospectrum has a $k^{-11/3}$ power law wavenumber dependence in the inertial-diffusive range. The asymptotic form (2.31) will be compared with results from LES in subsection 2.1.5, and with the SDIP result in subsection 2.3.6. To compare with the bound given by the cospectrum inequality we need to consider the effect of the

mean scalar gradient on the scalar spectrum in the inertial-diffusive range, and this will be the subject of the next subsection.

### 2.1.4 Effect of the scalar gradient on the scalar spectrum in the inertial-diffusive range

Here we will see how the Batchelor, Howells, and Townsend [2] result for the scalar spectrum is modified by the presence of a mean scalar gradient. Chasnov [5] studied the scalar spectrum in the inertial-diffusive range using large-eddy simulation (LES), and noted that the Batchelor result [2] for the scalar spectrum is still valid in the presence of a mean scalar gradient when the scalar dissipation is replaced by $\epsilon_c + 2\,D\,\mu^2$. Here we will confirm this using a direct rederivation of the result, taking into account the mean scalar gradient.

In the inertial-diffusive range we have already shown that an approximate equation for $\tilde{c}(\mathbf{k},t)$ is given by neglecting the time derivative in equation (2.26). Multiplying by a similar expression for $\tilde{c}(-\mathbf{k},t)$, and taking an ensemble average gives

$$\begin{aligned}\overline{\tilde{c}(\mathbf{k},t)\,\tilde{c}(-\mathbf{k},t)}\,D^2\,k^4 &= \mu^2\,\overline{\tilde{u}_1(\mathbf{k},t)\,\tilde{u}_1(-\mathbf{k},t)} \\ &\quad - \left(\frac{2\pi}{L}\right)^6 \sum_{\mathbf{p}}\sum_{\mathbf{q}} p_j\,q_i\,\overline{\tilde{u}_j(-\mathbf{k}-\mathbf{p},t)\,\tilde{u}_i(\mathbf{k}-\mathbf{q},t)\,\tilde{c}(\mathbf{p},t)\,\tilde{c}(\mathbf{q},t)} \\ &\quad + i\,\mu\,\left(\frac{2\pi}{L}\right)^3 \sum_{\mathbf{q}} q_i\,\overline{\tilde{u}_i(\mathbf{k}-\mathbf{q},t)\,\tilde{c}(\mathbf{q},t)\,\tilde{u}_1(\mathbf{k},t)}.\end{aligned} \tag{2.32}$$

Again using $|\mathbf{q}| \ll k$, $|\mathbf{p}| \ll k$, and assuming the statistical independence of modes at wavenumber $\mathbf{q}$ or $\mathbf{p}$ with modes at $\mathbf{k}-\mathbf{q}$, $\mathbf{k}$, or $\mathbf{k}-\mathbf{p}$, we find

$$\begin{aligned}\overline{\tilde{c}(\mathbf{k},t)\,\tilde{c}(-\mathbf{k},t)}\,D^2\,k^4 &= \mu^2\,\overline{\tilde{u}_1(\mathbf{k},t)\,\tilde{u}_1(-\mathbf{k},t)} \\ &\quad - \left(\frac{2\pi}{L}\right)^6 \sum_{\mathbf{p}}\sum_{\mathbf{q}} p_j\,q_i\,\overline{\tilde{u}_j(-\mathbf{k}-\mathbf{p},t)\,\tilde{u}_i(\mathbf{k}-\mathbf{q},t)}\;\overline{\tilde{c}(\mathbf{p},t)\tilde{c}(\mathbf{q},t)}.\end{aligned} \tag{2.33}$$

This may be simplified to

$$D^2\,k^4\,\tilde{Z}(\mathbf{k},t,t) = \mu^2\,\tilde{V}_{11}(\mathbf{k},t,t) + \tilde{V}_{11}(\mathbf{k},t,t)\,\left(\frac{2\pi}{L}\right)^3 \sum_{\mathbf{q}} q_j\,q_j\,\tilde{Z}(\mathbf{q},t,t). \tag{2.34}$$

The sum over $\mathbf{q}$ can be related to the scalar dissipation, and taking the limit $L \to \infty$ and performing a surface integral in wavenumbers space leads to

$$E_c(k) = \frac{2}{3}\,E(k) D^{-2}\,k^{-4}\,\left(\mu^2 + \frac{\epsilon_c}{2\,D}\right). \tag{2.35}$$

We are in the inertial range, and so using the appropriate form of the energy spectrum (2.30) we find

$$E_c(k) = \frac{1}{3} D^{-3}\,K\,\epsilon^{2/3}\,\epsilon_c\,k^{-17/3}\,\left(1 + \frac{2\,D\,\mu^2}{\epsilon_c}\right). \tag{2.36}$$

Equation (2.36) reduces to the Batchelor, Howells, and Townsend [2] result when the mean scalar gradient $\mu$ is set to zero. Thus the effect of the mean scalar gradient is to change the magnitude of the scalar spectrum, but not its wavenumber dependence. As Chasnov [5] noted, the effect of the mean scalar gradient can be captured by replacing the scalar dissipation with $\epsilon_c + 2\,D\,\mu^2$ in the original Batchelor, Howells, and Townsend [2] result. We have performed an LES using a different subgrid model to the one used by Chasnov [5], and we will compare with our results for the scalar spectrum and velocity-scalar cospectrum in the next subsection.

We are now in a position to compare our asymptotic result for the cospectrum in the inertial-diffusive range with the bound given by the cospectrum inequality. Substituting (2.30) and (2.36) into (2.21) we find

$$|C_{u_1 c}(k)| \leq \frac{2}{3}\,\mu\,K\,\epsilon^{2/3}\,k^{-11/3}\,D^{-1}\,\left(\frac{\epsilon_c}{2\,D\,\mu^2} + 1\right)^{1/2}. \tag{2.37}$$

Thus the bound exceeds the magnitude of our asymptotic result for the cospectrum by a factor $(\epsilon_c/(2\,D\,\mu^2) + 1)^{1/2}$.

### 2.1.5 Large-eddy simulation at low Schmidt number

We performed a large-eddy simulation (LES) to verify the asymptotic results (2.31) and (2.36) for the velocity-scalar cospectrum and scalar spectrum at low Schmidt number in the inertial-diffusive range. Our simulation is similar to the LES of Chasnov [5]. Chasnov made a comparison with the asymptotic form (2.36) for the scalar spectrum, and found excellent agreement in the far inertial-diffusive range, but the agreement in the near inertial-diffusive range was not as good. As was the case for Chasnov, we do not need a subgrid model for the scalar because we resolve the diffusive range, but our subgrid model for the velocity is different from that used by Chasnov.

The LES was performed with $64^3$ gridpoints, at a Taylor Reynolds number of 1500, and a Schmidt number of $2 \times 10^{-4}$. A statistically stationary state was reached by forcing the velocity at the low wavenumbers using the same forcing scheme as is described in section 2.4, and a mean scalar gradient acted as the source for the scalar variance. Statistics were collected over thirty large-eddy turnover times, and time-averaged spectra are reported.

We used the stretched-vortex SGS model of Misra and Pullin [32], with vortex alignment according to the locally resolved strain rates (model 1a), and a spiral-vortex type energy spectrum at the subgrid scales. Evaluation of the second-order velocity structure function was used to calculate the subgrid energy, see Voelkl *et al.* [47] and Pullin [38] for further details. This LES method has the advantage of dynamically giving a value for the Kolmogorov constant, which we then use in expressions (2.31) and (2.36).

The LES result for the scalar spectrum, and the asymptotic result given by (2.36) are compared in Figure 2.1. The Obukhov-Corrsin wavenumber corresponds to $k_C\,\eta \simeq 0.002$, and so we can see that in the inertial-diffusive range the agreement is quite good. The LES result for the velocity-scalar cospectrum, and the asymptotic result given by (2.31) are compared in Figure 2.2. The agreement is reasonable for wavenumbers in the inertial-diffusive range, although the asymptotic result is lower

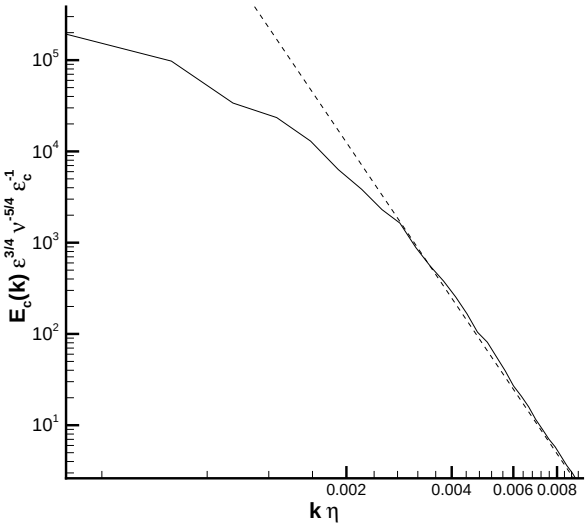


Figure 2.1: Comparison of the scalar spectrum from the LES (solid) and the low Schmidt number asymptotic form given by equation (2.36).

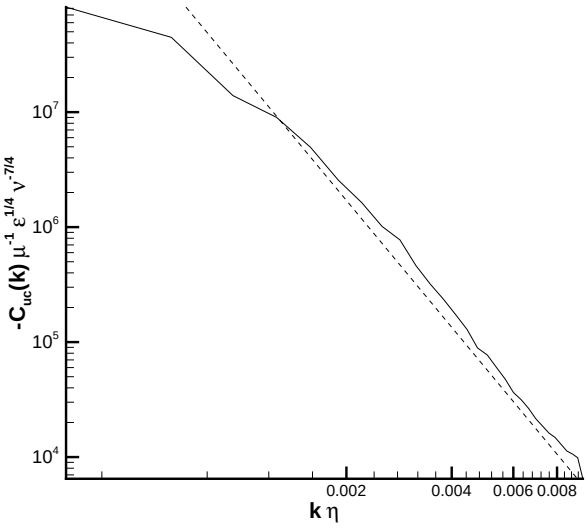


Figure 2.2: Comparison of the velocity-scalar cospectrum from the LES (solid) and the low Schmidt number asymptotic form given by equation (2.31).

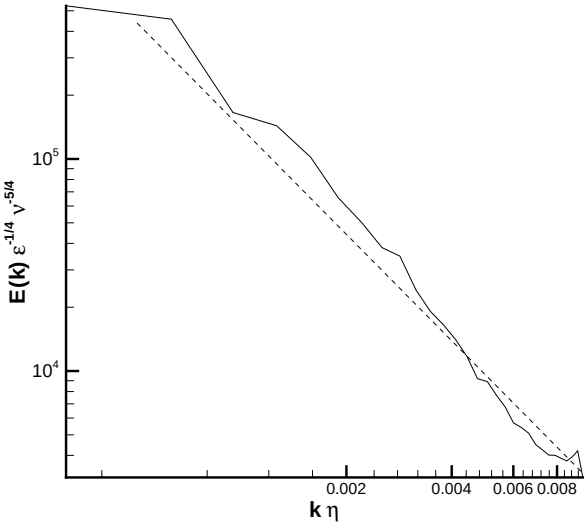


Figure 2.3: Comparison of the energy spectrum from the LES (solid) and inertial range form given by equation (2.30).

than the LES result. Thus, LES seems to confirm both asymptotic results for the velocity-scalar cospectrum and the scalar spectrum, although of course any mechanism that requires a resolved viscous range has been neglected in our LES. For reference, we show in Figure 2.3 the energy spectrum from the LES compared with the inertial-range form (2.30), where we have again used the Kolmogorov constant given by the LES.

## 2.2 Application of the stretched-spiral vortex model

Here we will use the stretched-spiral vortex model to calculate the velocity-scalar cospectrum. In subsection 2.2.1 a new solution is found to the advection diffusion equation where the scalar can show variation parallel to the vortex axis, and asymptotic expressions for the evolution of the velocity and scalar fields in the vortex tube are described. In subsection 2.2.2 expressions are derived for the cospectrum contributed by the axial velocity and also the velocity in the plane of the vortex. In subsection 2.2.3 the expressions for the cospectrum are evaluated for a particular

choice of initial conditions. The contribution from the axial velocity is evaluated using its asymptotic form for high wavenumber, but the contribution from the velocity in the plane of the vortex can only be evaluated numerically.

### 2.2.1 Evolution of scalar and velocity fields in a stretched vortex tube

We wish to find the evolution of the velocity and scalar fields in a vortex tube embedded in a background linear velocity field. It will be important in this section to distinguish between lab and vortex fixed frames, because the mean scalar gradient is assumed to be fixed with respect to the laboratory frame. Therefore, we adopt a temporary notation, where $x_i$ are vortex fixed axes, and $x_i'$ are laboratory coordinates. The vortex fixed coordinate, $x_3$, is aligned with the vortex tube axis. The velocity field of the vortex tube is assumed independent of $x_3$, but may have a component in the direction of the vortex axis. The scalar is in general a function of all three spatial coordinates. The following analysis generalizes that of Pullin and Lundgren [40], hereafter referred to as PL, by letting the scalar have an $x_3$ dependence. The effect of this change on the scalar spectrum is discussed in Appendix B.

It will be convenient for the moment to work with the total scalar field $c^t(\mathbf{x},t) = \mu\, x_1' + c(\mathbf{x},t)$, rather than the scalar fluctuation $c(\mathbf{x},t)$. The Navier-Stokes equations for the velocity $u_i$ and the vorticity $\omega_i$ are

$$\frac{\partial u_i}{\partial t} + u_j \frac{\partial u_i}{\partial x_j} = -\frac{\partial \pi}{\partial x_i} + \nu \nabla^2 u_i, \tag{2.38}$$

$$\frac{\partial \omega_i}{\partial t} + u_j \frac{\partial \omega_i}{\partial x_j} = \omega_j \frac{\partial u_i}{\partial x_j} + \nu \nabla^2 \omega_i, \tag{2.39}$$

and the advection-diffusion equation for the scalar $c^t(x_1, x_2, x_3, t)$ is

$$\frac{\partial c^t}{\partial t} + u_j \frac{\partial c^t}{\partial x_j} = D\, \nabla^2 c^t, \tag{2.40}$$

where $\pi$ is the pressure-density ratio, $\nu$ is the viscosity and $D$ is the scalar diffusivity.

The velocity field is decomposed as

$$u_i = v_i(x_1, x_2, t) + a_i(t)x_i, \tag{2.41}$$

with $a_1 + a_2 + a_3 = 0$ and $a_3 > a_2 > a_1$. Summation over $i$ is not implied. If the support of the vorticity is compact in a domain surrounding $x_1 = x_2 = 0$ then the velocity can be expressed in terms of a vector potential $\psi_i(x_1, x_2, t)$ as

$$v_1 = \frac{\partial \psi_3}{\partial x_2}, \qquad v_2 = -\frac{\partial \psi_3}{\partial x_1}, \qquad v_3 = \frac{\partial \psi_2}{\partial x_1} - \frac{\partial \psi_1}{\partial x_2}. \tag{2.42}$$

Now choose the gauge of $\psi_i$ so that $\partial \psi_i / \partial x_i = 0$. Then,

$$\omega_i(x_1, x_2, t) = -\nabla_2^2 \psi_i, \qquad \nabla_2^2 \equiv \frac{\partial^2}{\partial x_1^2} + \frac{\partial^2}{\partial x_2^2}. \tag{2.43}$$

We also define a reduced pressure $\pi^*$ as follows

$$\pi^*(x_1, x_2, t) = \pi + \frac{1}{2}(a_1^2 x_1^2 + a_2^2 x_2^2 + a_3^2 x_3^2). \tag{2.44}$$

Then we have the following equations for $\omega_3$, $v_3$ and $c^t$,

$$\frac{\partial \omega_3}{\partial t} + \left(a_1 x_1 + \frac{\partial \psi_3}{\partial x_2}\right)\frac{\partial \omega_3}{\partial x_1} + \left(a_2 x_2 - \frac{\partial \psi_3}{\partial x_1}\right)\frac{\partial \omega_3}{\partial x_2} + a_3 \omega_3 = \nu \nabla_2^2 \omega_3, \tag{2.45}$$

$$\frac{\partial v_3}{\partial t} + \left(a_1 x_1 + \frac{\partial \psi_3}{\partial x_2}\right)\frac{\partial v_3}{\partial x_1} + \left(a_2 x_2 - \frac{\partial \psi_3}{\partial x_1}\right)\frac{\partial v_3}{\partial x_2} + a_3 v_3 = \nu \nabla_2^2 v_3, \tag{2.46}$$

$$\frac{\partial c^t}{\partial t} + \left(a_1 x_1 + \frac{\partial \psi_3}{\partial x_2}\right)\frac{\partial c^t}{\partial x_1} + \left(a_2 x_2 - \frac{\partial \psi_3}{\partial x_1}\right)\frac{\partial c^t}{\partial x_2} = -\left(a_3 x_3 + v_3\right)\frac{\partial c^t}{\partial x_3} + D\nabla^2 c^t. \tag{2.47}$$

It can be seen that (2.45) and (2.43) ($i = 3$) are sufficient to determine $\omega_3(x_1, x_2, t)$ and $\psi_3(x_1, x_2, t)$. Once these are solved (2.46) can be solved for $v_3(x_1, x_2, t)$, and finally (2.47) can be solved for $c^t(x_1, x_2, x_3, t)$.

We wish to consider the case where there is a mean gradient, $\mu$, in the scalar in the lab frame. We assume the mean gradient is along the $x_1'$ axis, where $x_i'$ are lab coordinates. The scalar field at time zero may then be decomposed as the sum of the

linear gradient fixed in the lab frame, and a remainder, $c'(\mathbf{x},0) = c'(x_1,x_2,x_3,0)$,

$$\begin{aligned} c^t(t=0) &= \mu\, x_1' + c'(\mathbf{x},0) && (2.48)\\ &= \mu(M_{11}x_1 + M_{21}x_2 + M_{31}x_3) + c'(\mathbf{x},0), && (2.49)\end{aligned}$$

where $M_{ij}(\alpha,\beta,\gamma)$ is a rotation matrix describing a rotation from the $x_i'$ axes to the $x_i$ axes, such that $x_j' = M_{ij}x_i$, and where $(\alpha,\beta,\gamma)$ are the corresponding Euler angles [42]. Noting that the equation governing the scalar is linear, we decompose the scalar field at time $t$ as

$$c^t(\mathbf{x},t) = M_{11}\, c_1(\mathbf{x},t) + M_{21}\, c_2(\mathbf{x},t) + M_{31}\, c_3(\mathbf{x},t) + c'(\mathbf{x},t), \tag{2.50}$$

where

$$c_i(\mathbf{x},0) = \mu\, x_i, \tag{2.51}$$

and each of $c_1, c_2, c_3, c'$ solve equation (2.47). We now further specialize to the case of a time independent axisymmetric strain field, $a_1 = a_2 = -a/2$, $a_3 = a$, $a > 0$, and also set the Schmidt number equal to unity, $Sc = \nu/D = 1$.

**Solution for $c_3$ in terms of $v_3$**

A schematic is shown in Figure 2.4 of the winding of the axial velocity into a spiral. Scalar variations in the axial direction are distorted by the spiraling axial velocity, and we can capture this effect with the following analysis. We begin by defining the material derivative $D/Dt = \partial/\partial t + u_i\, \partial/\partial x_i$ and temporarily set $\nu = D = 0$. Then we can rewrite equation (2.47) for $c_3$ as $Dc_3/Dt = 0$, and it is clear that $c_3$ is conserved along paths $\chi_i(t)$ that satisfy $d\chi_i/dt = u_i$. Therefore, using the initial condition (2.51) we have that $c_3(\mathbf{x},t) = \mu\,\chi_3(0)$ where $\chi_i(t) = x_i$. We can also rewrite equation (2.46) as $Dv_3/Dt = -a\, v_3$, so that $v_3(\mathbf{X},t) = \exp(-a\,t)\, v_{30}$ where $v_{30}$ is a constant, and

$$\frac{d\chi_3(t)}{dt} = a\,\chi_3(t) + e^{-a\,t}\, v_{30}. \tag{2.52}$$

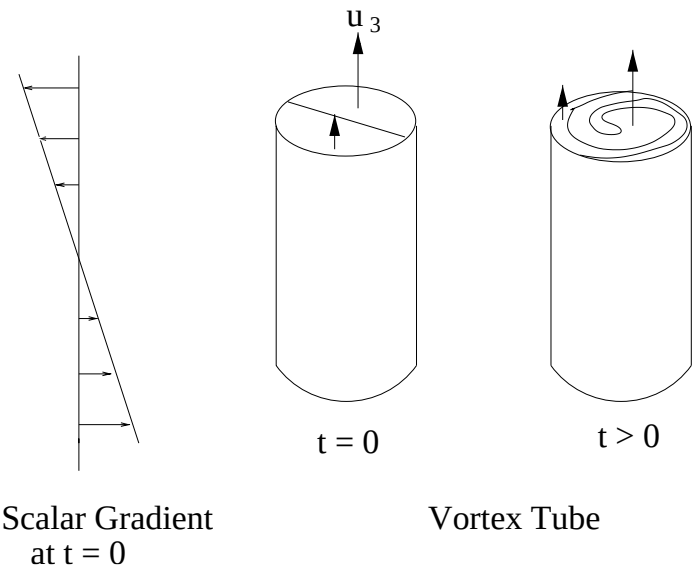


Figure 2.4: Schematic representation of the winding of the axial velocity in a vortex structure. Scalar variations in the axial direction are in turn distorted by the axial velocity.

This equation can be solved to give

$$\chi_3(0) = \chi_3(t)\, e^{-a\,t} - v_3(x_1, x_2, t)\, \frac{1}{a}\, \sinh(at), \tag{2.53}$$

so that

$$c_3(\mathbf{x}, t) = \mu\, (e^{-a\,t} x_3 - v_3(x_1, x_2, t)\, \frac{1}{a} \sinh(a\,t)). \tag{2.54}$$

It is easily verified by direct substitution that this solution (2.54) for $c_3$ is also valid in the case when $\nu \neq 0$ if $Sc = \nu/D = 1$. To simplify the analysis, we subsequently assume $Sc = 1$.

**Solutions for $c_1$, $c_2$ and the axial velocity and vorticity**

Both $c_1$ and $c_2$ have no $x_3$ dependence initially, and so from equation (2.47) it is clear that they will be independent of $x_3$ at later times. We are thus motivated to study solutions to equation (2.47) when there is no $x_3$ dependence,

$$\frac{\partial c_1}{\partial t} + \left(a_1 x_1 + \frac{\partial \psi_3}{\partial x_2}\right) \frac{\partial c_1}{\partial x_1} + \left(a_2 x_2 - \frac{\partial \psi_3}{\partial x_1}\right) \frac{\partial c_1}{\partial x_2} = D \nabla^2 c_1. \tag{2.55}$$

It is convenient to work in polar coordinates $(r, \theta)$ with $x_1 = r\cos\theta$, $x_2 = r\sin\theta$, and introduce the transformation [29],

$$\begin{aligned} S(t) &= e^{a\,t}, \\ \rho &= S(t)^{1/2}\, r, \\ \tau &= \frac{1}{a}\,(S(t)-1), \\ \psi_3(r,\theta,t) &= \Psi_3(\rho,\theta,\tau), \\ \omega_3(r,\theta,t) &= S(t)\,\mathcal{W}(\rho,\theta,\tau), \\ v_3(r,\theta,t) &= S(t)^{-1}\,\mathcal{U}(\rho,\theta,\tau), \\ c_1(r,\theta,t) &= \Phi(\rho,\theta,\tau). \end{aligned} \tag{2.56}$$

Equations (2.46) and (2.55) can then be expressed in essentially the same form,

$$\frac{\partial \mathcal{U}}{\partial t} + \frac{1}{\rho}\left(\frac{\partial \Psi_3}{\partial \theta}\frac{\partial \mathcal{U}}{\partial \rho} - \frac{\partial \Psi_3}{\partial \rho}\frac{\partial \mathcal{U}}{\partial \theta}\right) = \nu\,\nabla_2^2\,\mathcal{U}, \tag{2.57}$$

where the equation is also valid if $(\mathcal{U}, \nu)$ are replaced with $(\Phi, D)$. Approximate solutions for $\mathcal{W}$, $\Psi_3$, $\mathcal{U}$ and $\Phi$ can be found using a two time analysis [40]. These solutions are asymptotically correct for large $\tau$. The solution for the axial vorticity and the stream function takes the form

$$\mathcal{W} = \sum_{-\infty}^{\infty} \omega_n(\rho,\tau)\,\exp(i\,n\,\theta), \qquad \omega_{-n} = \omega_n^*, \tag{2.58}$$

$$\Psi_3 = \sum_{-\infty}^{\infty} \psi_n(\rho,\tau)\,\exp(i\,n\,\theta), \qquad \psi_{-n} = \psi_n^*, \tag{2.59}$$

where the Fourier coefficients for $n \neq 0$ are

$$\omega_n(\rho,\tau) = f_n(\rho)\,\exp(-i\,n\,\Omega(\rho)\,\tau\, - \nu\,n^2\,\Lambda^2\,\tau^3/3), \tag{2.60}$$

$$\psi_n(\rho,\tau) = \tau^{-2}\,h_n(\rho)\,\exp(-i\,n\,\Omega(\rho)\,\tau\, - \nu\,n^2\,\Lambda^2\,\tau^3/3), \tag{2.61}$$

with

$$h_n(\rho) = \frac{f_n(\rho)}{n^2\,\Lambda^2}, \qquad \Lambda(\rho) = \frac{d\Omega(\rho)}{d\rho}. \tag{2.62}$$

The $\theta$ averaged angular velocity $\Omega(\rho)$ is related to the zeroth harmonic of the vorticity and to $\psi_0$ by

$$\omega_0(\rho) = \frac{1}{\rho}\frac{\partial(\rho^2\Omega)}{\partial\rho}, \qquad \Omega(\rho) = -\frac{1}{\rho}\frac{\partial\psi_0}{\partial\rho}. \tag{2.63}$$

It should be noted that we assume $\Lambda < 0$ in order for the expansion in large $\tau$ to be valid. The expressions for $\omega_n$ are valid to $O(1)$ for $n \neq 0$. However $\omega_0$ (and hence $\Omega$) is constant in time to within terms of order $\tau^{-2}$. The functions $f_n(\rho)$ may be viewed as initial conditions that define a spiral vortex structure although the solution is of course only valid for large $\tau$. The above solution for the axial vorticity essentially describes the winding of the non-axisymmetric part of the vorticity field by the axisymmetric part (the core). The solution for the stream function may be rewritten in the form

$$\begin{aligned}
\Psi_3 &= \Psi^{(0)} + \tau^{-2}\,\Psi^{(2)}, \\
\Psi^{(2)} &= \sum_{-\infty, n\neq 0}^{\infty} \Psi_n^{(2)}\,\exp(i\,n(\theta - \Omega\tau)), \\
\Psi_n^{(2)} &= h_n(\rho)\,\exp(-\nu\,n^2\,\Lambda^2\,\tau^3/3).
\end{aligned} \tag{2.64}$$

The asymptotic solutions for the scalar and the axial velocity are then given by (to order $\tau^{-1}$)

$$\begin{aligned}
\Phi(\rho,\theta,\tau) &= \Phi^{(0)} + \tau^{-1} \sum_{-\infty, n\neq 0}^{\infty} \Phi_n^{(1)}\,\exp(i\,n(\theta - \Omega\,\tau)), \\
\Phi^{(0)} &= \sum_{-\infty}^{\infty} \Phi_n^{(0)}(\rho,\tau)\,\exp(i\,n(\theta - \Omega\,\tau)), \\
\Phi_n^{(0)} &= \check{\Phi}_n^{(0)}(\rho)\exp(-D\,n^2\,\Lambda^2\,\tau^3/3), \\
\Phi_n^{(1)} &= \frac{i}{\rho} \sum_{-\infty, m\neq 0}^{\infty} \left( m\,\Psi_m^{(2)}\,\frac{\partial\,\Phi_{n-m}^{(0)}}{\partial\,\rho} - (n-m)\,\frac{\partial\,\Psi_m^{(2)}}{\partial\,\rho}\,\Phi_{n-m}^{(0)} \right),
\end{aligned} \tag{2.65}$$

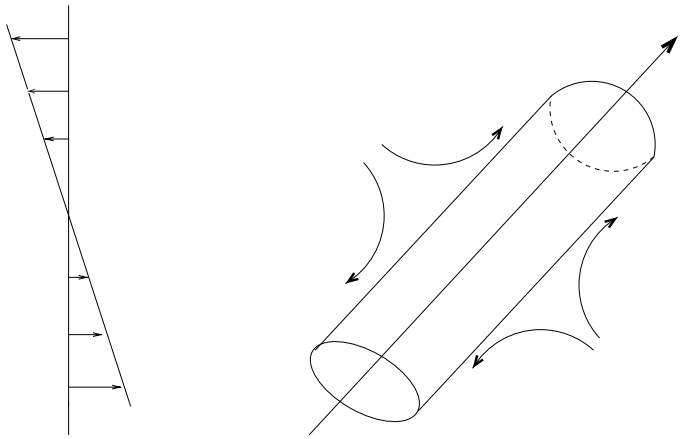


Figure 2.5: Schematic representation of a stretched vortex structure and the mean scalar gradient.

$$
\begin{aligned}
\mathcal{U}(\rho,\theta,\tau) &= \mathcal{U}^{(0)} + \tau^{-1} \sum_{-\infty, n\neq 0}^{\infty} \mathcal{U}_n^{(1)} \exp(i\, n(\theta - \Omega\,\tau)), \\
\mathcal{U}^{(0)} &= \sum_{-\infty}^{\infty} \mathcal{U}_n^{(0)}(\rho,\tau) \exp(i\, n(\theta - \Omega\,\tau)), \\
\mathcal{U}_n^{(0)} &= \check{\mathcal{U}}_n^{(0)}(\rho) \exp(-\nu\, n^2\, \Lambda^2\, \tau^3/3), \\
\mathcal{U}_n^{(1)} &= \frac{i}{\rho} \sum_{-\infty, m\neq 0}^{\infty} \left( m\, \Psi_m^{(2)}\, \frac{\partial\, \mathcal{U}_{n-m}^{(0)}}{\partial\, \rho} - (n-m)\, \frac{\partial\, \Psi_m^{(2)}}{\partial\, \rho}\, \mathcal{U}_{n-m}^{(0)} \right), \qquad (2.66)
\end{aligned}
$$

where the initial scalar field is given by the functions $\check{C}_n^{(0)}(\rho)$ and the initial axial velocity field is given by the functions $\check{\mathcal{U}}_n^{(0)}(\rho)$. It should be emphasized that this scalar solution is only valid when the initial conditions have no $x_3$ dependence, as is the case for $c_1$ and $c_2$.

### 2.2.2 Calculation of the cospectrum

We wish to calculate the velocity-scalar cospectrum using the stretched-spiral vortex model. The important elements of our calculation are shown schematically in Figure 2.5. We will consider the scalar gradient fixed in the lab frame. The vortex structures are stretched in the axial direction, and there is a random distribution of the orientation of the structure axes with respect to the lab frame.

We will first consider the shell-summed cospectrum defined by equation (2.2). Here we will again adopt the temporary notation where $x_i$ are vortex fixed axes, primed quantities indicate the lab frame, and of course $k = k'$, so that equation (2.2) is rewritten as

$$C_{u'_i c}(k) = \frac{1}{(2\pi)^3} \int_S \int_V \mathcal{R}_{u'_i c}(\mathbf{r}') e^{-i\,\mathbf{k}'\cdot\mathbf{r}'} d\mathbf{r}'\, dS_{k'}. \tag{2.67}$$

We suppose there is a box populated by a collection of stretched vortex tubes. The vortex tubes do not interact except in that each vortex tube is stretched on average by the other vortex tubes. We assume that the vortex structures are distributed sparsely enough so that the overlapping velocity and scalar fields from the vortex tubes do not contribute strongly to the fine scales. It is further assumed that a statistical equilibrium has been reached whereby the structures are created and decay at the same rate. The average in the definition of the scalar-velocity correlation (2.1) is then interpreted as an average over time, space, vortex orientation, and initial conditions of one vortex tube,

$$\mathcal{R}_{u'_i\, c}(\mathbf{r}') = N^c \left\langle < \int_0^{t_c} \int_V u'_i(\mathbf{x}', t)\, c(\mathbf{x}' + \mathbf{r}', t)\, d\mathbf{x}'\, dt\ > \right\rangle, \tag{2.68}$$

where $N^c$ is the rate of creation of vortex tubes per unit time and per unit volume, $t^c$ is a typical vortex lifetime, $\langle\rangle$ indicates an average over initial conditions, and $<>$ indicates an average over vortex orientation. The average over vortex orientation is defined using the Euler angles $\alpha, \beta, \gamma$ that rotate the lab frame to the vortex fixed frame [42],

$$< f(M_{ij}) >= \frac{1}{8\pi^2} \int_0^{2\pi} \int_0^{2\pi} \int_0^{\pi} f(M_{ij})\, P(\alpha, \beta, \gamma)\, \sin\alpha\, d\alpha\, d\beta\, d\gamma, \tag{2.69}$$

where $P(\alpha, \beta, \gamma)$ is the probability density function of the Euler angles, and $M_{ij}$ is the associated rotation matrix. To match with experiment we specialize to the case of an isotropic velocity field and set $P = 1$ so that all orientations are equally likely. We now rewrite equation (2.67) by changing the ordering of the averages, substituting $u'_i = M_{ji} u_j$ and changing integration variables from $\mathbf{r}'$ to $\mathbf{r}$, from $\mathbf{k}'$ to $\mathbf{k}$, and from

$\mathbf{x}'$ to $\mathbf{x}$. It is also convenient to replace the scalar fluctuation, $c(\mathbf{x},t)$, with the total scalar field, $c^t(\mathbf{x},t)$, and this is justified because the average of the velocity field is zero. Lastly, we substitute $v_j(\mathbf{x},t)$ for $u_j(\mathbf{x},t)$, neglecting any contribution from the strain field. The resulting expression is

$$C_{u_i'c}(k) = \frac{N^c}{(2\pi)^3} < \langle \int_S \int_V \int_0^{t_c} \int_V M_{ji}\, v_j(\mathbf{x},t)\, c^t(\mathbf{x}+\mathbf{r},t)\, e^{-i\,\mathbf{k}\cdot\mathbf{r}}\, d\mathbf{x}\, dt\, d\mathbf{r}\, dS_k \rangle > . \tag{2.70}$$

**Simplification using symmetries in the distribution of initial conditions**

Next we use some symmetries in the distribution of the initial conditions of the velocity and the scalar to simplify (2.70). For a given vortex tube let the initial $v_3$ distribution be $v_{30}$ (say at the time when the tube is created). We will consider the effects of the transformation $v_{30}$ to $-v_{30}$. Clearly $v_3(\mathbf{x},t)$ changes to $-v_3(\mathbf{x},t)$ because equation (2.46) is linear and homogeneous. It is also clear that $v_1$ and $v_2$ are unaffected as they have no $x_3$ dependence. From (2.51) we see that initially $\partial c_1/\partial x_3 = \partial c_2/\partial x_3 = 0$. Then by taking the partial derivative with respect to $x_3$ of equation (2.47) we see that $\partial c_1/\partial x_3 = \partial c_2/\partial x_3 = 0$ for all times. It is then clear from equation (2.47) that $v_3$ has no influence on the evolution of $c_1$ or $c_2$. Finally, it is clear that the first term in expression (2.54) for $c_3$ is unaffected by changes in $v_{30}$, and that the second term will change sign when $v_{30}$ changes sign.

Therefore, if we assume that for each initial distribution of velocities $v_1(\mathbf{x},0)$ and $v_2(\mathbf{x},0)$ that $v_3(\mathbf{x},0) = v_{30}$ is as likely as $v_3(\mathbf{x},0) = -v_{30}$, then performing the average over the initial conditions will eliminate some terms that we now neglect. At this stage we also neglect the remainder term $c'$ in the expression (2.50) for $c^t(\mathbf{x},t)$. This may be justified by noting that $c'(\mathbf{x},t)$ depends linearly on $c'(\mathbf{x},0)$, and making the approximation that $c'(\mathbf{x},0)$ and $v_j(\mathbf{x},0)$ are statistically independent. We therefore replace $M_{ji}\, v_j(\mathbf{x},t)\, c(\mathbf{x}+\mathbf{r},t)$ in expression (2.70) with

$$\begin{aligned}[M_{1i}v_1 + M_{2i}v_2](\mathbf{x},t)\ [M_{11}\, c_1 + M_{21}\, c_2 + M_{31}\, \mu\, e^{-at}\, x_3](\mathbf{x}+\mathbf{r},t) \quad - \\ M_{3i}v_3(\mathbf{x},t)\ [M_{31}\, \mu\, v_3\, \frac{1}{a}\, \sinh(at)](\mathbf{x}+\mathbf{r},t).\end{aligned} \tag{2.71}$$

For simplicity we now replace the average over initial conditions with one particular initial condition. Using the integrals

$$\frac{1}{8\pi^2}\int M_{ij}\,M_{k1}\sin\alpha\,d\alpha\,d\beta\,d\gamma=\frac{1}{3}\,\delta_{ik}\delta_{j1} \tag{2.72}$$

to perform the orientation average gives $C_{u'_2c}=C_{u'_3c}=0$ and,

$$\begin{aligned}C_{u'_1c}(k) &= \frac{1}{3}\,\frac{N^c}{(2\pi)^3}\int_S\int_V\int_0^{t_c}\int_V[v_1(\mathbf{x},t)\,c_1(\mathbf{x}+\mathbf{r},t)+v_2(\mathbf{x},t)\,c_2(\mathbf{x}+\mathbf{r},t)\\ &- v_3(\mathbf{x},t)\,\mu\,\frac{1}{a}\,\sinh(at)\,v_3(\mathbf{x}+\mathbf{r},t)\,]e^{-i\,\mathbf{k}\cdot\mathbf{r}}\,d\mathbf{x}\,dt\,d\mathbf{r}\,dS_k.\end{aligned} \tag{2.73}$$

Noting that $v_1, v_2, v_3, c_1, c_2$ have no $x_3$ dependence we can replace $N^c\int_0^{t_c}\int_V d\mathbf{x}\,dt$ with $N\int_0^{t_c}\int_{-\infty}^{\infty}\int_{-\infty}^{\infty}dx_1\,dx_2\,S(t)\,dt$ where $N$ is the rate of creation of vortex length per unit time and per unit volume, and the factor $S(t)$ arises from the lengthening over time of the vortex tube. Defining the two dimensional Fourier transform of a function $f(x_1,x_2)$ by

$$\hat{f}(k_1,k_2)=\frac{1}{4\pi^2}\int_{-\infty}^{\infty}\int_{-\infty}^{\infty}e^{-i\,k_1x_1-i\,k_2x_2}\,f(x_1,x_2)\,dx_1\,dx_2, \tag{2.74}$$

and dividing the expression (2.73) into contributions from the axial velocity (a) and planar velocity (p), we find that

$$C_{u'_1c}(k) = C^{(p)}_{u'_1c}(k)+C^{(a)}_{u'_1c}(k), \tag{2.75}$$

where

$$C^{(p)}_{u'_1c}(k)=\frac{N(2\pi)^2}{3}\int_0^{t_c}\int_0^{2\pi}(\hat{v}_1\,\hat{c_1}^*+\hat{v}_2\,\hat{c_2}^*)\,k\,d\theta_k\,S(t)\,dt, \tag{2.76}$$

$$C^{(a)}_{u'_1c}(k)=-\frac{N(2\pi)^2}{3}\int_0^{t_c}\int_0^{2\pi}\left(\mu\,\frac{1}{a}\,\sinh(at)\,\hat{v}_3\,\hat{v_3}^*\right)k\,d\theta_k\,S(t)\,dt, \tag{2.77}$$

and $k_1=k\,\cos\theta_k$ and $k_2=k\,\sin\theta_k$.

**Contribution from the planar velocity:** $C^{(p)}_{u_1' c}$

We now consider the contribution to the cospectrum from correlations between the planar velocities $(v_1, v_2)$ and $c_1$ and $c_2$ in equation (2.76). We can simplify the analysis by relating $(\hat{v}_1, \hat{v}_2)$ to $\hat{\omega}_3$. Using $\omega_i = \epsilon_{ijk}\, \partial v_k / \partial x_j$, assuming that the velocity field decays sufficiently quickly as $x_1$ or $x_2$ become large, and defining $k_3 = 0$ gives $\hat{\omega}_l = i\, \epsilon_{lmn}\, k_m \hat{v}_n$. The assumption of incompressibility gives $k_l\, \hat{v}_l = 0$. Therefore $\hat{v}_l$ is orthogonal to $k_l$ and $\hat{\omega}_l$, and,

$$\hat{v}_l = \alpha\, \epsilon_{lmn}\, k_m\, \hat{\omega}_n = -\alpha\, i\, k^2 \hat{v}_l. \tag{2.78}$$

Thus the scalar $\alpha$ is determined and $\hat{v}_l(k_1, k_2) = i\, k^{-2}\, \epsilon_{lmn}\, k_m\, \hat{\omega}_n$. We are interested in the components of the velocity in the plane,

$$\hat{v}_1(k_1, k_2) = \frac{i}{k}\, \sin\theta_k\, \hat{\omega}_3, \qquad \hat{v}_2(k_1, k_2) = -\frac{i}{k}\, \cos\theta_k\, \hat{\omega}_3. \tag{2.79}$$

Then from equation (2.76) we have that

$$C^{(p)}_{u_1' c}(k) = \frac{1}{3}\, i\, N\, (2\pi)^2 \int_0^{t_c} \int_0^{2\pi} \hat{\omega}_3\, (\sin\theta_k\, \hat{c}_1^* - \cos\theta_k\, \hat{c}_2^*)\; d\theta_k\, S(t)\, dt. \tag{2.80}$$

Letting

$$\omega_3 = \sum_{n=-\infty}^{\infty} \omega_n(r, t) \exp(i\, n\, \theta), \tag{2.81}$$

and using

$$\int_0^{2\pi} \exp(i\, n\, \theta - ikr \cos(\theta - \theta_k))\, d\theta = (-i)^n 2\pi J_n(kr) \exp(i\, n\, \theta_k), \tag{2.82}$$

gives

$$\hat{\omega}_3 = \frac{1}{2\pi} \sum_{n=-\infty}^{\infty} (-i)^n\, \exp(i\, n\, \theta_k)\, I_n^{\omega}(k, t), \tag{2.83}$$

where

$$I_n^{\omega}(k, t) = \int_0^{\infty} \omega_n(r, t)\, J_n(k\, r)\, r\, dr. \tag{2.84}$$

We will use the solution (2.65) for $c_1$ and $c_2$, but will neglect terms of order $\tau^{-1}$. Using the initial conditions (2.51) we see that for $c_1$

$$\check{\Phi}_1^{(0)} = \frac{\mu\,\rho}{2}, \qquad \check{\Phi}_{-1}^{(0)} = \frac{\mu\,\rho}{2}, \tag{2.85}$$

and that for $c_2$

$$\check{\Phi}_1^{(0)} = -\frac{i\,\mu\,\rho}{2}, \qquad \check{\Phi}_{-1}^{(0)} = \frac{i\,\mu\,\rho}{2}. \tag{2.86}$$

Note that because the solutions for the scalar and the vorticity are only valid asymptotically in time, we should specify the initial conditions at some initial time $t_1 > 0$. However, we make the approximation $t_1 \to 0$, and the resulting integrals are convergent at time zero.

It is convenient to define

$$\begin{aligned} I_1^c &= \frac{\mu}{2}\int_0^\infty \exp(-i\,\Omega(\rho)\,\tau - D\,\Lambda(\rho)^2\,\tau^3/3)\,J_1(k\,r)\,\rho\,r\,dr \\ &= \frac{\mu}{2(1+a\tau)}\int_0^\infty \exp(-i\,\Omega(\rho)\,\tau - D\,\Lambda(\rho)^2\,\tau^3/3)\,J_1\left(\frac{k\,\rho}{\sqrt{1+a\tau}}\right)\,\rho^2\,d\rho. \end{aligned} \tag{2.87}$$

Then using $J_{-1} = -J_1$ and equation (2.82) we have that

$$\hat{c}_1 = \frac{1}{2\pi}\left((-i)\,\exp(i\,\theta_k)\,I_1^c + (-i)^{-1}\,\exp(-i\,\theta_k)\,(-I_1^c)^*\right), \tag{2.88}$$

$$\hat{c}_2 = \frac{1}{2\pi}\left((-i)\,\exp(i\,\theta_k)\,I_1^c\,(-i) + (-i)^{-1}\,\exp(-i\,\theta_k)\,(-I_1^c)^*\,i\right). \tag{2.89}$$

Substituting (2.88), (2.89) and (2.83) into (2.80), and after some algebra we find

$$C_{u_1' c}^{(p)}(k) = \frac{1}{3}\,N\int_0^{t_c}\int_0^{2\pi} i\sum_{n=-\infty}^{\infty}(-i)^n\,\exp(i\,n\,\theta_k)\,I_n^\omega\,((I_1^c)^* - I_1^c)\,d\theta_k\,S(t)\,dt. \tag{2.90}$$

Therefore only $n = 0$ makes a contribution and

$$C_{u_1' c}^{(p)}(k) = \frac{4\pi}{3}\,N\int_0^{t_c} I_0^\omega\,Im(I_1^c)\,S(t)\,dt. \tag{2.91}$$

Finally we can evaluate $I_0^\omega$ in terms of $\Omega(r',0)$ as follows,

$$\begin{aligned} I_0^\omega &= \int_0^\infty J_0(k\,r)\,\omega_0(r,t) r\,dr \\ &= \int_0^\infty J_0\left(\frac{k\,\rho}{\sqrt{1+a\tau}}\right)\,\mathcal{W}_0(\rho,\tau)\rho\,d\rho, \end{aligned} \tag{2.92}$$

where $\mathcal{W}_0(\rho,\tau)$ is the $\theta$ average of $\mathcal{W}(\rho,\theta,\tau)$. Note that unlike the analysis in subsection 2.2.1 where $\Omega$ was taken as constant in time in the asymptotic solution for the scalar and vorticity spirals, we must now take into account the evolution in time of $\Omega(r',t)$ and $\mathcal{W}_0(r',t)$. It is easy to show that $\mathcal{W}_0$ evolves according to a heat equation in a cylindrical geometry [41]. This can be solved using a Green's function in terms of the vorticity distribution at $t=0$,

$$\mathcal{W}_0(\rho,\tau) = 2\pi \int_0^\infty \mathcal{W}_0(r',0)\left[\frac{1}{4\pi\nu\tau}\,\exp\left(\frac{-(\rho^2+r'^2)}{4\nu\tau}\right)\,I_0\left(\frac{\rho r'}{2\nu\tau}\right)\right] r' dr'. \tag{2.93}$$

Substituting this into (2.92) and performing the $\rho$ integral gives

$$I_0^\omega = \exp\left(\frac{-\nu\tau k^2}{1+a\tau}\right)\int_0^\infty\,J_0\left(\frac{r'k}{\sqrt{1+a\tau}}\right)\mathcal{W}_0(r',0)\;r'\,dr'. \tag{2.94}$$

If we use (2.63) to relate $\omega_0$ to $\Omega$ and note that $\omega_0$ and $\mathcal{W}_0$ coincide at $t=0$, we find that

$$I_0^\omega = \exp\left(\frac{-\nu\tau k^2}{1+a\tau}\right)\,k\,(1+a\tau)^{-1/2}\,\int_0^\infty\,J_1\left(\frac{r'k}{\sqrt{1+a\tau}}\right)\Omega(r',0)\;r'^2\,dr'. \tag{2.95}$$

This expression for $I_0^\omega$ cannot be evaluated using the method of stationary phase unlike the corresponding integrals for higher harmonics. Therefore $C^{(p)}_{u_1' c}(k)$ does not have a universal form at high wavenumber, and in fact depends on the choice of $\Omega(r',0)$. Combining equations (2.91), (2.87) and (2.95) gives

$$C^{(p)}_{u_1' c}(k) = \frac{2\pi\,\mu}{3}\,k\,N\,\int_0^{t_c}\exp\left(\frac{-\nu\tau k^2}{1+a\tau}\right)\,(1+a\tau)^{-3/2}\,S(t)\,T_1(\tau,k)\,T_2(\tau,k)\,dt \tag{2.96}$$

where

$$T_1(\tau,k) = -\int_0^\infty J_1\left(\frac{k\,\rho}{\sqrt{1+a\tau}}\right)\,\sin(\Omega\,\tau)\,\exp(-D\,\Lambda^2\,\tau^3/3)\,\rho^2\,d\rho \tag{2.97}$$

$$T_2(\tau,k) = \int_0^\infty J_1\left(\frac{r'k}{\sqrt{1+a\tau}}\right)\,\Omega(r',0)\;r'^2\,dr' \tag{2.98}$$

This expression is evaluated for a particular choice of vortex core in subsection 2.2.3.

Unlike the calculation of $C^{(a)}_{u_1'c}$ discussed in the next section, here we only calculate the lowest order contribution to $C^{(p)}_{u_1'c}$. This is because of the complexity involved in proceeding to higher order, and also because, as we have seen, the asymptotic form of $C^{(p)}_{u_1'c}$ is dependent on the initial conditions. We will use this lowest order contribution in §2.2.3 to show that the planar contribution is comparable in magnitude to the axial contribution.

**Contribution from the axial velocity: $C^{(a)}_{u_1'c}$**

We now wish to consider the contribution from correlations between the axial velocity $v_3$ and the second term of $c_3$. Using expression (2.77) and defining

$$v_3(r,\theta,t) = \sum_{n=-\infty}^{\infty} v_{3,n}(r,t)\;\exp(i\,n\,\theta), \tag{2.99}$$

we find that

$$C^{(a)}_{u_1'c}(k) = -\frac{\mu}{3a}\,k\,N\,2\pi\int_0^{t_c}\sum_{n=-\infty}^{\infty}|I^u_n|^2\;\sinh(at)\,S(t)\,dt, \tag{2.100}$$

where

$$I^u_n = \int_0^\infty J_n(kr)\,v_{3,n}(r,t)\,r\,dr. \tag{2.101}$$

This is similar in structure to the expression for the energy spectrum contributed by the axial velocity [40]. Note that this contribution is negative, consistent with the experimental results of Mydlarski and Warhaft [34], and our DNS results in section 2.4. We can now use the asymptotic solution for $v_3$ to evaluate $I^u_n$. We first consider

the contribution from the $\mathcal{U}^{(0)}$ term. Using (2.66), the integral in $r$ for $I_n^u$ may be evaluated using the method of stationary phase, giving

$$|I_n^u|^2 = \frac{\rho_n\,|\check{\mathcal{U}}_n^{(0)}(\rho_n)|^2}{S^{7/2}\,\Lambda'(\rho_n)\,k\,\tau\,n}\,\exp\left(-\frac{2\,\nu\,n^2\,\Lambda^2(\rho_n)\tau^3}{3}\right), \tag{2.102}$$

where $\rho_n$ is the point of stationary phase. If we approximate $S(t) \simeq a\,\tau$ (valid for $a\,\tau \gg 1$) then $\rho_n$ is related to $\tau$ by

$$\tau \simeq \left(\frac{k}{n\,a^{1/2}\,|\Lambda(\rho_n)|}\right)^{2/3}. \tag{2.103}$$

We now approximate $\sinh(at)$ by $\frac{1}{2}\exp(at)$ (making an $O(\tau^{-2})$ error) and change integration variable from $t$ to $\rho = \rho_n$. Using $|\check{\mathcal{U}}_{-n}^{(0)}| = |\check{\mathcal{U}}_n^{(0)}|$ and letting $t_c \to \infty$ we find,

$$\begin{aligned} C_{u_1' c}^{(a)}(k)^{(0)} &= -\frac{4\pi\mu N}{9}\,k^{-5/3}\,a^{-8/3}\,\exp\left(-\frac{2\,\nu\,k^2}{3\,a}\right)\sum_{n=1}^{\infty} n^{2/3} \\ &\quad\times\int_0^{\infty}\rho\,|\check{\mathcal{U}}_n^{(0)}(\rho)|^2\,|\Lambda(\rho)|^{2/3}\,d\rho, \end{aligned} \tag{2.104}$$

where we have neglected the zeroth harmonic.

### The next-order contribution from $C_{u_1' c}^{(a)}$

Now consider the next-order contribution by including terms involving $\mathcal{U}_n^{(1)}$. We keep only terms $O(\tau^{-1})$ and use stationary phase to evaluate the $r$ integral to find

$$|I_n^u|^2 = \frac{\rho_n\,\left(\check{\mathcal{U}}_n^{(0)}(\rho_n)\,\mathcal{U}_n^{(1)}(\rho_n)^* + \mathcal{U}_n^{(1)}(\rho_n)\,\check{\mathcal{U}}_n^{(0)}(\rho_n)^*\right)}{S^{7/2}\,\Lambda'(\rho_n)\,k\,\tau^2\,n}\,\exp\left(-\frac{\nu\,n^2\,\Lambda^2(\rho_n)\tau^3}{3}\right). \tag{2.105}$$

Again approximating $\sinh(at)$ by $\frac{1}{2}\exp(at)$ for $at \gg 1$, changing variables from $t$ to $\rho_n = \rho$, using $|\check{\mathcal{U}}_{-n}^{(0)}| = |\check{\mathcal{U}}_{n}^{(0)}|$ and letting $t_c \to \infty$ we find

$$\begin{aligned} C_{u_1' c}^{(a)}(k)^{(1)} &= -\frac{8\pi\mu N}{9}\, k^{-7/3}\, a^{-7/3}\, \exp\left(-\frac{\nu\, k^2}{3\, a}\right) \sum_{n=1}^{\infty} n^{4/3} \\ &\quad \times \int_0^{\infty} |\Lambda(\rho)|^{4/3}\, Re\left(\check{\mathcal{U}}_n^{(0)}(\rho)\Pi_n^*\right)\, d\rho, \end{aligned} \tag{2.106}$$

where

$$\begin{aligned} \Pi_n &= i \sum_{m\neq 0} \exp\left(-\frac{\nu\, k^2\, (m^2 + (n-m)^2)}{3\, a\, n^2}\right) \\ &\quad \times \left(\frac{f_m(\rho)}{m\,\Lambda^2}\, \frac{\partial}{\partial\rho}(\check{\mathcal{U}}_{n-m}^{(0)}(\rho)) - \frac{n-m}{m^2}\check{\mathcal{U}}_{n-m}^{(0)}(\rho)\frac{\partial}{\partial\rho}\left(\frac{f_m(\rho)}{\Lambda^2}\right)\right). \end{aligned} \tag{2.107}$$

This contribution may be positive or negative, and may change sign as $k$ varies. Note that the coefficient for this contribution is an integral involving the initial conditions for the axial velocity ($\check{\mathcal{U}}_n^{(0)}(\rho)$), the axial vorticity ($f_m(\rho)$) and the radial derivative of the theta averaged angular velocity ($\Lambda = d\Omega/d\rho$). The following argument could be made to make this coefficient zero. The functions $f_n(r)$ describe the initial condition for the axial vorticity. We can write without loss of generality $f_n(r) = \exp(i\, n\, \theta_n + i\, n\, \delta)\, |f_n(r)|$ where the $\theta_n$ are constant offset angles and $\delta$ then fixes the orientation of the non-axisymmetric part of the initial axial vorticity. Then $C_{u_1' c}^{(a)}(k)^{(1)}$ only depends on $\delta$ through $\Pi_n^*$. It is clear that if we assume $\delta$ is distributed uniformly for a given set of functions $\check{\mathcal{U}}_n^{(0)}(\rho)$ then $C_{u_1' c}^{(a)}(k)^{(1)}$ will be zero. That is, if the initial conditions for the axial vorticity and the axial velocity are uncorrelated then this first-order correction to $C_{u_1' c}^{(a)}$ will give no contribution. Indeed changing the sign of the $f_m$'s and leaving everything else constant will change the sign of this contribution.

Recall that earlier in the derivation we assumed that for a given initial condition for the velocity in the plane of the vortex, that either direction was as likely for the initial condition of the axial velocity. In other words it was assumed that the statistics of the initial velocity field do not possess chirality. This is consistent with the existence of a correlation between the orientation of the initial conditions of the

axial velocity and the axial vorticity. Indeed changing the sign of $\check{\mathcal{U}}_n^{(0)}(\rho)$ has no effect on $C^{(a)}_{u_1' c}(k)^{(1)}$.

In summary, we have found an expression for the axial contribution as a sum of two terms. The first term, expression (2.104), has a $k^{-5/3}$ power law range. This is produced by the winding of the initial axial velocity field by the axisymmetric vortex core. The next-order term, expression (2.106), has a $k^{-7/3}$ power law range, and arises from the lowest order effect of the non-axisymmetric vorticity on the evolution of the axial velocity.

### 2.2.3 Result for a specific choice of initial conditions

We now evaluate (2.96), (2.104) and (2.106) for a particular choice of initial conditions. This will enable us to make a numerical comparison with experiment, theory, and simulation in a later section. We no longer need to distinguish between laboratory and vortex fixed coordinates, and so drop the prime indicating laboratory coordinates. For simplicity and consistency we will choose simple initial conditions similar to those considered for the scalar spectrum by PL. We will use a line vortex as the initial condition for the vortex core so that

$$\Omega(\rho, 0) = \frac{\Gamma}{2\pi\,\rho^2}, \qquad \Lambda(\rho, 0) = -\frac{\Gamma}{\pi\,\rho^3}, \tag{2.108}$$

where $\Gamma$ is the circulation. In general this choice for the vortex core might cause problems as $\rho \to 0$, but our choice for the non-axisymmetric part of the axial vorticity and the axial velocity will ensure that the integrals in (2.104) and (2.106) converge.

#### Contribution of the axial velocity

We first consider the contribution of the axial velocity. The initial condition for the non-axisymmetric component of the axial vorticity is chosen to be

$$\omega_3(r, \theta, 0) = 2\, f_0\, g(\rho)\, \sin(2\theta), \tag{2.109}$$

so that $f_2 = -i\, f_0\, g$ and $f_{-2} = i\, f_0\, g$ where $f_0$ is a dimensional constant. We also assume the initial condition for the axial velocity to be

$$v_3(r,\theta,0) = 2\, u_0\, g(\rho)\, \cos\theta, \tag{2.110}$$

so that $\check{\mathcal{U}}_1^{(0)} = u_0\, g$ and $\check{\mathcal{U}}_{-1}^{(0)} = u_0\, g$. Then

$$\begin{aligned} C_{u_1 c}^{(a)}(k) &= -\frac{4\pi\,\mu\,N}{9}\, k^{-5/3}\, a^{-8/3}\, \exp(-\frac{2\nu\, k^2}{3\, a})\, u_0^2\, B_1 \\ &\quad -\frac{8\pi\,\mu\,N}{9}\, k^{-7/3}\, a^{-7/3}\, \exp(-\frac{2\nu\, k^2}{a})\, f_0\, u_0^2\, B_2, \end{aligned} \tag{2.111}$$

where

$$B_1 = \int_0^\infty \rho\, g(\rho)^2\, |\Lambda(\rho)|^{2/3}\, d\rho, \tag{2.112}$$

$$B_2 = \int_0^\infty |\Lambda(\rho)|^{4/3}\, \left( \frac{g^2}{2\,\Lambda^2} \frac{d\, g}{d\, \rho} + \frac{g^2}{4}\, \frac{d}{d\,\rho}\left(\frac{g}{\Lambda^2}\right)\right) d\rho. \tag{2.113}$$

We now choose a simple form for $g(\rho)$. Letting $r_0$ be a characteristic vortex radius we set $g(\rho) = 1$ for $r_0/2 < \rho < r_0$, and zero otherwise. Note that the cutoffs in $g(\rho)$ do not create a spurious contribution at high wavenumber to the form of the cospectrum as we only use $g(\rho)$ to evaluate coefficients for the axial velocity contribution. Then $B_1$ and $B_2$ may be evaluated, taking care to deal with the derivatives at the cutoffs in $g(\rho)$,

$$B_1 = \left(\frac{\Gamma}{\pi}\right)^{2/3} \log 2, \qquad B_2 = \frac{3\pi^{2/3}}{8}\, \frac{r_0^2}{\Gamma^{2/3}}. \tag{2.114}$$

We next approximate the strain rate using $a = (\epsilon/(15\nu))^{1/2}$ and choose $f_0 = \Gamma/r_0^2$, $u_0 = \Gamma/r_0$. Then we can write

$$\begin{aligned} &\frac{C_{u_1 c}^{(a)}(k)}{\mu\, \epsilon^{-1/4}\, \nu^{7/4}} = \\ &-\frac{1}{36}\, \log 2\, \pi^{1/3}\, 15^{-1/6}\, (k\eta)^{-5/3}\, \exp(-2.58\,(k\eta)^2)\, \left(\frac{N\, r_0^2}{a}\right) \left(\frac{\Gamma}{\nu}\right)^{8/3} \left(\frac{a\, r_0^2}{4\nu}\right)^{-2} \\ &-\frac{1}{48}\, \pi^{5/3}\, 15^{-1/3}\, (k\eta)^{-7/3}\, \exp(-7.75\,(k\eta)^2)\, \left(\frac{N\, r_0^2}{a}\right)\, \left(\frac{\Gamma}{\nu}\right)^{7/3}\, \left(\frac{a\, r_0^2}{4\nu}\right)^{-2}, \end{aligned} \tag{2.115}$$

where $\eta$ is the Kolmogorov length scale. It is interesting to find the ratio of the two terms in the above expression,

$$(k\eta)^{-2/3}\,\frac{3\pi^{4/3}}{4\log 2}\,15^{-1/6}\,\left(\frac{\Gamma}{\nu}\right)^{-1/3}\,\exp(-5.17\,(k\eta)^2). \tag{2.116}$$

Thus the second term becomes less important as the vortex Reynolds number increases.

It is now necessary to estimate $N\,r_0^2/a$, $\Gamma/\nu$ and $a\,r_0^2/(4\nu)$. We assume a value of $\Gamma/\nu = 1000$ and let $r_0$ be given by the Taylor length scale. In section 2.5 we compare with the experiment of Mydlarski and Warhaft [34], and so all other parameters except $N$ are taken from the table of parameters in that paper for a Taylor Reynolds number of 582. Also in order to compare with this experiment we will need to convert our shell-summed cospectrum to a one-dimensional cospectrum. The appropriate relationship is derived in Appendix A,

$$C_{u_1c}^{1D}(k_3) = \frac{3}{4}\int_{k_3}^{\infty}\,\frac{k^2+{k_3}^2}{k^3}\,C_{u_1c}(k)\,dk. \tag{2.117}$$

We note the factor of 2 in the relationship between the one-dimensional cross spectrum and cospectrum. It is interesting to observe that if the one-dimensional cospectrum had been measured in the same direction as the velocity component used ($u_1$) (i.e., if $C_{u_1c}^{1D}(k_1)$ had been measured), then the axial velocity would give no contribution because the axial velocity does not generate small scale scalar structure in the axial direction.

To estimate $N$ we find an expression involving $N$ for the energy dissipation from the model and compare it with the experimental value. The energy dissipation for the model is given by

$$\epsilon = 3\nu a^2 + 2\nu\int_0^{\infty}\,k^2\,\left(E_0(k)+E_s(k)+E_{\omega_\theta}\right)dk. \tag{2.118}$$

The first term is the dissipation from the strain field. The remaining three terms are the dissipation associated with the vortex core, (axial) vortex spiral, and axial

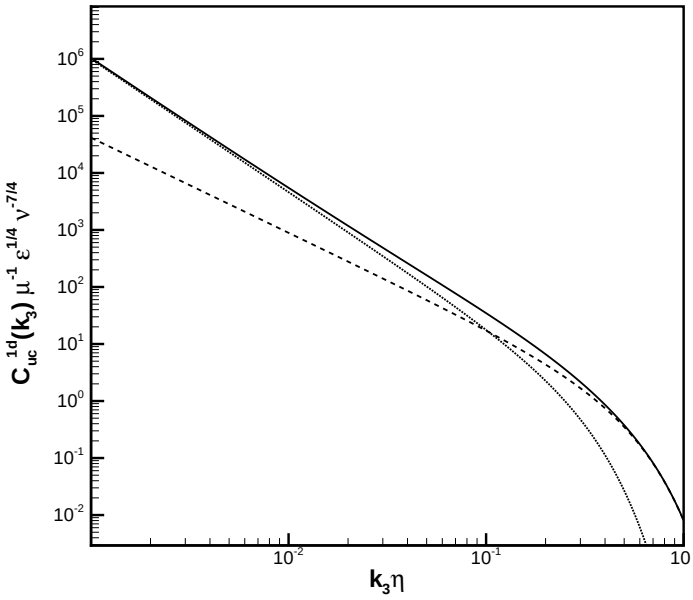


Figure 2.6: The 1D cospectrum contributed by the axial velocity from the stretched-spiral vortex model. Dashed, -5/3 component. Dotted, -7/3 component. Solid, both components.

velocity, respectively. This is equation (37) in Pullin and Saffman [41], except that we now also include the leading order dissipation from the axial velocity. An expression for $E_{\omega_\theta}$ is given by equation (66) of PL [40]. Expressions for $E_s$ and $E_0$ are given in Pullin and Saffman [41], and were evaluated for the current choice of initial conditions. The core dissipation was found to be

$$2\nu \int_0^\infty k^2\, E_0\, dk = \frac{\Gamma^2\, N}{8\,\pi} \int_{\tau_1}^{\tau_2} \frac{1 + a\tau}{\tau}\, d\tau. \tag{2.119}$$

To obtain a finite value we must choose reasonable time cutoffs $\tau_1$ and $\tau_2$, and, following Pullin *et. al.* [39] we choose $a\tau_1 = 1$ and $\tau_2 = (\Gamma/\nu)^{-2/3}\, 10\, r_0^2/(4\nu)$.

The normalized one-dimensional cospectrum contributed by the axial velocity, obtained from (2.115) and (2.117), is shown in Figure 2.6 where the $k^{-5/3}$ and the $k^{-7/3}$ terms are also shown separately for comparison.

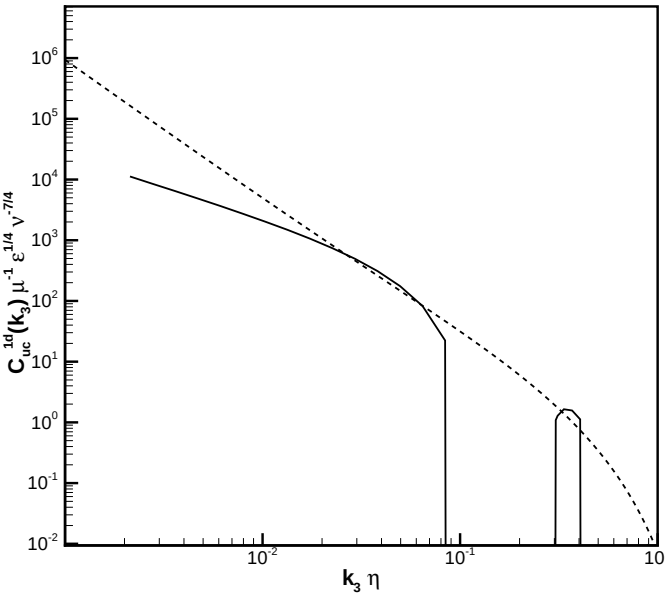


Figure 2.7: Comparison of the 1D cospectrum contributed by the axial velocity and the planar velocity from the stretched-spiral vortex model. Solid, planar contribution. Dashed, axial contribution.

### Contribution of the planar velocity

Equation (2.96) for the contribution to the cospectrum of the velocity in the plane of the vortex cannot in general be evaluated analytically or asymptotically. It was instead evaluated numerically for different choices of the initial condition for the vortex core. A combination of the monte-carlo integration routine 'Vegas' [9] and the double exponential routine of T. Ooura [35] was used. The double exponential routine was used to speed convergence of the oscillatory $I_1^c$ integral for large $\rho$. This method of numerical integration was first used to evaluate the energy spectrum and reasonable agreement with Lundgren's asymptotic result [29] was found. In the case of an initial condition for the vortex core of a line vortex (2.108) the situation is simplified because the $I_0^\omega$ integral can be performed explicitly. The resulting contribution to the one-dimensional cospectrum for this initial condition is shown on a log-log scale in Figure 2.7. compared with the axial contribution.

Note that the planar contribution is not of one sign, unlike the experimental result. This is typical of results obtained for other choices of the initial condition for

the vortex core. Also the upper cutoff in time has an effect on this contribution, and if a cutoff is not used the core winds up more and more of the gradient so that the integrals do not converge. The planar contribution for this initial condition has two distinct ranges. The first range (for low wavenumber) is a $k^{-1}$ range and is of one sign. At higher wavenumber there is an oscillatory spectrum with a $k^{-5/3}$ envelope. However, both of these ranges are specific to this choice of $\Omega$ because the integral in $I_0^\omega$ is not in general dominated by a point of stationary phase, and its form varies for different $\Omega$'s.

In section 2.5 we will compare the axial contribution to the cospectrum with results from experiment, simulation, and the SDIP.

### 2.2.4 Comments on the stretched-spiral vortex model result

Here we will give some additional comments and physical interpretation of the stretched-spiral vortex model result for the velocity-scalar cospectrum. We have shown that the velocity-scalar cospectrum result is a sum of a component from the axial velocity, and a component from the planar velocity. The solution to the advection-diffusion equation given by expression (2.54) shows that the axially-varying scalar and the axial velocity evolve in a very similar way, as they are both wound into a spiral by the axisymmetric vorticity, the main difference being caused by the effect of stretching. As the spiral turns wind closer together over time, smaller and smaller structure is created. However, for a given time and wavenumber the contribution to the cospectrum is dominated by the spiral structure at a certain radius. This dominance is expressed in the stationary phase approximation used in subsection (2.2.2). Thus, in the stretched-spiral vortex model, the eddies or small scale structure correspond to the structure of the turns of the spiral.

In contrast, the contribution to the cospectrum from the planar velocity does not have an asymptotic wavenumber dependence independent of initial conditions. The reason for this is that while the axial velocity, the scalar, and the axial vorticity are all wound into spirals of a similar form, a given component of the planar velocity has

a different kind of evolution because of the pressure term in equation (2.38). Thus, the physical mechanism of spiral winding does not apply, and a range of different wavenumber behaviors are possible depending on initial conditions.

## 2.3 Sparse direct-interaction perturbation

Here we will apply the SDIP to mixing of a passive scalar in the presence of a mean scalar gradient. In particular, we will use the SDIP to calculate the velocity-scalar cospectrum for a range of Schmidt numbers. It is worth emphasizing that we will consider a statistically isotropic velocity field, but a statistically non-isotropic scalar field. Fortunately, we will be able to use incompressibility of the velocity field and the statistical axisymmetry of the scalar field to describe the cospectrum using a single isotropic function. The resulting SDIP equations are still considerably more complicated than those derived for the scalar spectrum in the isotropic case [14].

Before going into the details of the SDIP calculation of the cospectrum, it will be useful to give a brief critical assessment of the SDIP. The SDIP is based upon three assumptions, as will be explained in subsection 2.3.3. The first two assumptions have been verified for simpler dynamical systems in Goto and Kida [13, 15]. The third assumption involves statistical independence of certain quantities, and is unlikely to be a good approximation. The SDIP equations are identical to those of the Lagrangian renormalized approximation [21], a theory that is based on the truncation of a renormalized perturbation series. Neither derivation of the SDIP equations has been rigorously justified, and the SDIP may not be a rational approximation to the exact dynamics, see also the discussion by Saffman [44]. Nonetheless, the SDIP calculation of the turbulent energy spectrum [24] shows good agreement with experiment. The SDIP calculation of the scalar spectrum [14] gives power-law scaling regimes in agreement with phenomenology, but the Obukhov-Corrsin constant is significantly different from experimental values. It is notable that the agreement achieved with the scalar and energy spectra does not require adjustable parameters.

In subsection 2.3.1 we describe the basic formulation and equations. In subsections

2.3.3 and 2.3.4 we derive an integral equation for the cospectrum using the SDIP. We solve this equation in the inertial-convective range in subsection 2.3.5, and numerically for the entire wavenumber range in subsection 2.3.6 for a range of Schmidt numbers. Lastly, we find the asymptotic solution to the SDIP equation for the cospectrum in the limit of low Schmidt number in subsection 2.3.7.

### 2.3.1 Basic formulation

The notation we will use is consistent with that of Goto and Kida [14]. A more detailed account of some of the basic equations can be found in section II of that paper, although it should be noted that they deal with a statistically isotropic scalar field without a mean gradient. We again adopt the convention for denoting integrals, where the associated infinitesimal is placed beside the integration sign, to improve the clarity of some of our expressions. We are considering passive scalar mixing by an incompressible, statistically homogeneous and isotropic velocity field, $u_i(\mathbf{x},t)$, and where the scalar is assumed to have a mean scalar gradient, $\mu$, in the 1 direction, so that we can decompose the scalar as $\mu\, x_1 + c(\mathbf{x},t)$.

The velocity field evolves according to the Navier-Stokes equations,

$$\frac{\partial}{\partial t}\, u_i(\mathbf{x},t) + u_j(\mathbf{x},t)\, \frac{\partial}{\partial x_j}\, u_i(\mathbf{x},t) = -\frac{\partial}{\partial x_i}\, \pi(\mathbf{x},t) + \nu\, \frac{\partial^2}{\partial x_j \partial x_j}\, u_i(\mathbf{x},t), \tag{2.120}$$

where $\pi(\mathbf{x},t)$ is the pressure density ratio, and the continuity condition,

$$\frac{\partial}{\partial x_i}\, u_i(\mathbf{x},t) = 0. \tag{2.121}$$

The scalar fluctuation evolves according to the advection-diffusion equation given by equation (2.25). It is convenient to make use of a Lagrangian position function, $\phi(\mathbf{x},t|\mathbf{x}',t')$, defined by

$$\phi(\mathbf{x},t|\mathbf{x}',t') = \delta^3(\mathbf{x} - \mathbf{y}(t|\mathbf{x}',t')), \tag{2.122}$$

where a fluid element that is located at $\mathbf{x}'$ at time $t'$, is located at $\mathbf{y}(t|\mathbf{x}', t')$ at time $t \geq t'$. The Lagrangian position function evolves according to

$$\frac{\partial}{\partial t}\,\phi(\mathbf{x}, t|\mathbf{x}', t') + u_j(\mathbf{x}, t)\,\frac{\partial}{\partial x_j}\,\phi(\mathbf{x}, t|\mathbf{x}', t') = 0 \tag{2.123}$$

with initial condition

$$\phi(\mathbf{x}, t|\mathbf{x}', t) = \delta^3(\mathbf{x} - \mathbf{x}'). \tag{2.124}$$

We can then define Lagrangian velocity and scalar fields as

$$u_i^L(t|\mathbf{x}, t') = \int d^3\mathbf{x}'\, u_i(\mathbf{x}', t)\,\phi(\mathbf{x}', t|\mathbf{x}, t'), \tag{2.125}$$

and

$$c^{(L)}(t|\mathbf{x}, t') = \int d^3\mathbf{x}'\, c(\mathbf{x}', t)\,\phi(\mathbf{x}', t|\mathbf{x}, t'). \tag{2.126}$$

The velocity and scalar Lagrangian auto-correlation functions are

$$V_{ij}(\mathbf{r}, t, t') = \overline{u_i^L(t|\mathbf{x} + \mathbf{r}, t')\,u_j(\mathbf{x}, t')}, \tag{2.127}$$

and

$$Z(\mathbf{r}, t, t') = \overline{c^{(L)}(t|\mathbf{x} + \mathbf{r}, t')\,c(\mathbf{x}, t')}. \tag{2.128}$$

We wish to calculate the velocity-scalar cospectrum, and so define Lagrangian cross-correlation functions,

$$W_i(\mathbf{r}, t, t') = \overline{c^{(L)}(t|\mathbf{x} + \mathbf{r}, t')\,u_i(\mathbf{x}, t')}, \tag{2.129}$$

and

$$Y_i(\mathbf{r}, t, t') = \overline{u_i^L(t|\mathbf{x} + \mathbf{r}, t')\,c(\mathbf{x}, t')}. \tag{2.130}$$

Having defined the basic statistical quantities in physical space, we now move to Fourier space. The SDIP is formulated by first assuming that the flow is in a periodic box of side $L$. The velocity field $u_i(\mathbf{x}, t)$ can then be decomposed as in equation (2.8),

and the inverse Fourier transform is given by (2.9). Similar transforms are defined for the other variables. The limit $L \to \infty$ will be taken at a later stage.

We will now write the governing equations in Fourier space. The incompressibility of the velocity field implies that $k_i\,\tilde{u}_i(\mathbf{k},t) = 0$. The Navier-Stokes equations (2.120) become

$$\left[\frac{\partial}{\partial t} + \nu\,k^2\right]\tilde{u}_i(\mathbf{k},t) = -\frac{i}{2}\left(\frac{2\pi}{L}\right)^3 \tilde{P}_{ijm}(\mathbf{k}) \sum_{\substack{\mathbf{p}\\(\mathbf{k}+\mathbf{p}+\mathbf{q}=0)}} \sum_{\mathbf{q}} \tilde{u}_j(-\mathbf{p},t)\,\tilde{u}_m(-\mathbf{q},t), \quad (2.131)$$

where $\tilde{P}_{ijm}(\mathbf{k}) = k_m\,\tilde{P}_{ij}(\mathbf{k}) + k_j\,\tilde{P}_{im}(\mathbf{k})$, and the incompressible projection operator is given by $\tilde{P}_{ij}(\mathbf{k}) = \delta_{ij} - k_i k_j/k^2$. The scalar advection-diffusion equation (2.25) becomes equation (2.26) in Fourier space, but here we will use the equivalent symmetric form,

$$\left[\frac{\partial}{\partial t} + D\,k^2\right]\tilde{c}(\mathbf{k},t) = -\mu\,\tilde{u}_1(\mathbf{k},t) - i\,k_j\left(\frac{2\pi}{L}\right)^3 \sum_{\substack{\mathbf{p}\\(\mathbf{k}+\mathbf{p}+\mathbf{q}=0)}} \sum_{\mathbf{q}} \tilde{u}_j(-\mathbf{p},t)\,\tilde{c}(-\mathbf{q},t). \quad (2.132)$$

The evolution equation for the Lagrangian position function (2.123) becomes

$$\frac{\partial}{\partial t}\tilde{\phi}(\mathbf{k},t|\mathbf{k}',t') = -i\,k_j\left(\frac{2\pi}{L}\right)^3 \sum_{\substack{\mathbf{p}\\(\mathbf{k}+\mathbf{p}+\mathbf{q}=0)}} \sum_{\mathbf{q}} \tilde{u}_j(-\mathbf{p},t)\,\tilde{\phi}(-\mathbf{q},t|\mathbf{k}',t') \quad (2.133)$$

with initial condition

$$\tilde{\phi}(\mathbf{k},t|\mathbf{k}',t') = \frac{L^3}{(2\pi)^6}\,\delta^3_{\mathbf{k}+\mathbf{k}'}, \quad (2.134)$$

where $\delta^3_{\mathbf{k}+\mathbf{k}'} = 1$ if $\mathbf{k} = -\mathbf{k}'$, and $\delta^3_{\mathbf{k}+\mathbf{k}'} = 0$ otherwise. The Fourier transforms of the

Lagrangian velocity and scalar fields evolve according to

$$\begin{aligned}\frac{\partial}{\partial t}\tilde{v}_i(t|\mathbf{k},t') &= -\frac{(2\pi)^6}{L^3}\,\nu\sum_{\mathbf{p}} p^2\,\tilde{u}_i(\mathbf{p},t)\,\tilde{\phi}(-\mathbf{p},t|\mathbf{k},t') \\ &- i\,\frac{(2\pi)^9}{L^6}\sum_{\substack{\mathbf{p}\\(\mathbf{p}+\mathbf{q}+\mathbf{r}=0)}}\sum_{\mathbf{q}}\sum_{\mathbf{r}}\frac{r_i\,r_m\,r_n}{r^2}\,\tilde{u}_m(\mathbf{p},t)\,\tilde{u}_n(\mathbf{q},t)\,\tilde{\phi}(\mathbf{r},t|\mathbf{k},t'),\end{aligned} \tag{2.135}$$

and

$$\frac{\partial}{\partial t}\tilde{c}^{(L)}(t|\mathbf{k},t') = -\mu\,\tilde{v}_1(t|\mathbf{k},t') - \frac{(2\pi)^6}{L^3}\,D\sum_{\mathbf{p}} p^2\,\tilde{c}(\mathbf{p},t)\,\tilde{\phi}(-\mathbf{p},t|\mathbf{k},t'). \tag{2.136}$$

This may be seen by taking a time derivative of the Fourier space counterparts of (2.125) and (2.126),

$$\tilde{v}_i(t|\mathbf{k},t') = \frac{(2\pi)^6}{L^3}\sum_{\mathbf{k}'}\tilde{u}(\mathbf{k}',t)\,\tilde{\phi}(-\mathbf{k}',t|\mathbf{k},t'), \tag{2.137}$$

and

$$\tilde{c}^{(L)}(t|\mathbf{k},t') = \frac{(2\pi)^6}{L^3}\sum_{\mathbf{k}'}\tilde{c}(\mathbf{k}',t)\,\tilde{\phi}(-\mathbf{k}',t|\mathbf{k},t'). \tag{2.138}$$

The diffusive term in (2.136) is written incorrectly in the paper by Goto and Kida[14], although this makes no difference after the SDIP approximations are made.

Turning now to the two-point statistics, we find

$$\tilde{V}_{ij}(\mathbf{k},t,t') = \left(\frac{2\pi}{L}\right)^3\overline{\tilde{v}_i(t|\mathbf{k},t')\,\tilde{u}_j(-\mathbf{k},t')}, \tag{2.139}$$

$$\tilde{Z}(\mathbf{k},t,t') = \left(\frac{2\pi}{L}\right)^3\overline{\tilde{c}^{(L)}(t|\mathbf{k},t')\,\tilde{c}(-\mathbf{k},t')}, \tag{2.140}$$

$$\tilde{W}_i(\mathbf{k},t,t') = \left(\frac{2\pi}{L}\right)^3\overline{\tilde{c}^{(L)}(t|\mathbf{k},t')\,\tilde{u}_i(-\mathbf{k},t')}, \tag{2.141}$$

$$\tilde{Y}_i(\mathbf{k},t,t') = \left(\frac{2\pi}{L}\right)^3\overline{\tilde{v}_i(t|\mathbf{k},t')\,\tilde{c}(-\mathbf{k},t')}. \tag{2.142}$$

We will later need evolution equations for $\tilde{W}_i(\mathbf{k},t,t')$ and $\tilde{Y}_i(\mathbf{k},t,t')$ when calculating the cospectrum. For one-time correlations we have that

$$\begin{aligned}\left[\frac{\partial}{\partial t}+(\nu+D)\,k^2\right]\tilde{W}_i(\mathbf{k},t,t) &= -\mu\,\tilde{V}_{1i}(\mathbf{k},t,t)\\ &\quad - i\,k_j\left(\frac{2\pi}{L}\right)^6 \sum_{\substack{\mathbf{p}\\(\mathbf{k}+\mathbf{p}+\mathbf{q}=0)}}\sum_{\mathbf{q}} \overline{\tilde{u}_j(-\mathbf{p},t)\,\tilde{c}(-\mathbf{q},t)\,\tilde{u}_i(-\mathbf{k},t)}\\ &\quad + \frac{i}{2}\left(\frac{2\pi}{L}\right)^6 \tilde{P}_{ijm}(\mathbf{k}) \sum_{\substack{\mathbf{p}\\(-\mathbf{k}+\mathbf{p}+\mathbf{q}=0)}}\sum_{\mathbf{q}} \overline{\tilde{u}_j(-\mathbf{p},t)\,\tilde{u}_m(-\mathbf{q},t)\,\tilde{c}(\mathbf{k},t)},\end{aligned} \tag{2.143}$$

and $\tilde{Y}_i(\mathbf{k},t,t)=\tilde{W}_i(-\mathbf{k},t,t)$. For two-time correlations we have that

$$\frac{\partial}{\partial t}\tilde{W}_i(\mathbf{k},t,t') = -\mu\,\tilde{V}_{1i}(\mathbf{k},t,t') - D\,\frac{(2\pi)^9}{L^6}\sum_{\mathbf{p}} p^2\,\overline{\tilde{c}(\mathbf{p},t)\,\tilde{\phi}(-\mathbf{p},t|\mathbf{k},t')\,\tilde{u}_i(-\mathbf{k},t')}, \tag{2.144}$$

$$\begin{aligned}\frac{\partial}{\partial t}\tilde{Y}_i(\mathbf{k},t,t') &= -i\,\frac{(2\pi)^{12}}{L^9}\sum_{\substack{\mathbf{p}\\(\mathbf{p}+\mathbf{q}+\mathbf{r}=0)}}\sum_{\mathbf{q}}\sum_{\mathbf{r}} \frac{r_i\,r_m\,r_n}{r^2}\,\overline{\tilde{u}_m(\mathbf{p},t)\,\tilde{u}_n(\mathbf{q},t)\,\tilde{\phi}(\mathbf{r},t|\mathbf{k},t')\,\tilde{c}(-\mathbf{k},t')}\\ &\quad - \nu\,\frac{(2\pi)^9}{L^6}\sum_{\mathbf{p}} p^2\,\overline{\tilde{u}_i(\mathbf{p},t)\,\tilde{\phi}(-\mathbf{p},t|\mathbf{k},t')\,\tilde{c}(-\mathbf{k},t')}.\end{aligned} \tag{2.145}$$

It will be necessary to make use of linear response functions in the SDIP calculation. The Eulerian and Lagrangian scalar response functions are defined as

$$\tilde{G}^{(E)}(\mathbf{k},t|\mathbf{k}',t') = \frac{\delta\,\tilde{c}(\mathbf{k},t)}{\delta\,\tilde{c}(\mathbf{k}',t')}, \tag{2.146}$$

$$\tilde{G}^{(L)}(t|\mathbf{k},\mathbf{k}',t') = \frac{\delta\,\tilde{c}^{(L)}(t|\mathbf{k},t')}{\delta\,\tilde{c}(\mathbf{k}',t')}, \tag{2.147}$$

with evolution equations

$$\left[\frac{\partial}{\partial t} + D\,k^2\right] \tilde{G}^{(E)}(\mathbf{k},t|\mathbf{k}',t') = -i\,k_j \left(\frac{2\pi}{L}\right)^3 \sum_{\substack{\mathbf{p} \\ (\mathbf{k}+\mathbf{p}+\mathbf{q}=0)}} \sum_{\mathbf{q}} \tilde{u}_j(-\mathbf{p},t)\,\tilde{G}^{(E)}(-\mathbf{q},t|\mathbf{k}',t'), \tag{2.148}$$

$$\frac{\partial}{\partial t}\tilde{G}^{(L)}(t|\mathbf{k},\mathbf{k}',t') = -D\,\frac{(2\pi)^6}{L^3} \sum_{\mathbf{p}} p^2\,\tilde{G}^{(E)}(\mathbf{p},t|\mathbf{k}',t')\,\tilde{\phi}(-\mathbf{p},t|\mathbf{k},t'), \tag{2.149}$$

and initial conditions

$$\tilde{G}^{(E)}(\mathbf{k},t'|\mathbf{k}',t') = \tilde{G}^{(L)}(t'|\mathbf{k},\mathbf{k}',t') = \frac{L^3}{(2\pi)^6}\,\delta^3_{\mathbf{k}+\mathbf{k}'}. \tag{2.150}$$

Here $\delta$ is a functional derivative, and our notation is consistent so that, for example, $\delta\,\tilde{c}(\mathbf{k},t)/\delta\,\tilde{c}(\mathbf{k}',t')$ is a Fourier transform with respect to $\mathbf{x}$, followed by a a Fourier transform with respect to $\mathbf{x}'$ of $\delta\,c(\mathbf{x},t)/\delta\,c(\mathbf{x}',t')$. Similarly, we define Eulerian and Lagrangian velocity response functions as

$$\tilde{G}^{(E)}_{ij}(\mathbf{k},t|\mathbf{k}',t') = \frac{\delta\,\tilde{u}_i(\mathbf{k},t)}{\delta\,\tilde{u}_j(\mathbf{k}',t')}, \tag{2.151}$$

$$\tilde{G}^{(L)}_{ij}(t|\mathbf{k},\mathbf{k}',t') = \frac{\delta\,\tilde{v}_i(t|\mathbf{k},t')}{\delta\,\tilde{u}_j(\mathbf{k}',t')}, \tag{2.152}$$

with initial conditions

$$\tilde{G}^{(E)}_{ij}(\mathbf{k},t'|\mathbf{k}',t') = \tilde{G}^{(L)}_{ij}(t'|\mathbf{k},\mathbf{k}',t') = \frac{L^3}{(2\pi)^6}\,\delta_{ij}\,\delta^3_{\mathbf{k}+\mathbf{k}'}. \tag{2.153}$$

Details of the evolution equations for $\tilde{G}^{(E)}_{ij}(\mathbf{k},t|\mathbf{k}',t')$ and $\tilde{G}^{(L)}_{ij}(t|\mathbf{k},\mathbf{k}',t')$ may be found in Kida and Goto[24].

It is often more convenient to work with incompressible projections of $\tilde{V}_{ij}(\mathbf{k},t,t')$, $\tilde{G}^{(L)}_{ij}(t|\mathbf{k},\mathbf{k}',t')$, and $\tilde{Y}_i(\mathbf{k},t,t')$, and so we define

$$\tilde{Q}_{ij}(\mathbf{k},t,t') = \tilde{P}_{im}(\mathbf{k})\,\tilde{V}_{mj}(\mathbf{k},t,t'), \tag{2.154}$$

$$\tilde{G}_{ij}(\mathbf{k},t,t') = \frac{(2\pi)^6}{L^3}\,\overline{\tilde{G}^{(L)}_{im}(t|\mathbf{k},-\mathbf{k},t')}\,\tilde{P}_{mj}(\mathbf{k}), \tag{2.155}$$

$$\tilde{X}_i(\mathbf{k},t,t') = \tilde{P}_{im}(\mathbf{k})\,\tilde{Y}_m(\mathbf{k},t,t'). \tag{2.156}$$

Finally, after taking the limit $L \to \infty$ we can relate $\tilde{V}_{ij}(\mathbf{k},t,t)$ to the shell-summed energy spectrum, $E(k)$, $\tilde{Z}(\mathbf{k},t,t)$ to the shell-summed scalar spectrum, $E_c(k)$, and $\tilde{W}_i(\mathbf{k},t,t)$ to the shell-summed velocity-scalar cospectrum, $C_{u_1c}(k)$, see equations (2.16), (2.17), and (2.18), respectively. The shell-summed cospectrum can also be related to $\tilde{Y}$ by noting that $\tilde{W}_1(\mathbf{k},t,t) = \tilde{Y}_1(\mathbf{k},t,t)$.

### 2.3.2 DIA decompositions

We will now use the SDIP to calculate the velocity-scalar cospectrum. It will be convenient from now on in this section to generalize to the case of an arbitrary mean scalar gradient $\mu_i$. The basis of the approximation is the decomposition of the field variables into the sum of non-direct-interaction (NDI) fields, denoted by the superscript (0), and the deviation fields, denoted with the superscript (1). For example, we decompose the scalar field as

$$\tilde{c}(\mathbf{k},t) = \tilde{c}^{(0)}(\mathbf{k},t\|\mathbf{k}_0,\mathbf{p}_0,\mathbf{q}_0) + \tilde{c}^{(1)}(\mathbf{k},t\|\mathbf{k}_0,\mathbf{p}_0,\mathbf{q}_0), \tag{2.157}$$

where $\mathbf{k}_0$, $\mathbf{p}_0$, and $\mathbf{q}_0$ are a triad of wavevectors such that $\mathbf{k}_0 + \mathbf{p}_0 + \mathbf{q}_0 = 0$. The initial conditions for this decomposition are given at time $t_0$ as

$$\tilde{c}^{(0)}(\mathbf{k},t_0\|\mathbf{k}_0,\mathbf{p}_0,\mathbf{q}_0) = \tilde{c}(\mathbf{k},t_0), \qquad \tilde{c}^{(1)}(\mathbf{k},t_0\|\mathbf{k}_0,\mathbf{p}_0,\mathbf{q}_0) = 0. \tag{2.158}$$

The evolution of $\tilde{c}^{(0)}$ is governed by

$$\begin{aligned}\left[\frac{\partial}{\partial t} + D\,k^2\right]\tilde{c}^{(0)}(\mathbf{k},t\|\mathbf{k}_0,\mathbf{p}_0,\mathbf{q}_0) &= -\mu_j\,\tilde{u}_j(\mathbf{k},t) \\ &\quad - i\,k_j\left(\frac{2\pi}{L}\right)^3 \sum_{\substack{\mathbf{p}\\(\mathbf{k}+\mathbf{p}+\mathbf{q}=0)}} \sum_{\mathbf{q}}{}' \tilde{u}_j(-\mathbf{p},t)\,\tilde{c}^{(0)}(-\mathbf{q},t\|\mathbf{k}_0,\mathbf{p}_0,\mathbf{q}_0),\end{aligned} \tag{2.159}$$

where $\sum\sum'$ denotes a summation that excludes interactions between the triad $\mathbf{k}_0$, $\mathbf{p}_0$, and $\mathbf{q}_0$. Subtracting (2.159) from (2.132) we find

$$\begin{aligned}
\left[\frac{\partial}{\partial t} + D\,k^2\right]\tilde{c}^{(1)}(\mathbf{k},t\|\mathbf{k}_0,\mathbf{p}_0,\mathbf{q}_0) = \\
&- i\,k_j\left(\frac{2\pi}{L}\right)^3 \sum_{\substack{\mathbf{p}\\(\mathbf{k}+\mathbf{p}+\mathbf{q}=0)}} \sum_{\mathbf{q}}{}' \;\tilde{u}_j(-\mathbf{p},t)\,\tilde{c}^{(1)}(-\mathbf{q},t\|\mathbf{k}_0,\mathbf{p}_0,\mathbf{q}_0) \\
&- i\,\delta^3_{\mathbf{k}-\mathbf{k}_0}\,k_{0j}\,\tilde{u}_j(-\mathbf{p}_0,t)\,\tilde{c}^{(0)}(-\mathbf{q}_0,t\|\mathbf{k}_0,\mathbf{p}_0,\mathbf{q}_0) \\
&- i\,\delta^3_{\mathbf{k}-\mathbf{k}_0}\,k_{0j}\,\tilde{u}_j(-\mathbf{q}_0,t)\,\tilde{c}^{(0)}(-\mathbf{p}_0,t\|\mathbf{k}_0,\mathbf{p}_0,\mathbf{q}_0) \\
&+ i\,\delta^3_{\mathbf{k}+\mathbf{k}_0}\,k_{0j}\,\tilde{u}_j(\mathbf{p}_0,t)\,\tilde{c}^{(0)}(\mathbf{q}_0,t\|\mathbf{k}_0,\mathbf{p}_0,\mathbf{q}_0) \\
&+ i\,\delta^3_{\mathbf{k}+\mathbf{k}_0}\,k_{0j}\,\tilde{u}_j(\mathbf{q}_0,t)\,\tilde{c}^{(0)}(\mathbf{p}_0,t\|\mathbf{k}_0,\mathbf{p}_0,\mathbf{q}_0) \\
&+ (\mathbf{k}_0 \to \mathbf{p}_0 \to \mathbf{q}_0 \to \mathbf{k}_0).
\end{aligned} \tag{2.160}$$

Similar decompositions are made for the Eulerian velocity field, $\tilde{u}(\mathbf{k},t)$, the position function, $\tilde{\phi}(\mathbf{k},t|\mathbf{k}',t')$, the Eulerian velocity response function $\tilde{G}^{(E)}_{ij}(\mathbf{k},t|\mathbf{k}',t')$, and the Lagrangian velocity response function $\tilde{G}^{(L)}_{ij}(t|\mathbf{k},\mathbf{k}',t')$, see Kida and Goto [24]. We also decompose the Eulerian scalar response function, $\tilde{G}^{(E)}(\mathbf{k},t|\mathbf{k}',t')$, see Goto and Kida [14]. The deviation fields can then be expressed in terms of the NDI fields and the response functions. For example, the scalar deviation field is given by

$$\begin{aligned}
\tilde{c}^{(1)}(\mathbf{k},t\|\mathbf{k}_0,\mathbf{p}_0,\mathbf{q}_0) &= -i\,k_j\,\frac{(2\pi)^9}{L^6}\int_{t_0}^{t} dt'\,\tilde{G}^{E(0)}(\mathbf{k},t|-\mathbf{k},t'\|\mathbf{k}_0,\mathbf{p}_0,\mathbf{q}_0) \\
&\times\ [\,\delta^3_{\mathbf{k}-\mathbf{k}_0}\,\tilde{u}_j(-\mathbf{p}_0,t')\,\tilde{c}^{(0)}(-\mathbf{q}_0,t'\|\mathbf{k}_0,\mathbf{p}_0,\mathbf{q}_0) \\
&+\ \delta^3_{\mathbf{k}-\mathbf{k}_0}\,\tilde{u}_j(-\mathbf{q}_0,t')\,\tilde{c}^{(0)}(-\mathbf{p}_0,t'\|\mathbf{k}_0,\mathbf{p}_0,\mathbf{q}_0) \\
&+\ \delta^3_{\mathbf{k}+\mathbf{k}_0}\,\tilde{u}_j(\mathbf{p}_0,t')\,\tilde{c}^{(0)}(\mathbf{q}_0,t'\|\mathbf{k}_0,\mathbf{p}_0,\mathbf{q}_0) \\
&+\ \delta^3_{\mathbf{k}+\mathbf{k}_0}\,\tilde{u}_j(\mathbf{q}_0,t')\,\tilde{c}^{(0)}(\mathbf{p}_0,t'\|\mathbf{k}_0,\mathbf{p}_0,\mathbf{q}_0) \\
&+\ (\mathbf{k}_0 \to \mathbf{p}_0 \to \mathbf{q}_0 \to \mathbf{k}_0)\,]\,.
\end{aligned} \tag{2.161}$$

### 2.3.3 Derivation of closed evolution equations

The main purpose of the SDIP is to express third-order correlations in terms of second-order correlations so that closed evolution equations for second order quantities can be derived. There are three main assumptions in the SDIP procedure:

i The magnitude of the deviation field is smaller than that of the NDI field for times $(t - t_0)$ within the correlation timescale of the velocity field.

ii Any two Fourier modes of the NDI fields without direct interaction are statistically independent of each other. For example, $\tilde{c}^{(0)}(\mathbf{k}_0, t \| \mathbf{k}_0, \mathbf{p}_0, \mathbf{q}_0)$, $\tilde{c}^{(0)}(\mathbf{p}_0, t' \| \mathbf{k}_0, \mathbf{p}_0, \mathbf{q}_0)$, and $\tilde{u}_k^{(0)}(\mathbf{q}_0, t'' \| \mathbf{k}_0, \mathbf{p}_0, \mathbf{q}_0)$ are statistically independent.

iii The NDI position function field, $\tilde{\phi}^0$, is statistically independent of the other Eulerian quantities, such as $\tilde{u}_i^{(0)}$ and $\tilde{c}^{(0)}$.

Additional statistical assumptions were needed in Kida and Goto [24] involving the position response function, but this function is not used here. Assumptions (i) and (ii) were tested for a model system in Goto and Kida [13, 15], but assumption (iii) is difficult to justify.

SDIP approximations to (2.143) and (2.144) are derived in Appendix C using the DIA decompositions and the above three assumptions. The results are

$$\left[\frac{\partial}{\partial t} + (\nu + D)\, k^2\right] \tilde{W}_i(\mathbf{k}, t, t) = \left(\frac{2\pi}{L}\right)^3 \sum_{\substack{\mathbf{p} \\ (\mathbf{k}+\mathbf{p}+\mathbf{q}=0)}} \sum_{\mathbf{q}} \int_{t_0}^{t} dt'\, \Theta_1(\mathbf{k}, \mathbf{p}, \mathbf{q}, t, t') - \mu_j\, \tilde{V}_{ji}(\mathbf{k}, t, t), \tag{2.162}$$

where

$$
\begin{aligned}
&\Theta_1(\mathbf{k},\mathbf{p},\mathbf{q},t,t') = \\
&k_j \Big( \tilde{Q}_{ib}(-\mathbf{k},t,t')\,\tilde{W}_c(-\mathbf{q},t,t')\,\Big[p_c\,\tilde{G}_{jb}(-\mathbf{p},t,t') + p_b\,\tilde{G}_{jc}(-\mathbf{p},t,t')\Big] \\
&+ (i \leftrightarrow j, \mathbf{k} \leftrightarrow \mathbf{p})\Big) \\
&+ k_j\,q_l\,\exp[-D\,q^2\,(t-t')]\Big[\tilde{Q}_{jl}(-\mathbf{p},t,t')\,\tilde{X}_i(-\mathbf{k},t,t') + \tilde{Q}_{il}(-\mathbf{k},t,t')\,\tilde{X}_j(-\mathbf{p},t,t')\Big] \\
&+ \frac{1}{2}\,\tilde{P}_{ijm}(\mathbf{k})\,\Big(\tilde{Q}_{mc}(\mathbf{q},t,t')\,\tilde{W}_b(\mathbf{k},t,t')\Big[p_c\,\tilde{G}_{jb}(\mathbf{p},t,t') + p_b\,\tilde{G}_{jc}(\mathbf{p},t,t')\Big] \\
&+ (j \leftrightarrow m, \mathbf{p} \leftrightarrow \mathbf{q})\Big) \\
&+ \frac{1}{2}\,k_l\,\tilde{P}_{ijm}(\mathbf{k})\,\exp[-D\,q^2\,(t-t')]\Big[\tilde{Q}_{jl}(\mathbf{p},t,t')\,\tilde{X}_m(\mathbf{q},t,t') + \tilde{Q}_{ml}(\mathbf{q},t,t')\,\tilde{X}_j(\mathbf{p},t,t')\Big],
\end{aligned}
\tag{2.163}
$$

and

$$
\left[\frac{\partial}{\partial t} + D\,k^2\right]\tilde{W}_i(\mathbf{k},t,t') = -\mu_j\,\tilde{V}_{ji}(\mathbf{k},t,t'). \tag{2.164}
$$

It is easier to work with $\tilde{X}_i(\mathbf{k},t,t')$ rather than $\tilde{Y}_i(\mathbf{k},t,t')$, and so the SDIP approximation to the incompressible projection of equation (2.145) is derived in Appendix D,

$$
\begin{aligned}
&\left[\frac{\partial}{\partial t} + \nu\,k^2\right]\tilde{X}_i(\mathbf{k},t,t') \\
&= -2\,\left(\frac{2\pi}{L}\right)^3 \sum_{\substack{\mathbf{p} \\ (\mathbf{k}+\mathbf{p}+\mathbf{q}=0)}} \sum_{\mathbf{q}} \tilde{P}_{il}(\mathbf{k})\,\frac{q_l\,q_m\,q_n\,q_j}{q^2}\,\tilde{X}_n(\mathbf{k},t,t')\int_{t'}^{t} dt''\,\tilde{Q}_{mj}(\mathbf{p},t,t'').
\end{aligned}
\tag{2.165}
$$

Taking the $L \to \infty$ limit, the system of integro-differential equations to be solved can be summarized as

$$
\begin{aligned}
\left[\frac{\partial}{\partial t} + (\nu + D)\,k^2\right]\tilde{W}_i(\mathbf{k},t,t) &= \int d\mathbf{p} \int d\mathbf{q}\;\delta^3_{\mathbf{k}+\mathbf{p}+\mathbf{q}} \int_{t_0}^{t} dt'\,\Theta_1(\mathbf{k},\mathbf{p},\mathbf{q},t,t') \\
&- \mu_j\,\tilde{V}_{ji}(\mathbf{k},t,t),
\end{aligned}
\tag{2.166}
$$

$$\left[\frac{\partial}{\partial t}+\nu\,k^2\right]\tilde{X}_i(\mathbf{k},t,t') \\ =-2\,\tilde{P}_{il}(\mathbf{k})\int d\mathbf{p}\int d\mathbf{q}\;\delta^3_{\mathbf{k}+\mathbf{p}+\mathbf{q}}\,\frac{q_l\,q_m\,q_n\,q_j}{q^2}\,\tilde{X}_n(\mathbf{k},t,t')\int_{t'}^{t}dt''\,\tilde{Q}_{mj}(\mathbf{p},t,t''), \tag{2.167}$$

together with equation (2.164) for $\tilde{W}_i(\mathbf{k},t,t')$, and the initial condition

$$\tilde{X}_i(\mathbf{k},t,t)=\tilde{W}_i(-\mathbf{k},t,t). \tag{2.168}$$

This is a closed system of equations for $\tilde{W}_i(\mathbf{k},t,t')$ and $\tilde{X}_i(\mathbf{k},t,t')$ once the velocity field statistics $\tilde{V}_{ij}(\mathbf{k},t,t')$, $\tilde{Q}_{ij}(\mathbf{k},t,t')$, and $\tilde{G}_{ij}(\mathbf{k},t,t')$ are specified.

### 2.3.4 Spatial symmetries and stationarity

We now use the spatial symmetries and stationarity of the problem to simplify our equations. The velocity field is isotropic and stationary, and so we can write

$$\tilde{Q}_{ij}(\mathbf{k},t,t')=\frac{1}{2}\,\tilde{P}_{ij}(\mathbf{k})\,Q^{\dagger}(k,t-t'), \tag{2.169}$$

$$\tilde{G}_{ij}(\mathbf{k},t,t')=\tilde{P}_{ij}(\mathbf{k})\,G^{\dagger}(k,t-t'). \tag{2.170}$$

Note that although $\tilde{G}_{ij}(\mathbf{k},t,t')$ does not satisfy $k_i\,\tilde{G}_{ij}(\mathbf{k},t,t')=0$ in the general case, the incompressible property $k_j\,\tilde{G}_{ij}(\mathbf{k},t,t')=0$ is sufficient to give the form (2.170) in the isotropic case. Similarly, the condition $k_j\,\tilde{V}_{ij}(\mathbf{k},t,t')=0$ together with isotropy is sufficient to ensure that

$$\tilde{V}_{ij}(\mathbf{k},t,t')=\frac{1}{2}\,\tilde{P}_{ij}(\mathbf{k})V^{\dagger}(k,t-t'). \tag{2.171}$$

The definition of $\tilde{Q}_{ij}(\mathbf{k},t,t')$ (2.154) then implies that $V^{\dagger}(k,t)=Q^{\dagger}(k,t)$. We turn now to statistical quantities involving the scalar. Axisymmetry and the condition $k_i\,\tilde{W}_i(\mathbf{k},t,t')=0$ imply that

$$\tilde{W}_i(\mathbf{k},t,t')=f(k,t,t',\mu,k_j\mu_j)\,\left(\mu_i-k_i\,\frac{k_s\,\mu_s}{k^2}\right). \tag{2.172}$$

The scalar, and therefore $\tilde{W}_i(\mathbf{k},t,t')$, depend linearly on the mean scalar gradient $\mu_i$ after initial fluctuations decay, and so we can write

$$\tilde{W}_i(\mathbf{k},t,t') = \tilde{P}_{ij}(\mathbf{k})\,\mu_j\,W^\dagger(k,t-t'). \tag{2.173}$$

Using a similar argument for the form of $\tilde{X}_i(\mathbf{k},t,t')$, we find

$$\tilde{X}_i(\mathbf{k},t,t') = \tilde{P}_{ij}(\mathbf{k})\,\mu_j\,X^\dagger(k,t-t'). \tag{2.174}$$

Substituting (2.171) and (2.173) into (2.164) leads to

$$\left[\frac{\partial}{\partial t} + D\,k^2\right] W^\dagger(k,t) = -\frac{1}{2}\,Q^\dagger(k,t), \tag{2.175}$$

and this may be solved to give

$$W^\dagger(k,t) = \left(-\frac{1}{2}\int_0^t Q^\dagger(k,t')\,\exp[D\,k^2\,t']\,dt' + W^\dagger(k,0)\right)\exp[-D\,k^2\,t]. \tag{2.176}$$

Making a comparison between the evolution equation for $\tilde{Q}_{ij}(\mathbf{k},t,t')$ in Kida and Goto [24], and the evolution equation (2.165) for $\tilde{X}_i(\mathbf{k},t,t')$ here, it is easy to show that $X^\dagger(k,t)$ and $Q^\dagger(k,t)$ have the same evolution equation. This can be written as

$$\left[\frac{\partial}{\partial t} + \nu\,k^2 + \hat{\eta}(k,t)\right] X^\dagger(k,t) = 0, \tag{2.177}$$

where

$$\hat{\eta}(k,t) = \frac{4\pi}{3}\,k^5\int_0^\infty dp\;p^{10/3}\,s_2(p^{2/3})\int_0^t dt'\,Q^\dagger(k\,p,t'), \tag{2.178}$$

and

$$s_2(p) = \frac{3}{32\,p^5}\left(\frac{(1-p^3)^4}{2p^{3/2}}\log\left[\frac{1+p^{3/2}}{|1-p^{3/2}|}\right] - \frac{1+p^3}{3}\,(3p^6-14p^3+3)\right). \tag{2.179}$$

Therefore

$$X^\dagger(k,t) = \frac{Q^\dagger(k,t)}{Q^\dagger(k,0)}\,W^\dagger(k,0), \tag{2.180}$$

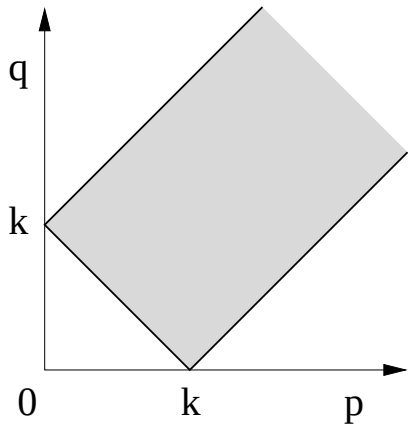


Figure 2.8: Integration region used in the SDIP integrals, denoted by $\triangle_k$.

where we have used (2.168). Finally, we substitute into the integro-differential equation (2.166) for $\tilde{W}_i(\mathbf{k}, t, t)$. Taking into account (2.176) and (2.180), and after considerable algebra, we find

$$2\,k^2\,(\nu + D)\,W^\dagger(k,0) + Q^\dagger(k,0) = \frac{1}{2}\int\int_{\triangle_k} dp\,dq\,\frac{\pi\,p\,q}{k}\,\frac{s_1(k,p,q)}{q^2}\,\int_0^\infty dt\,\Theta_2(k,p,q,t), \tag{2.181}$$

where

$$\begin{aligned}
\Theta_2(k,p,q,t) &= (k^2-q^2)(k^2-p^2+q^2)\,Q^\dagger(k,t)\,W^\dagger(q,t)\,Q^\dagger(p,t)\,Q^\dagger(p,0)^{-1} \\
&+ \left((p^2-q^2)^2 - k^2(p^2-3q^2)\right)\,Q^\dagger(p,t)\,W^\dagger(q,t)\,Q^\dagger(k,t)\,Q^\dagger(k,0)^{-1} \\
&+ \exp[-D\,q^2\,t]\,Q^\dagger(k,t)\,Q^\dagger(p,t)\,q^2 \\
&\qquad \times \left(-4\,k^2\,W^\dagger(k,0)\,Q^\dagger(k,0)^{-1} + (k^2+p^2-q^2)\,W^\dagger(p,0)\,Q^\dagger(p,0)^{-1}\right) \\
&+ \left(2p^2\,(q^2+k^2-p^2) - 4\,q^2\,k^2\right)\,Q^\dagger(p,t)\,W^\dagger(k,t)\,Q^\dagger(q,t)\,Q^\dagger(q,0)^{-1} \\
&+ \exp[-D\,k^2\,t]\,\left((p^2-q^2)^2 - k^2(p^2-3q^2)\right)\,Q^\dagger(p,t)\,W^\dagger(q,0)\,Q^\dagger(q,t)\,Q^\dagger(q,0)^{-1},
\end{aligned} \tag{2.182}$$

and

$$s_1(k,p,q) = \frac{(k+p+q)(k+p-q)(k-p+q)(-k+p+q)}{4\,p^2\,k^2}. \tag{2.183}$$

The wavenumber integral is given by $\int\int_{\triangle_k} = \int_0^\infty dp \int_{|k-p|}^{k+p} dq$, and the region of integration is illustrated in Figure 2.8. Note that we have let $(t - t_0) \to \infty$, and this

is justified by the exponential decay of $Q^\dagger(k,t)$ with respect to $t$. The linear integral equation (2.181) together with (2.176) is sufficient to determine $W^\dagger(k,0)$ when $Q^\dagger(k,t)$ has been specified.

### 2.3.5 Inertial-convective range

Here we will solve (2.181) and (2.176) for $W^\dagger(k,0)$ in the inertial-convective range, that is in the wavenumber range where viscosity and diffusivity are unimportant. We introduce a non-dimensional wavenumber $\kappa = k/k_K$, and a non-dimensional time $\tau_k = t\,\epsilon^{1/3}\,k^{2/3}$, where $k_K = (\epsilon/\nu^3)^{1/4}$ is the Kolmogorov wavenumber. It was shown in Kida and Goto [24] that according to the SDIP, the velocity correlation function $Q^\dagger(k,t)$ can be written as

$$Q^\dagger(k,t) = \frac{1}{2\pi}\,K\,\epsilon^{2/3}\,k^{-11/3}\,Q(\kappa,\tau_k), \tag{2.184}$$

where $K = 1.722$ is the Kolmogorov constant. In particular, in the inertial range we have that

$$Q^\dagger(k,t) = \frac{1}{2\pi}\,K\,\epsilon^{2/3}\,k^{-11/3}\,Q(0,\tau_k). \tag{2.185}$$

Assuming we are in the inertial-convective range means that we can effectively set $\nu$ and $D$ to zero in equations (2.176), (2.181), and (2.182). Thus, there are no characteristic scales, and we can look for solutions of the form

$$W^\dagger(k,0) = -\frac{1}{2\pi}\,\zeta\,\epsilon^{1/3}\,k^{-13/3}, \tag{2.186}$$

where $\zeta$ is a constant to be determined. Then, by (2.176),

$$W^\dagger(k,t) = W^\dagger(k,0)\,\left(1 + \frac{K}{2\,\zeta}\,H(0,k^{2/3}\,\epsilon^{1/3}\,t)\right), \tag{2.187}$$

where the more general function $H(\kappa,\tau_k)$ is defined by

$$H(\kappa,\tau_k) = \exp[-\kappa^{4/3}\,\tau_k/Sc]\int_0^{\tau_k} d\tau_k'\,Q(\kappa,\tau_k')\,\exp[\kappa^{4/3}\,\tau_k'/Sc]. \tag{2.188}$$

Note $H(\kappa, \tau_k)$ will be used in subsection 2.3.6 for non-zero $\kappa$.

Substituting (2.185), (2.187), and (2.186) into (2.181), the powers of $k$ factor out, and we find after some changes of integration variables that

$$\zeta = -\frac{1}{b_1}(1 + b_2\, K), \tag{2.189}$$

where

$$\begin{aligned}
b_1 &= \frac{1}{4}\int\int_{\triangle_1} dp\, dq\, \frac{s_1(1,p,q)}{q^2}\, p\, q \\
&\times \Big[(1-q^2)\,(1-p^2+q^2)\, q^{-13/3}\, d_1(p) + (1+p^2-q^2)\, q^2\, p^{-13/3}\, d_1(p) \\
&- 4\, q^2\, p^{-11/3}\, d_1(p) + \left((p^2-q^2)^2 - (p^2-3q^2)\right)\, p^{-11/3}\, q^{-13/3}\, d_1(p) \\
&+ \left(2p^2(q^2+1-p^2) - 4q^2\right)\, p^{-13/3}\, f\left(\frac{q}{p}\right) \\
&+ \left((p^2-q^2)^2 - (p^2-3q^2)\right)\, p^{-13/3}\, q^{-13/3}\, f\left(\frac{q}{p}\right)\Big], \qquad (2.190) \\
b_2 &= \frac{1}{8}\int\int_{\triangle_1} dp\, dq\, \frac{s_1(1,p,q)}{q^2}\, p\, q \\
&\times \Big[(1-q^2)\,(1-p^2+q^2)\, q^{-13/3}\, d_2(p,q) \\
&+ \left((p^2-q^2)^2 - (p^2-3q^2)\right)\, p^{-11/3}\, q^{-13/3}\, d_2(p,q) \\
&+ \left(2p^2(q^2+1-p^2) - 4q^2\right)\, p^{-11/3}\, d_3(p,q)\Big], \qquad (2.191)
\end{aligned}$$

and

$$\begin{aligned}
d_1(p) &= \int_0^\infty d\tau_k\, Q(0,\tau_k)\, Q(0, p^{2/3}\,\tau_k), \qquad (2.192) \\
d_2(p,q) &= \int_0^\infty d\tau_k\, Q(0,\tau_k)\, Q(0, p^{2/3}\,\tau_k)\, H(0, q^{2/3}\,\tau_k), \qquad (2.193) \\
d_3(p,q) &= \int_0^\infty d\tau_k\, Q(0, p^{2/3}\,\tau_k)\, Q(0, q^{2/3}\,\tau_k)\, H(0,\tau_k). \qquad (2.194)
\end{aligned}$$

Several of the terms in (2.191) and (2.191) contain non-integrable singularities, but these can be shown to cancel each other to give finite values for $b_1$ and $b_2$. It is such cancellations of singularities that allow Lagrangian reformulations of the

DIA to give an energy spectrum with a $k^{-5/3}$ wavenumber dependence in the inertial range; see Leslie [27]. To evaluate the constant $\zeta$ we need to specify $Q(0, \tau_k)$. Comparing with Kida and Goto [24] we find that their function $\check{Q}^\dagger(\tau_k)$ is given by $\check{Q}^\dagger(\tau_k) = Q(0, K^{-1/2}\,\tau_k)$, and we repeated their numerical calculation to determine $\check{Q}^\dagger(\tau_k)$. Performing the integrals in (2.191) and (2.191) we found $b_1 = -0.44$ and $b_2 = 0.070$, implying $\zeta = 2.6$. The numerical integrations were carried out using adaptive Gauss-Konrod integration routines from the GNU Scientific Library [10].

The shell-summed cospectrum can be evaluated using (2.18) and (2.173) to give

$$C_{u_1 c}(k) = -\frac{4}{3}\,\mu\,\zeta\,\epsilon^{1/3}\,k^{-7/3}. \tag{2.195}$$

Thus, the SDIP agrees with the Lumley [28] form for the cospectrum in the inertial-convective range (1.2), and also gives the constant of proportionality.

### 2.3.6 Numerical solution of the SDIP equations

Here we will numerically solve (2.181) and (2.176) for $W^\dagger(k, 0)$ with finite values of the viscosity and diffusivity. To begin with we derive a convenient non-dimensional form of the equations to be solved by defining the Schmidt number, $Sc = \nu/D$, and the non-dimensional function $W(\kappa)$ by

$$W^\dagger(k, 0) = -\frac{1}{2\pi}\,\zeta\,\epsilon^{1/3}\,k^{-13/3}\,W(\kappa). \tag{2.196}$$

The limit $\kappa \to 0$ represents the inertial-convective range, and so from (2.186) we expect $W(0) = 1$. Some further changes of integration variables result in the following linear integral equation for $W(\kappa)$

$$N_1(\kappa)\,W(\kappa) + N_2(\kappa) + \int_0^\infty dq\,N_3(\kappa, q)\,W(\kappa\,q) = 0, \tag{2.197}$$

where

$$\begin{aligned} N_1(\kappa) &= 2\,\kappa^{4/3}\left(1+\frac{1}{Sc}\right)\zeta \\ &- K\,\zeta\int_0^\infty dq\int_{|1-q|}^{1+q} dp\int_0^\infty d\tau_k\;\frac{p}{q}\,s_1(1,p,q)\,p^{-11/3}\,Q(\kappa\,p,\tau_k\,p^{2/3}) \\ &\times \Big[-\exp[-\kappa^{4/3}\,q^2\,\tau_k/Sc]\,q^2\,Q(\kappa,\tau_k)\,Q(\kappa,0)^{-1} \\ &+ \exp[-\kappa^{4/3}\,\tau_k/Sc]\left(\frac{1}{2}\,p^2(q^2+1-p^2)-q^2\right)Q(\kappa\,q,\tau_k\,q^{2/3})\,Q(\kappa\,q,0)^{-1}\Big], \end{aligned} \tag{2.198}$$

$$\begin{aligned} N_2(\kappa) &= -K\,Q(\kappa,0)-\frac{1}{8}\,K^2\int_0^\infty dq\int_{|1-q|}^{1+q} dp\int_0^\infty d\tau_k\;\frac{p}{q}\,s_1(1,p,q)\,Q(\kappa\,p,\tau_k\,p^{2/3}) \\ &\times \Big[(1-q^2)(1-p^2+q^2)\,Q(\kappa,\tau_k)\,Q(\kappa\,p,0)^{-1}\,H(\kappa\,q,\tau_k\,q^{2/3})\,q^{-13/3} \\ &+ ((p^2-q^2)^2-p^2+3\,q^2)\,Q(\kappa,\tau_k)\,Q(\kappa,0)^{-1}\,H(\kappa\,q,\tau_k\,q^{2/3})\,p^{-11/3}\,q^{-13/3} \\ &+ (2\,p^2(q^2+1-p^2)-4\,q^2)\,Q(\kappa\,q,\tau_k\,q^{2/3})\,Q(\kappa\,q,0)^{-1}\,H(\kappa,\tau_k)\,p^{-11/3}\Big], \end{aligned} \tag{2.199}$$

$$\begin{aligned} N_3(\kappa,q) &= -\frac{1}{4}\,\zeta\,K\,q^{-13/3}\int_{|1-q|}^{1+q} dp\int_0^\infty d\tau_k\;\frac{p}{q}\,s_1(1,p,q) \\ &\times\Big[(1-q^2)(1-p^2+q^2)\,Q(\kappa,\tau_k)\,Q(\kappa\,p,\tau_k\,p^{2/3})\,Q(\kappa\,p,0)^{-1}\,\exp[-\kappa^{4/3}\,q^2\,\tau_k/Sc] \\ &+((p^2-q^2)^2-p^2+3\,q^2)\,p^{-11/3}\,Q(\kappa\,p,\tau_k\,p^{2/3}) \\ &\quad\times\Big(Q(\kappa,\tau_k)\,Q(\kappa,0)^{-1}\,\exp[-\kappa^{4/3}\,q^2\,\tau_k/Sc]+ \\ &\qquad Q(\kappa\,q,\tau_k\,q^{2/3})\,Q(\kappa\,q,0)^{-1}\,\exp[-\kappa^{4/3}\,\tau_k/Sc]\Big) \\ &+p^2(1+q^2-p^2)\,Q(\kappa,\tau_k)\,Q(\kappa\,q,\tau_k\,q^{2/3})\,Q(\kappa\,q,0)^{-1}\,\exp[-\kappa^{4/3}\,p^2\,\tau_k/Sc]\Big]. \end{aligned} \tag{2.200}$$

Equation (2.197) is an inhomogeneous Fredholm integral equation of the second kind. As written, the integrals giving $N_1(\kappa)\,W(\kappa)$ and $\int_0^\infty dq\,N_3(\kappa,q)\,W(\kappa\,q)$ do not converge, because of a non-integrable singularity at $(p\to 0, q\to 1)$. These singularities do cancel each other, but involve the unknown function $W(\kappa)$ in a way that makes

adding and subtracting the singularity difficult. Therefore, the method of solution chosen was to use a Newton-Raphson solver. This simplifies the problem because calculation of the residuals requires finding the left hand side of the equation, but not each individual term. Although the equation is linear, in practice two iterations were required for good accuracy.

There is also an integrable singularity at $(p \to 1, q \to 0)$ in the integral involving $N_3(\kappa, q)$, and this was dealt with by transforming the $q$ integration from the semi-infinite interval to $(-1, 1)$, and then using a Gauss-Jacobi rule with an appropriate weighting function. The $p$ and $\tau_k$ integrations were performed using adaptive Gauss-Konrod integration routines from the GNU Scientific Library [10]. The Jacobian needed for the Newton-Raphson solver was calculated using finite differences, and interpolations were performed using cubic and bicubic spline interpolation for $W(\kappa)$, and $Q(\kappa, \tau_k)$, respectively.

The results were found to be converged when the integral equation was evaluated at twenty points, and when for the $q$ integration the integrand was evaluated at twenty-four points. The integral equation was evaluated at the same points as where $W(\kappa)$ was stored, but these points were chosen to be different from the quadrature points for the $q$ integration. This was necessary because $W$ enters the $q$ integral as $W(\kappa q)$, and so for small $\kappa$ the $q$ integration must extend to large values for accuracy. A rescaling to a form with $W(q)$ was not possible without the undesirable effect of making the location of the singular points a function of $\kappa$.

Solving (2.197) obviously requires knowledge of the two-time, two-point velocity statistics through the function $Q(\kappa, \tau_k)$. Initially, model functions were used, but in order to have a more consistent calculation of the cospectrum all results presented here use the SDIP prediction for $Q(\kappa, \tau_k)$. This was obtained by repeating the calculation of Kida and Goto [24], involving the solution of a coupled system of a non-linear integral equation, and a second order integro-differential equation. Our results for $Q(\kappa, 0)$ were found to match their reported results to within graphing accuracy.

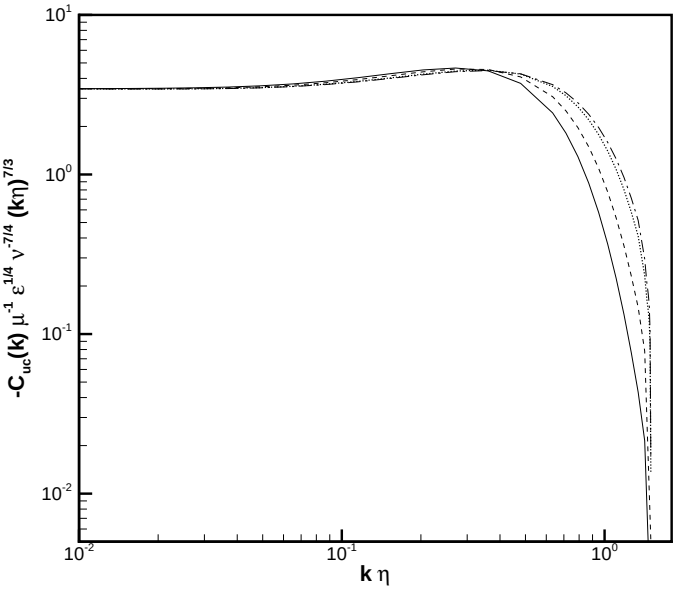


Figure 2.9: SDIP results for the compensated shell-summed velocity-scalar cospectrum at Schmidt numbers 1 (solid), 2 (dashed), 10 (dotted), and 100 (dash-dotted).

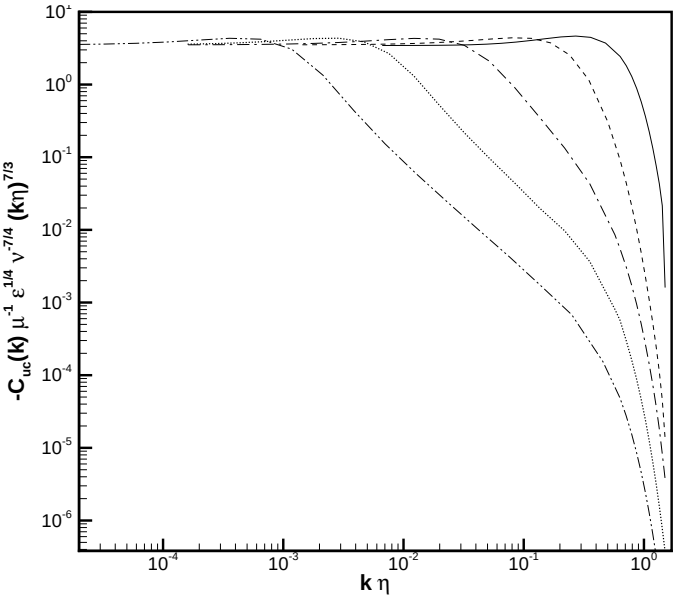


Figure 2.10: SDIP results for the compensated shell-summed velocity-scalar cospectrum at Schmidt numbers 1 (solid), $10^{-1}$ (dashed), $10^{-2}$ (dash-dotted), $10^{-3}$ (dotted), and $10^{-4}$ (dash-dot-dotted).

The shell-summed cospectrum is related to $W(\kappa)$ by

$$C_{u_1c}(k) = -\frac{4}{3}\,\mu\,\zeta\,\epsilon^{1/3}\,k^{-7/3}\,W(\kappa), \tag{2.201}$$

and so $W(\kappa)$ represents a non-dimensional compensated cospectrum. Figure 2.9 shows the results for the compensated shell-summed cospectrum for a range of Schmidt numbers greater than one. As might be expected the cospectrum decays slower for increasing Schmidt number, but nonetheless smoothly approaches the inertial-convective limit in each case. Note we did not enforce the inertial-convective limit, $W(0) = 1$, so that this condition is a check on the consistency of our results with the inertial-convective calculation. There is a characteristic bump structure, which is located at approximately $0.3\,k_K$ for Schmidt number unity. The cospectrum quickly reaches an asymptotic form for large Schmidt number, and when graphed there was no visible difference between the cospectra at Schmidt numbers one hundred, and one thousand. As was discussed in section (2.1) there seems to be no power-law behavior in the viscous-convective range. The compensated shell-summed cospectrum is shown in Figure 2.10 for a range of small Schmidt numbers. Again there is a smooth approach to the inertial-convective limit in each case. The asymptotic form for low Schmidt number will be discussed in subsection 2.3.7, but we note in Figure 2.10 the approach to a power law in the inertial-diffusive range. Comparison with experiment, DNS, and the stretched-spiral vortex model will be made in section 2.5 at a Schmidt number of order unity.

### 2.3.7 The SDIP equations at low Schmidt number

Here we will derive the asymptotic form of equation (2.197) for low Schmidt number. We will then compare with the numerical solution of (2.197), and the non-SDIP asymptotic result of section 2.1. To make the analysis more clear we follow the method of Goto and Kida [14] by introducing the rescaled quantities $\kappa = \kappa_s\,Sc^{\alpha}$, $W(\kappa) = W_s(\kappa_s)\,Sc^{\beta}$, where $\kappa_s$ and $W_s$ are assumed to be order unity as $Sc \to 0$. Here $\alpha$ and $\beta$ are unrelated to the Euler angles of subsection 2.2.2. The Kolmogorov

wavenumber and the Obukhov-Corrsin wavenumber then correspond to $\alpha = 0$ and $\alpha = 3/4$, respectively. We wish to consider wavenumbers $k \gg k_C$ and so $\alpha < 3/4$. Typical exponential factors involving the Schmidt number are rewritten as

$$\exp[-\kappa^{4/3}\,\tau_k/Sc] = \exp[-\kappa_s^{4/3}\,\tau_k\,Sc^{4\alpha/3-1}] \simeq 0, \tag{2.202}$$

because $4\alpha/3 - 1 < 0$. Therefore in equation (2.197) we can neglect $N_3$, and $N_1$ is approximated by

$$N_1 \simeq 2\,\kappa_s^{4/3}\,Sc^{4\alpha/3-1}\,\zeta. \tag{2.203}$$

Care must be taken with the function $H(\kappa, \tau_k)$, which is written using the rescaled quantities as

$$H(\kappa, \tau_k) = \int_0^{\tau_k} d\tau_k'\,Q(\kappa, \tau_k')\,\exp[-\kappa_s^{4/3}\,Sc^{4\alpha/3-1}\,(\tau_k - \tau_k')]. \tag{2.204}$$

Noting that $\tau_k \geq \tau_k'$ we have that

$$N_2 \simeq -K\,Q(\kappa_s\,Sc^{\alpha}, 0). \tag{2.205}$$

The relevant scaling for $W_s(\kappa_s)$ is then $\beta = -4\alpha/3 + 1$, with the result

$$W_s(\kappa_s) = \frac{K\,Q(\kappa_s\,Sc^{\alpha}, 0)}{2\,\kappa_s^{4/3}\,\zeta}. \tag{2.206}$$

In the inertial-diffusive range we have $k \ll k_K$, so that $\alpha > 0$, and

$$W_s(\kappa_s) = \frac{K}{2\,\kappa_s^{4/3}\,\zeta}. \tag{2.207}$$

Returning to unscaled variables we have that

$$W(\kappa) = \frac{K\,Q(\kappa, 0)\,Sc}{2\,\kappa^{4/3}\,\zeta}, \qquad k \gg k_C, \tag{2.208}$$

$$W(\kappa) = \frac{K\,Sc}{2\,\kappa^{4/3}\,\zeta}, \qquad k_C \ll k \ll k_K. \tag{2.209}$$

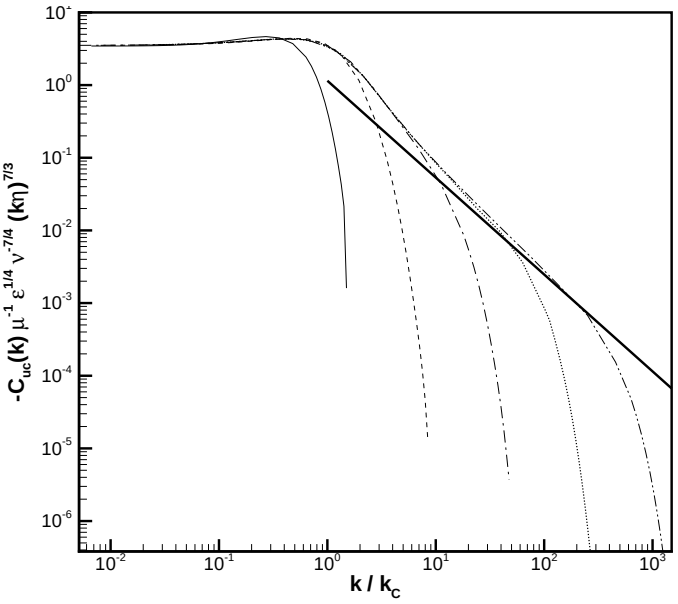


Figure 2.11: SDIP results for the compensated shell-summed velocity-scalar cospectrum at low Schmidt numbers (same key as Figure 2.10). Here the wavenumber has been normalized with the Obukhov-Corrsin wavenumber, and the thick solid line shows the inertial-diffusive asymptotic result given by equation (2.31).

The corresponding form for the shell-summed cospectrum is

$$C_{u_1c}(k) = -\frac{2\,\mu}{3\,D\,k^2}\,E(k), \qquad k \gg k_C, \tag{2.210}$$

and for $k_C \ll k \ll k_K$ we recover expression (2.31). Therefore the SDIP equation is consistent with the asymptotic result of subsection 2.1.3 for the inertial-diffusive range that was derived using the simpler Batchelor, Howells, and Townsend [2] type analysis. The SDIP asymptotic form (2.210) is more general since it applies in the viscous-diffusive range also.

In Figure 2.11 we compare the numerical solution to the SDIP equation at a range of $Sc \leq 1$ with the inertial-diffusive power law form (2.31). We have scaled the wavenumber with the Obukhov-Corrsin wavenumber rather than the Kolmogorov wavenumber, so that the normalized inertial-diffusive asymptotic result is Schmidt number independent. The approach to the power law form is evident for the lower Schmidt number cospectra. In Figure 2.12 we make a comparison at $Sc = 10^{-4}$ of the

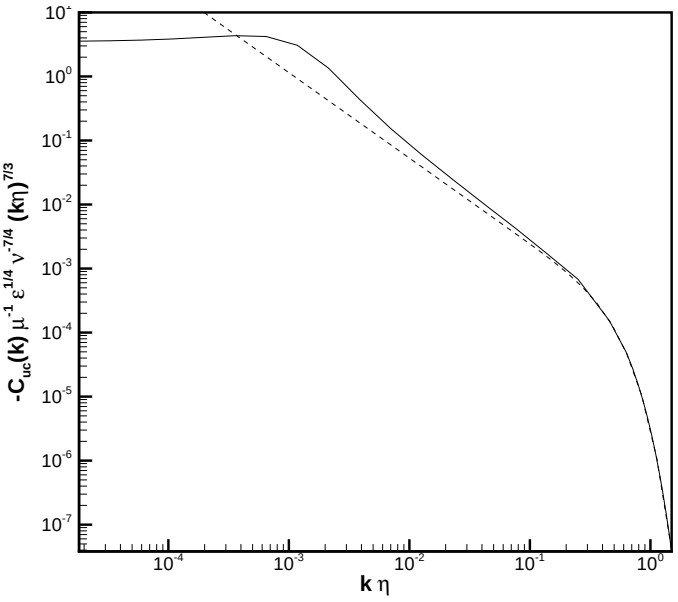


Figure 2.12: SDIP result for the compensated shell-summed velocity-scalar cospectrum at Schmidt number $10^{-4}$ (solid) compared with the SDIP asymptotic form given by equation (2.210) (dashed).

SDIP asymptotic form (2.210), and the SDIP numerical result. The agreement of the numerical result with the SDIP asymptotic form is excellent in the viscous-diffusive range.

Finally, to summarize our results for the effect of Schmidt number on the cospectrum, Figure 2.13 shows the shell-summed cospectrum in uncompensated form for Schmidt numbers $10^{-4}$, 1, and $10^4$, making clear the two distinct power law ranges for small Schmidt number. At large Schmidt number the relatively small effect of changes in Schmidt number is evident, at least when the wavenumber is scaled with the Kolmogorov wavenumber, corresponding to varying the diffusivity with the viscosity and energy dissipation held constant.

## 2.4 Direct numerical simulation

We performed a DNS with $512^3$ grid points on the QSC supercomputer to investigate the small scale mixing of a passive scalar by a statistically isotropic turbulent velocity field in the presence of a mean scalar gradient. In particular the velocity-scalar

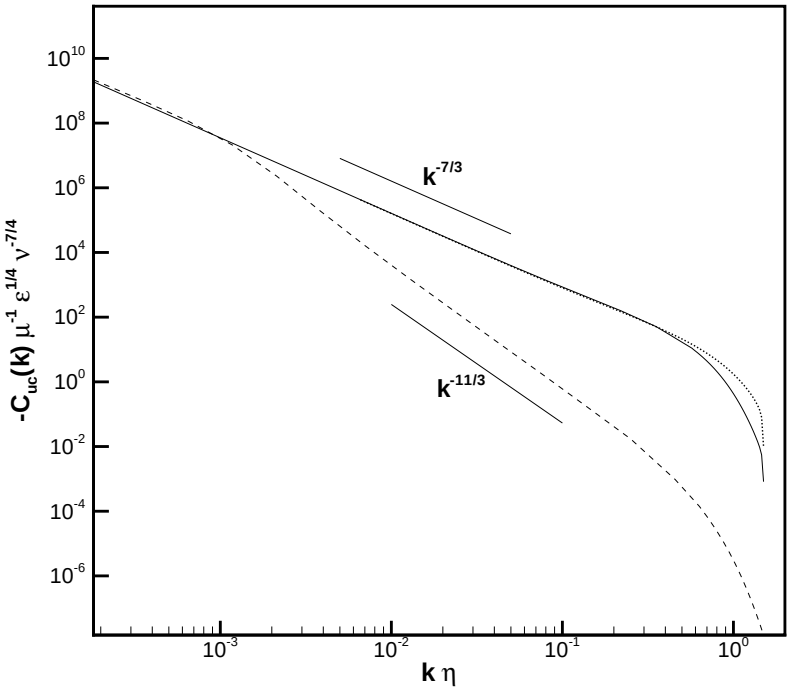


Figure 2.13: SDIP results for the shell-summed velocity-scalar cospectrum (uncompensated) at Schmidt numbers $10^{-4}$ (dashed), 1 (solid), and $10^{4}$ (dotted). The power laws $k^{-7/3}$ and $k^{-11/3}$ are also shown for reference.

cospectrum, and the modal time correlations of the velocity and scalar fields were calculated.

### 2.4.1 Description of the DNS

We solved the incompressible Navier-Stokes equations for the velocity field, and the advection-diffusion equation for the scalar, using a Fourier-Galerkin pseudospectral code in a cube of side $2\,\pi$ with periodic boundary conditions. Although the scalar has a mean gradient, the scalar fluctuation, $c(\mathbf{x},t)$, is statistically homogeneous, and so can be well represented using periodic functions. The velocity field is decomposed as in equation (2.8), but where now $L = 2\pi$, and the sum over $\mathbf{k}$ is over a finite set of modes, $k = -n_k/2, \cdots, n_k/2 - 1$, corresponding to $n_k^3$ modes in total. A similar decomposition is made for the scalar fluctuation. The velocity field was forced at the large scales so that it became statistically stationary in time. The method used was to force 20 Fourier modes, with wavevectors $\mathbf{k}$ such that $1 < |\mathbf{k}| < 2$, see Misra and Pullin [32]. The forcing coefficients were chosen so that the energy injection rate $\sum \tilde{f}_i(\mathbf{k},t)\,\tilde{u}_i(-\mathbf{k},t)$ was constant, where $\hat{f}_i(\mathbf{k},t)$ are the Fourier modes of the forcing field. The mean gradient acted as a source for the variance of the scalar fluctuation, and the scalar field also became statistically stationary in time. Integrating factors were used for the viscous and diffusive terms, so that the governing equations for the velocity and the scalar modes are given by

$$\begin{aligned}
&\frac{\partial}{\partial t}\left(\exp[\nu\,k^2\,t]\,\tilde{u}_i(\mathbf{k},t)\right) = \\
&\qquad -\exp[-\nu\,k^2\,t]\left(\tilde{P}_{ij}(\mathbf{k})\sum_{\mathbf{k}=\mathbf{p}+\mathbf{q}} i\,p_k\,\tilde{u}_j(\mathbf{p},t)\,\tilde{u}_k(\mathbf{q},t) - \tilde{f}_i(\mathbf{k},t)\right), \\
&\frac{\partial}{\partial t}\left(\exp[D\,k^2\,t]\,\tilde{c}(\mathbf{k},t)\right) = \\
&\qquad -\exp[-D\,k^2\,t]\left(\sum_{\mathbf{k}=\mathbf{p}+\mathbf{q}} i\,p_k\,\tilde{c}(\mathbf{p},t)\,\tilde{u}_k(\mathbf{q},t) + \mu\,\tilde{u}_1(\mathbf{k},t)\right),
\end{aligned} \tag{2.211}$$

where the incompressible projection operator is given by $\tilde{P}_{ij}(\mathbf{k}) = \delta_{ij} - k_i k_j/k^2$, see Mei-Jiau Huang [18]. A second-order explicit Runge-Kutta scheme was used for time-

| Grid | $R_\lambda$ | $T_{stat}/T_{eddy}$ | $Sc$ | $k_{max}\eta$ | $R_l$ | $< c^2 > /(\mu l_\epsilon)^2$ | $k_0\, l$ | $C$ |
|---|---|---|---|---|---|---|---|---|
| $512^3$ | 265 | 10.5 | 0.7 | 1.05 | 1901 | 0.45 | 1.00 | 0.48 |
| $256^3$ | 167 | 9.3 | 0.7 | 1.00 | 779 | 0.38 | 0.99 | 0.51 |

Table 2.1: Simulation parameters for the stationary period of the DNS.

stepping, and a 3/2 dealiasing method was used for the non-linear terms.

Parameters describing the simulation are shown in Table 2.1. Values are also reported for a smaller run with 256 grid points. Here $T_{eddy}$ is the eddy turnover time, $T_{stat}$ is the time over which the statistics are collected, $R_\lambda$ is the Taylor Reynolds number, $k_{max}$ is the largest dynamically significant wavenumber, $\eta$ is the Kolmogorov length, $R_l$ is the Reynolds number based on the integral length scale $l$, the turbulent length scale is $l_\epsilon = u_{rms}^3/\epsilon$ where $\epsilon$ is the dissipation, $k_0$ is the smallest wavenumber, and $C$ is the Courant number. The Courant number used was relatively low because the time-step was fixed so that two-time statistics could be collected easily.

### 2.4.2 Results of the DNS

First we will show some instances of the scalar and vorticity fields in the DNS to illustrate the structure of the flow. A two-dimensional $512^2$ cross-section of the total scalar field is shown in Figure 2.14, where we have included the mean scalar gradient in the horizontal direction. There appears to be many sharp interfaces in the scalar field, and these are known as ramp-cliff structures because of their distinctive signature in one dimension. See, for example, Warhaft [48] for a review of these structures and how they relate to isotropy of the scalar field at the small scales. Figure 2.15(a) shows an isosurface of vorticity magnitude corresponding to the intense vorticity in a cube representing one sixty-fourth of the entire computational domain. The intense vorticity is organized into tube-like structures that are sometimes referred to as worms, see Jimenez *et al.* [19]. Such structures in the vorticity field are part of the motivation for the stretched-spiral vortex model. Isosurfaces of the scalar field are shown in Figure 2.15(b), and we can see that the field contains sheet-like rather than tube-like structures. Brethouwer *et al.* [4] have studied the influence

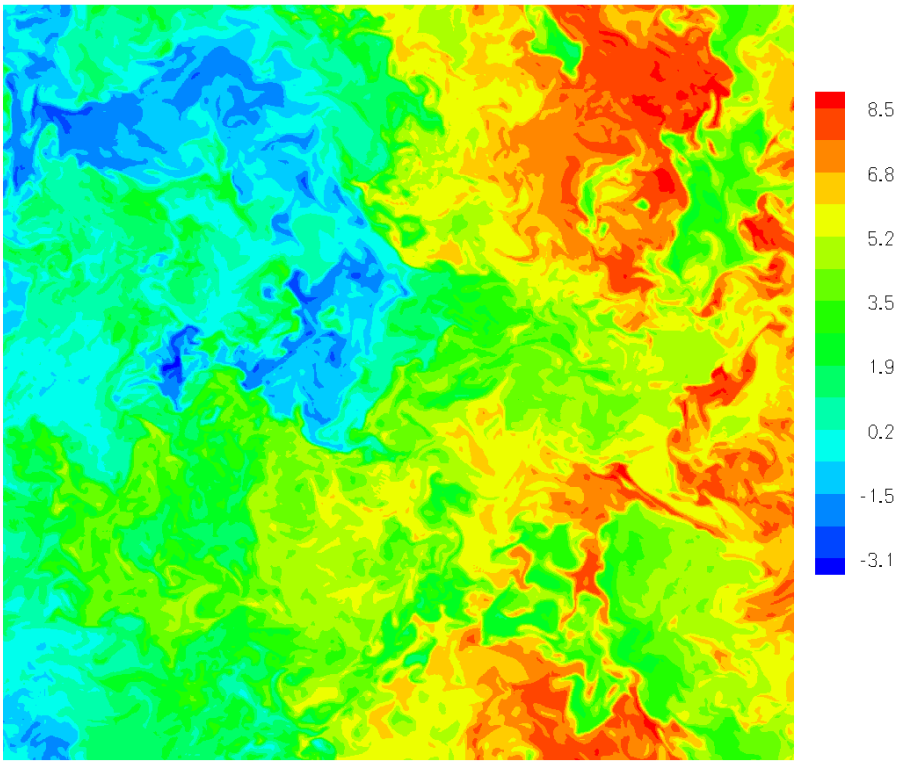


Figure 2.14: Cross-section of the total scalar field with $512^2$ gridpoints, including the mean gradient in the horizontal direction. The scalar values are normalized as $(c + \mu\, x_1)/(\mu\, l)$.

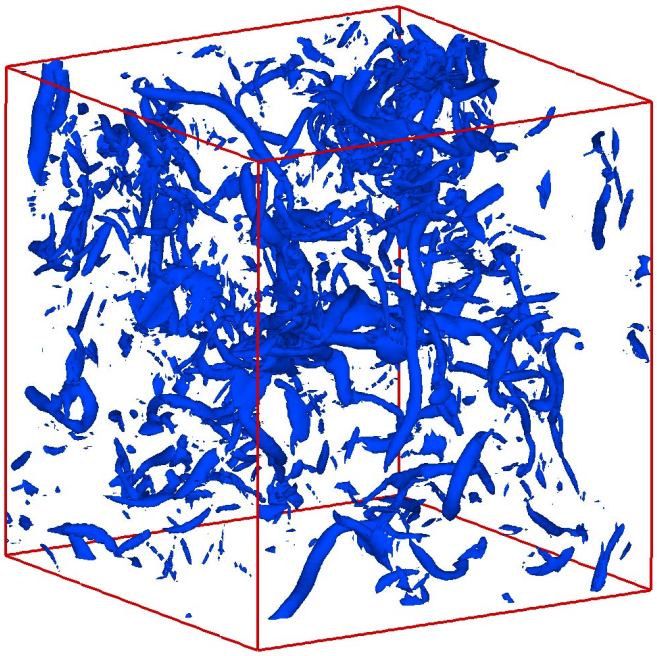

(a)

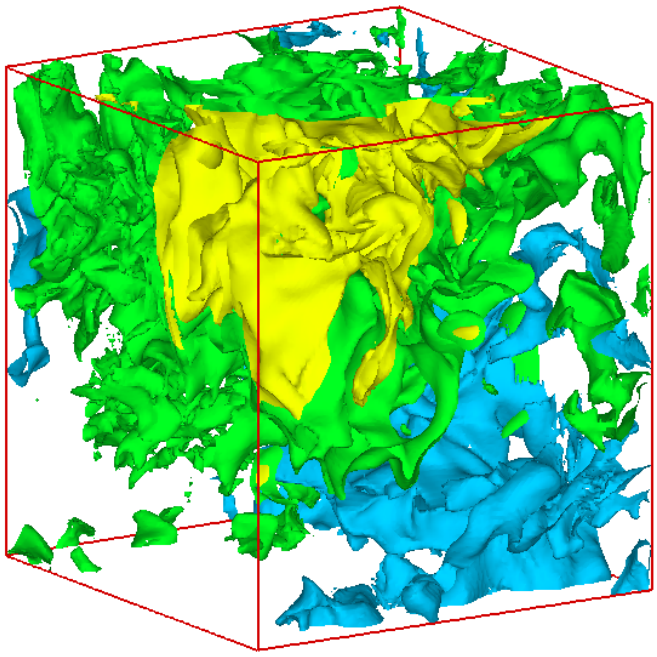

(b)

Figure 2.15: Isosurfaces of the vorticity magnitude and the scalar fluctuation. The volume shown is 1/64 of the compuational domain. (a) Isosurface of the magnitude of the vorticity, at a value three standard deviations above the mean value. (b) Isosurfaces of the scalar fluctuation at $c/(\mu\, l)$ of $-2.0$ (yellow), 0.0 (green), 2.0 (blue).

of Schmidt number on the morphology of the scalar field, albeit at relatively low Reynolds number, and found that at low Schmidt number the scalar sheets were wound into distinctive spiral structures.

We turn now to the time-averaged spectral characteristics of the flow. The shell averaged energy spectrum in compensated form is shown in Figure 2.16(a) for both the $256^3$ and $512^3$ runs. The beginning of the inertial range and the bump in the dissipation range are apparent. The shell averaged scalar spectrum is shown in Figure 2.16(b). Again there is a bump at the beginning of the dissipation range, but the slope at the beginning of the inertial convective range is considerably shallower than minus five-thirds.

Also shown in Figure 2.16(b) is the scalar spectrum that results from the stretched-spiral vortex model calculation of Pullin and Lundgren [40]. We plot the result given by equations (107) and (108) of that paper, for a Schmidt number of 0.7. The vortex Reynolds number was chosen to be 200 rather than 1000, so that it was at least less than the Taylor Reynolds number of the DNS with which we wish to compare. Note that at a Schmidt number of 0.7, the first order scalar dissipation, given by equation (109) of that paper, could not be neglected. The result is a combination of a $k^{-1}$ term and a $k^{-5/3}$ term, representing the first two terms in an asymptotic series. The agreement with the DNS result is quite good, although the DNS scalar spectrum is somewhat lower in the viscous diffusive range. A comparison, not shown here, using a vortex Reynolds number of 1000 also gave reasonable agreement. Pullin and Lundgren [40] made a comparison with experiment at Schmidt numbers 7 and 700, and it is interesting to see that the model seems to compare well at a Schmidt number of 0.7 also.

The shell-summed velocity-scalar cospectra for the two simulations are shown in Figure 2.17(a) compared with a $k^{-7/3}$ power law. The slope is a little shallower than a $k^{-7/3}$ at the beginning of the inertial-convective range. In Figure 2.17(b) we show the cospectrum for the larger simulation compared with the upper bound for the magnitude of the cospectrum derived from inequality (2.21). As might be expected, the bound is closest to the actual value for low wavenumbers.

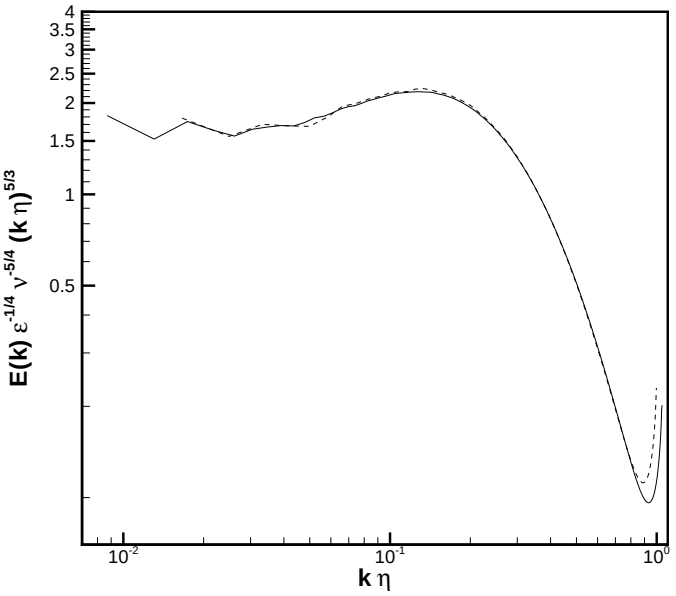


(a)

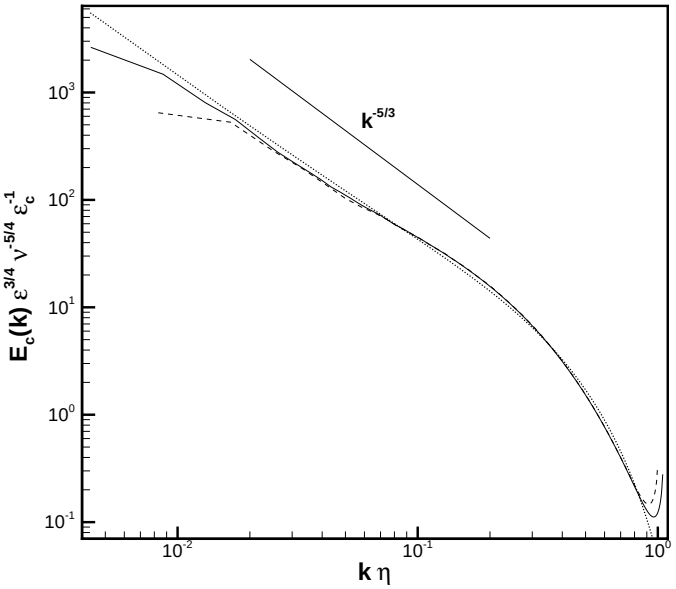


(b)

Figure 2.16: Spectra from the DNS at $512^3$ (full line) and $256^3$ (dashed line): (a) energy spectra in compensated form, (b) scalar spectra compared with $k^{-5/3}$, and the stretched-spiral vortex result from reference [40] (dotted line).

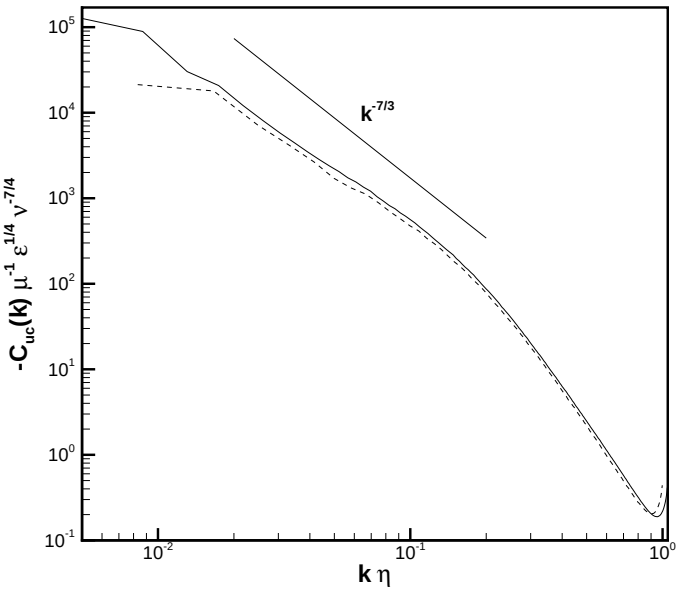


(a)

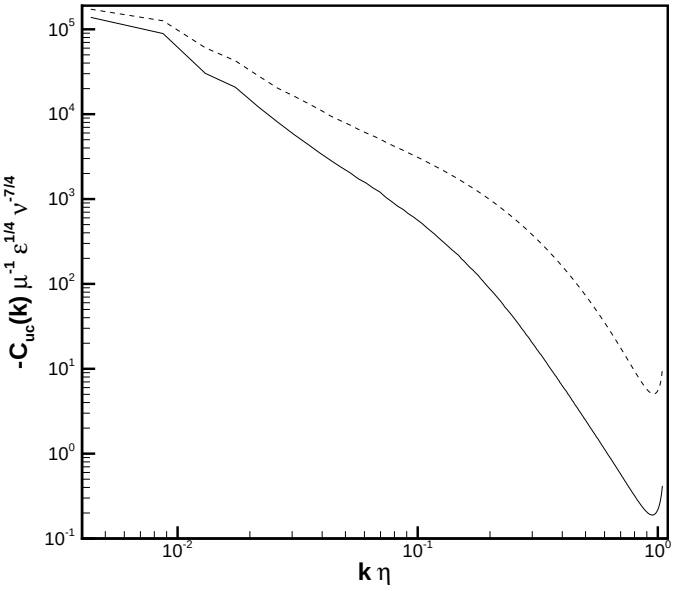


(b)

Figure 2.17: (a) Velocity-scalar cospectra from the DNS at $512^3$ (full line) and $256^3$ (dashed line) compared with a $k^{-7/3}$ power law. (b) Velocity-scalar cospectrum from the DNS at $512^3$ (full line) compared with the upper bound for the magnitude of the cospectrum given by the cospectrum inequality (dashed line).

Results from the DNS for the modal time correlations of the velocity and scalar fields are discussed in section 3.3.

## 2.5 Comparison of results from theory, simulation, and experiment

We make a comparison of the DNS results for the cospectrum with the stretched-spiral vortex model result of section 2.2.3, the SDIP result of section 2.3.2, and the experimental result of Mydlarski and Warhaft [34]. The Schmidt number is 0.7 for the DNS and the SDIP calculation. In the case of the stretched-spiral vortex model the Schmidt number is restricted to be one, see section 2.2.1. For this model we also only consider the component of the cospectrum due to axial motion in the vortex structures, see section 2.2.3 for further details. The experimental result was for the one-dimensional velocity-temperature cospectrum, $C_{u_1c}^{1D}(k_3)$, at $R_\lambda$ of 582, and a Schmidt number of 0.71. Note that in the experiment the direction of the scalar gradient, and hence the scalar flux, was perpendicular to the direction in which the cospectrum was measured. The experimental data was quite noisy, and so we have applied a one-third octave smoothing filter. Mydlarski and Warhaft attributed the noisiness of the cospectrum to the fact that no mathematical limitation keeps the cospectrum either positive or negative. To make the comparison, we convert the SDIP and stretched-spiral vortex model shell-summed cospectra to one-dimensional cospectra using equation (2.117). The one-dimensional cospectrum was calculated directly in the DNS.

The cospectra are shown in Figure (2.18) in compensated form, where we have also shown a straight line representing the inertial-convective SDIP result. The shapes of the cospectra are quite similar in all cases, although the SDIP cospectrum is closer than the other cospectra to a $k^{-7/3}$ power law in the inertial-convective range. The DNS has a similar spectral slope to that of the experimental result which was reported as $k^{-2}$. The result from the stretched-spiral vortex model is quite low in

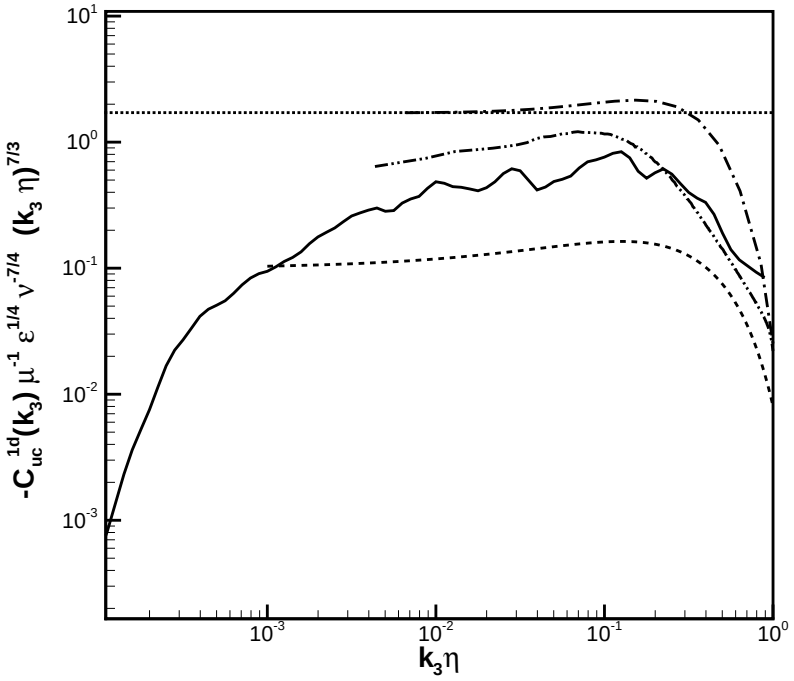


Figure 2.18: Comparison of compensated one-dimensional velocity-scalar cospectra from the stretched-spiral vortex model (dashed), experimental data from reference [34] at $R_\lambda = 582$ (solid), DNS at $R_\lambda = 265$ (dash-dot-dot), SDIP inertial-convective (dotted), and SDIP (dash-dot).

magnitude relative to the other results, although we note that the exact magnitude of the cospectrum result from this model is dependent on several rough estimates, and only the contribution of the axial velocity is shown. The SDIP cospectrum seems to be too large in magnitude in the inertial-convective range, and in this context it is worth noting that the SDIP value for the Obukhov-Corrsin constant differs from experimental values by a factor of about a half.

# Chapter 3 Modal Time Correlations

In this chapter we consider Eulerian two-point, two-time correlations of a turbulent velocity field, and of a passive scalar mixed by a turbulent velocity field. Integral expressions are derived for the modal time correlation functions of the velocity field, and of the scalar field, using the stretched-spiral vortex model. These expressions are evaluated using asymptotic methods for high wavenumber, and alternatively using numerical integration. If the motion of the centers of the vortex structures is neglected, then an inertial time scaling $(\epsilon k^2)^{-1/3}$, where $\epsilon$ is the energy dissipation rate, is found to collapse the velocity and scalar modal time correlation functions to universal forms. Allowing the centers of the vortex structures to move introduces a sweeping timescale, $(u_{rms}k)^{-1}$, where $u_{rms}$ is the rms velocity of the centers of the vortex structures. The sweeping timescale dominates the inertial timescale for sufficiently large wavenumber. Results are also reported for the direct numerical simulation at a Taylor Reynolds number of 265. As was mentioned in Chapter 1, the velocity modal time correlation function has previously been calculated using DNS [16, 22, 36, 45], but here we have calculated both the velocity and scalar modal time correlation functions. They coincide for large enough wavenumber, and are found to collapse to universal forms when a sweeping timescale is used.

In section 3.1 we define the modal time correlation functions for the velocity and the scalar, and briefly discuss some of their properties. Expressions for these functions are derived using the stretched-spiral vortex model in subsection 3.2.1, and these expressions are evaluated asymptotically in subsection 3.2.2, and numerically in subsection 3.2.3. The effect of motion of the centers of the vortex structures is considered in subsection 3.2.4. Finally, in section 3.3, the DNS results are reported, and a comparison with the stretched-spiral vortex model is made.

## 3.1 The modal time correlation function

We consider homogeneous turbulence, and begin by defining the two-time, two-point velocity correlation at time $t$ by

$$\mathcal{R}_{ij}(\mathbf{r},t,\sigma) = \overline{u_i(\mathbf{x},t)\,u_j(\mathbf{x}+\mathbf{r},t+\sigma)}, \tag{3.1}$$

where the overbar is taken to be an ensemble average. Then the shell-summed two-time velocity cross-spectrum at time $t$ is defined by

$$\mathcal{F}_{ij}(k,t,\sigma) = \frac{1}{(2\pi)^3}\int_S\int_V \mathcal{R}_{ij}(\mathbf{r},t,\sigma)e^{-i\mathbf{k}\cdot\mathbf{r}}d\mathbf{r}\,dS_k, \tag{3.2}$$

where the integral over $V$ indicates a volume integral over all space, and the integral over $S$ indicates a surface integral over a spherical shell in wavenumber space. Note that this shell average in wavenumber ensures that $\mathcal{F}_{ij}(k,t,\sigma)$ is a real quantity. The usual shell-summed energy spectrum is given by $E(k,t) = 1/2\,\mathcal{F}_{jj}(k,t,0)$, where the summation over $j$ is implied. The modal time correlation function at time $t$, $R(k,t,\sigma)$, is then defined by, (see Comte-Bellot and Corrsin [6])

$$R(k,t,\sigma) = \frac{\mathcal{F}_{jj}(k,t,\sigma)}{2\,\left(E(k,t)\,E(k,t+\sigma)\right)^{1/2}}, \tag{3.3}$$

so that $R(k,t,0) = 1$. It is straightforward to show that

$$\frac{\partial}{\partial\,\sigma}\,R(k,t,\sigma)\bigg|_{\sigma=0} = 0, \tag{3.4}$$

even when the turbulence is non-stationary; see Appendix F. We will be concerned with the case of stationary turbulence, so that we may omit references to $t$ and define

$$R(k,\sigma) = \frac{\mathcal{F}_{jj}(k,\sigma)}{2\,E(k)}. \tag{3.5}$$

Similarly for a passive scalar, $c(\mathbf{x},t)$, we define the two-point, two-time scalar

correlation function, $R^c(\mathbf{r}, \sigma)$,

$$\mathcal{R}^c(\mathbf{r}, \sigma) = \overline{c(\mathbf{x}, t)\, c(\mathbf{x} + \mathbf{r}, t + \sigma)}, \tag{3.6}$$

the shell-summed, two-time scalar cross-spectrum, $\mathcal{F}_c(k, \sigma)$,

$$\mathcal{F}_c(k, \sigma) = \frac{1}{(2\pi)^3} \int_S \int_V \mathcal{R}^c(\mathbf{r}, \sigma) e^{-i\mathbf{k}\cdot\mathbf{r}} d\mathbf{r}\, dS_k, \tag{3.7}$$

and the scalar modal correlation function, $R^c(k, \sigma)$,

$$R^c(k, \sigma) = \frac{\mathcal{F}_c(k, \sigma)}{E_c(k)}, \tag{3.8}$$

where $E_c(k) = \mathcal{F}_c(k, 0)$ is the scalar power spectrum. It is easily verified that the property $\frac{\partial}{\partial \sigma} R^c(k, \sigma) \big|_{\sigma=0} = 0$ also holds.

A more intuitive understanding of the modal correlation functions follows from considering turbulence in a cube of finite volume with periodic boundary conditions, as is often considered in numerical simulation of homogeneous turbulence. Then the velocity modal correlation function for a given discrete wavenumber represents the autocorrelation in time of the Fourier mode of the velocity field for that wavenumber, normalized by the variance of that Fourier mode. A similar interpretation follows in the case of the scalar.

Investigators typically look for a characteristic timescale, $\tau_c(k)$, such as the sweeping or inertial timescales introduced earlier, so that the velocity modal correlation function has the similarity form,

$$R(k, \sigma) = g\left(\frac{\sigma}{\tau_c(k)}\right). \tag{3.9}$$

We will also attempt to find such a scaling for the scalar modal time correlation function, although in general we expect the timescale and similarity function may be different from that found in the case of the velocity.

## 3.2 Application of the stretched-spiral vortex model

### 3.2.1 Vortex structures with stationary centers

We wish to calculate the modal correlation functions using the stretched-spiral vortex model. In order to do the simplest possible analysis (at least as a first step), we do not explicitly consider the effects of a mean scalar gradient fixed in a lab frame, and so $c(\mathbf{x}, t)$ now more properly refers to the total scalar field rather than a fluctuation about a mean gradient. Also, we do not let the scalar vary in the direction of the vortex axis, and we use the lowest-order solution for the scalar from expressions (2.65). We will assume that the centers of the vortex structures are stationary; the velocity and scalar modal correlation functions will be denoted $\check{R}(k, \sigma)$ and $\check{R}^c(k, \sigma)$, respectively in this case. Gross motion of the vortex structures will be considered in subsection 3.2.4.

As in subsection 2.2.1, the velocity field in a typical stretched vortex tube is decomposed as

$$u_i = v_i(x_1, x_2, t) + a_i(t) x_i \tag{3.10}$$

where summation over $i$ is not implied, $a_1 = a_2 = -a/2$, $a_3 = a$, $a > 0$, and the strain-rate $a$ is assumed constant. Note that we are now working with coordinates centered in the vortex structure and with the $x_3$ direction aligned with the vortex axis. We make the simplifying assumption that the axial velocity $v_3(x_1, x_2, t)$ is zero. The two-dimensional Fourier transform of the velocity and scalar fields, $\hat{v}_j(k_1, k_2, t)$ and $\hat{c}_j(k_1, k_2, t)$, respectively, are defined by (2.74). Our starting point is equation (B16) from Pullin and Saffman [41] for a general cross-spectrum, applied to $\mathcal{F}_{jj}(k, \sigma)$ and $\mathcal{F}_c(k, \sigma)$, and modified to include a time average over the lifetime of the vortex

$$\mathcal{F}_{jj}(k, \sigma) = 4\,\pi^2\,N\,k \int_0^\infty \int_0^{2\pi} \hat{v}_j(k_1, k_2, t)\,\hat{v}_j^*(k_1, k_2, t+\sigma)\,d\theta_k\,S(t)\,dt, \tag{3.11}$$

$$\mathcal{F}_c(k, \sigma) = 4\,\pi^2\,N\,k \int_0^\infty \int_0^{2\pi} \hat{c}(k_1, k_2, t)\,\hat{c}^*(k_1, k_2, t+\sigma)\,d\theta_k\,S(t)\,dt, \tag{3.12}$$

where $k_1 = k\,\cos\theta_k$ and $k_2 = k\,\sin\theta_k$. Here, $S(t) = \exp(a\,t)$ is a stretching factor due

to the uniform strain rate $a$, and $N$ is the rate of creation of vortex tube length per unit time, and per unit volume. Note that the stretching factor is $S(t)$ rather than $S(t+\sigma)$ because we take the length of the shorter tube when considering correlations between two tubes of different lengths.

We must now decide on an appropriate expression for $E(k)$ in the definition of $\check{R}(k,\sigma)$, equation (3.5). Guided by the definition of $\check{R}(k,t,\sigma)$ in the case of non-stationary turbulence, we take a geometric average of the energy spectra associated with the velocity fields starting from $t=0$ and $t=\sigma$,

$$\begin{aligned} E(k) &= \left(2\,\pi^2\,N\,k\int_0^\infty\int_0^{2\pi}\hat{v}_j(k_1,k_2,t)\,\hat{v}_j^*(k_1,k_2,t)\,d\theta_k\,S(t)\,dt\right)^{1/2} \\ &\times \left(2\,\pi^2\,N\,k\int_0^\infty\int_0^{2\pi}\hat{v}_j(k_1,k_2,t+\sigma)\,\hat{v}_j^*(k_1,k_2,t+\sigma)\,d\theta_k\,S(t)\,dt\right)^{1/2}. \end{aligned} \tag{3.13}$$

Note that we choose $S(t)$ rather than $S(t+\sigma)$ in the second term in parenthesis so that $N$ is still the correct normalization factor. It is straightforward to check that when expressions (3.11) and (3.13) are used in definition (3.5), then the property (3.4) remains valid. Similarly we choose

$$\begin{aligned} E_c(k) &= \left(4\,\pi^2\,N\,k\int_0^\infty\int_0^{2\pi}\hat{c}(k_1,k_2,t)\,\hat{c}^*(k_1,k_2,t)\,d\theta_k\,S(t)\,dt\right)^{1/2} \\ &\times \left(4\,\pi^2\,N\,k\int_0^\infty\int_0^{2\pi}\hat{c}(k_1,k_2,t+\sigma)\,\hat{c}^*(k_1,k_2,t+\sigma)\,d\theta_k\,S(t)\,dt\right)^{1/2}. \end{aligned} \tag{3.14}$$

If the velocity field of the vortex decays sufficiently fast far from the origin, we have that $\hat{v}_l(k_1,k_2,t) = i\,k^{-2}\,\epsilon_{lmn}\,k_m\,\hat{\omega}_n(k_1,k_2,t)$, where $\omega_i(x_1,x_2,t)$ is the vorticity field, and $\hat{\omega}_i(k_1,k_2,t)$ is its Fourier transform. Assuming that $\omega_1 = \omega_2 = 0$, and using $k_l\,\hat{\omega}_l = 0$, it is then easy to show from equations (3.5) and (3.11) that

$$\check{R}(k,\sigma)\,E(k) = \frac{1}{k}\,2\,\pi^2\,N\int_0^\infty\int_0^{2\pi}\hat{\omega}_3(k_1,k_2,t)\,\hat{\omega}_3^*(k_1,k_2,t+\sigma)\,d\theta_k\,S(t)\,dt, \tag{3.15}$$

where $E(k)$ is given by

$$\begin{aligned} E(k) &= \left(\frac{1}{k}\,2\,\pi^2\,N\int_0^\infty\int_0^{2\pi}\hat{\omega}_3(k_1,k_2,t)\,\hat{\omega}_3^*(k_1,k_2,t)\,d\theta_k\,S(t)\,dt\right)^{1/2} \\ &\times \left(\frac{1}{k}\,2\,\pi^2\,N\int_0^\infty\int_0^{2\pi}\hat{\omega}_3(k_1,k_2,t+\sigma)\,\hat{\omega}_3^*(k_1,k_2,t+\sigma)\,d\theta_k\,S(t)\,dt\right)^{1/2}. \end{aligned} \tag{3.16}$$

Decomposing $\omega_3(r,\theta,t)$ as in equation (2.81), gives that

$$\check{R}(k,\sigma)=\frac{\sum_{n=-\infty}^{\infty}\int_0^\infty I_n^\omega(k,t)\,I_n^{\omega*}(k,t+\sigma)\,S(t)\,dt}{(\sum_{n=-\infty}^{\infty}A_n^\omega(k,\sigma))^{1/2}\,(\sum_{n=-\infty}^{\infty}A_n^\omega(k,0))^{1/2}}, \tag{3.17}$$

where

$$A_n^\omega(k,\sigma)=\int_0^\infty |I_n^\omega(k,t+\sigma)|^2\,S(t)\,dt, \tag{3.18}$$

and $I_n^\omega(k,t)$ is given by (2.84). This can be simplified by using $I_{-n}^\omega = I_n^{\omega*}\,(-1)^n$ to give that $I_{-n}^\omega(k,t)\,I_{-n}^{\omega*}(k,t+\sigma)=I_n^{\omega*}(k,t)\,I_n^\omega(k,t+\sigma)$. Omitting the zeroth harmonic contribution we have that

$$\check{R}(k,\sigma)=\frac{\sum_{n=1}^{\infty}\int_0^\infty Re(I_n^\omega(k,t)\,I_n^{\omega*}(k,t+\sigma))\,S(t)\,dt}{(\sum_{n=1}^{\infty}A_n^\omega(k,\sigma))^{1/2}\,(\sum_{n=1}^{\infty}A_n^\omega(k,0))^{1/2}}. \tag{3.19}$$

Similarly for the passive scalar,

$$\check{R}^c(k,\sigma)=\frac{\sum_{n=1}^{\infty}\int_0^\infty Re(I_n^c(k,t)\,I_n^{c*}(k,t+\sigma))\,S(t)\,dt}{(\sum_{n=1}^{\infty}A_n^c(k,\sigma))^{1/2}\,(\sum_{n=1}^{\infty}A_n^c(k,0))^{1/2}}, \tag{3.20}$$

where $c(r,\theta,t)=\sum_{n=-\infty}^{\infty}\mathcal{C}_n(r,t)\,\exp(i\,n\,\theta)$, and $A_n^c$ and $I_n^c$ are defined by replacing $\omega_n$ with $\mathcal{C}_n$ in equation (2.84), and $I_n^\omega$ with $I_n^c$ in equation (3.18).

It remains to specify $\omega_n(r,t)$ and $\mathcal{C}_n(r,t)$. A more detailed analysis of the asymptotic solutions we will use is given in section 2.2.1, but we will summarize the results needed here. Following Lundgren [29], we introduce stretched coordinates $\rho$ and $\tau$ given by

$$\rho = S(t)^{1/2}\,r, \qquad \tau=\frac{1}{a}\,(S(t)-1). \tag{3.21}$$

We also define $\Omega(\rho)$ as the azimuthally averaged angular velocity, related to $\omega_0$ by

$$\omega_0 = \frac{1}{r}\frac{\partial(r^2\,\Omega)}{\partial\, r}, \tag{3.22}$$

and set $\Lambda(\rho) = d\Omega(\rho)/d\rho$. Then the following approximate solution to the Navier-Stokes equations is asymptotically accurate for large time,

$$\omega_n(r,t) = S(t)\, f_n(\rho)\, \exp(-i\, n\, \Omega(\rho)\, \tau - \nu\, n^2\, \Lambda(\rho)^2\, \tau^3/3), \qquad n \geq 1. \tag{3.23}$$

Here $\nu$ is the viscosity, and the arbitrary functions $f_n(\rho)$ specify the initial condition of the vorticity.

The scalar differs from the vorticity in that it is not amplified by stretching, and it can be shown that [40]

$$\mathcal{C}_n(r,t) = g_n(\rho)\, \exp(-i\, n\, \Omega(\rho)\, \tau - D\, n^2\, \Lambda(\rho)^2\, \tau^3/3), \qquad n \geq 1. \tag{3.24}$$

is a solution to the scalar advection diffusion equation, asymptotically accurate for large time, where $D$ is the diffusivity and $g_n(\rho)$ are arbitrary functions specifying the initial condition for the scalar. Comparing with expressions (2.65), we see that (3.24) is the lower order part of the asymptotic solution for the scalar.

### 3.2.2 Asymptotic evaluation

We will now use an asymptotic analysis to evaluate the expressions (3.19) and (3.20) for $\check{R}(k,\sigma)$ and $\check{R}^c(k,\sigma)$, respectively. First we concentrate on $\check{R}(k,\sigma)$, and use the method of stationary phase to evaluate $I_n^\omega(k,t)$ for large wavenumber and large time

[29],

$$\begin{aligned} I_n^\omega(k,t) &= \int_0^\infty J_n\left(\frac{k\,\rho}{(1+a\,\tau)^{1/2}}\right) f_n(\rho)\,\exp(-i\,n\,\Omega(\rho)\,\tau - \nu\,n^2\,\Lambda(\rho)^2\,\tau^3\,/3)\,\rho\,d\rho \\ &\simeq (1+a\,\tau)^{1/4}\,k^{-1/2}\,\rho_s^{1/2}\,f_n(\rho_s)\,(n\,\Delta(\rho_s)\,\tau)^{-1/2}\,i^{n+1/2}\,\times \\ &\quad \exp(i(-k\,\rho_s\,(1+a\,\tau)^{-1/2} - n\,\Omega(\rho_s)\,\tau - \pi/4) - n^2\,\tau^3\,\nu\,\Lambda^2(\rho_s)/3), \end{aligned} \tag{3.25}$$

where we have assumed $\Lambda(\rho)$ is monotonic, $\Delta(\rho) = d\Lambda(\rho)/d\rho$, and the point of stationary phase $\rho_s$ is given by $k + n\,\Lambda(\rho_s)\,\tau\,(1+a\tau)^{1/2} = 0$. Further assuming that only large $(a\,\tau)$ will be important gives

$$k\,n^{-1}\,\Lambda(\rho_s)^{-1}\,a^{-1/2}\tau^{-3/2} = 1 + O\left(\frac{1}{a\tau}\right). \tag{3.26}$$

The integral $I_n^\omega(k, t+\sigma)$ is approximated by the right hand side of equation (3.25) evaluated at $t+\sigma$, so that $\tau$ is replaced by

$$\tau' = \frac{1}{a}\,(e^{a\sigma}\,(a\,\tau + 1) - 1), \tag{3.27}$$

and $\rho_s$ is replaced by $\rho_s'$ where $k + n\,\Lambda(\rho_s')\,\tau'\,(1+a\tau')^{1/2} = 0$. Noting that $\Lambda^2(\rho_s')\,\tau'^3 \simeq \Lambda^2(\rho_s)\,\tau^3$ for a given $n$ and $k$ implies that the viscous parts of $I_n^\omega(k,t)$ and $I_n^\omega(k, t+\sigma)$ are similar for large $(a\tau)$.

We now restrict the range of delay times $\sigma$ that we are concerned with so that we can relate $I_n^\omega(k, t+\sigma)$ to $I_n^\omega(k,\sigma)$. Let $r_0$ be the characteristic length scale for $\Omega(\rho)$, and assume for simplicity that this is the same for $f_n(\rho)$. We then restrict attention to the range $(k\,r_0)^{2/3}\,(a\,\sigma)^2 \ll 1$ and $(k\,r_0) \gg 1$, so that $(a\sigma) \ll 1$. However $(kr_0)^{2/3}(a\sigma)$ is assumed to be order one or greater. Then to leading order $\rho_s' \simeq \rho_s$, $f_n(\rho_s') \simeq f_n(\rho_s)$, $\tau_s' \simeq \tau_s$, and $\Delta(\rho_s') \simeq \Delta(\rho_s)$, where higher order terms are a factor $(a\sigma)$ smaller in magnitude. However care must be taken with the argument of the complex exponential in equation (3.25), $w_n(\rho) = -k\,\rho_s\,(a\,\tau)^{-1/2} - n\,\Omega(\rho_s)\,\tau$. When we substitute our asymptotic expressions for $I_n^\omega(k,t)$ and $I_n^\omega(k, t+\sigma)$ in the numerator of

equation (3.19) for $\check{R}(k,\sigma)$, $(w_n(\rho_s') - w_n(\rho_s))$ cannot be neglected. Making a change of integration variables from $t$ to $\rho_s$ in equation (3.19), we find that

$$\check{R}(k,\sigma) \simeq \frac{\sum_{n=1}^{\infty} n^{-4/3} \int_0^{\infty} \Lambda(\rho_s)^{-4/3} |f_n(\rho_s)|^2 \rho_s \cos(w_n(\rho_s') - w_n(\rho_s)) d\rho_s}{\sum_{n=1}^{\infty} n^{-4/3} \int_0^{\infty} \Lambda(\rho_s)^{-4/3} |f_n(\rho_s)|^2 \rho_s \, d\rho_s}. \quad (3.28)$$

The viscous parts of $I_n^{\omega}(k, t+\sigma)$ and $I_n^{\omega}(k,t)$ are identical and independent of $t$ to within the current approximation, and so factor out.

It remains to find $w_n(\rho_s') - w_n(\rho_s)$ to leading order; see Appendix G. The result is

$$w_n(\rho_s') - w_n(\rho_s) = k^{2/3} \sigma \, n^{1/3} \, a^{2/3} \, e(\rho_s) + O((k\, r_0)^{2/3} \, (a\, \sigma)^2) + O(a\sigma), \quad (3.29)$$

where

$$e(\rho_s) = \left( \frac{|\Lambda(\rho_s)|^{1/3} \rho_s}{2} - \frac{\Omega(\rho)}{|\Lambda(\rho_s)|^{2/3}} \right). \quad (3.30)$$

Substituting into equation (3.28) we find

$$\check{R}(k,\sigma) \simeq \frac{\sum_{n=1}^{\infty} n^{-4/3} \int_0^{\infty} |\Lambda(\rho_s)|^{-4/3} |f_n(\rho_s)|^2 \rho_s \cos(k^{2/3} \sigma \, n^{1/3} \, a^{2/3} \, e(\rho_s)) \, d\rho_s}{\sum_{n=1}^{\infty} n^{-4/3} \int_0^{\infty} |\Lambda(\rho_s)|^{-4/3} |f_n(\rho_s)|^2 \rho_s \, d\rho_s}, \quad (3.31)$$

and so to leading order $\check{R}(k,\sigma)$ only depends on $k$ and $\sigma$ in the combination $k^{2/3}\sigma$, in a similar way to the inertial time scaling.

The analysis for the scalar goes through in a similar way. Comparing the expressions for the vorticity (3.23) and the scalar (3.24), we see that the scalar is similar to the vorticity except for the stretching factor $S(t)$. This leads to an extra factor $(a\tau)^{-1} \simeq k^{-2/3} \, n^{2/3} \, |\Lambda(\rho_s)|^{2/3} \, a^{-2/3}$ in the approximation for $I_n^c(k,t)$, and we find that

$$\check{R}^c(k,\sigma) \simeq \frac{\sum_{n=1}^{\infty} \int_0^{\infty} |g_n(\rho_s)|^2 \rho_s \cos(k^{2/3} \sigma \, n^{1/3} \, a^{2/3} \, e(\rho_s)) \, d\rho_s}{\sum_{n=1}^{\infty} \int_0^{\infty} |g_n(\rho_s)|^2 \rho_s \, d\rho_s}. \quad (3.32)$$

It is interesting to note that there is no dependence on the diffusivity in expression (3.32).

If we further assume that $a \simeq (\epsilon/(15\nu))^{1/2}$, and let $\Gamma$ and $r_0$ be the characteristic

circulation and length scales of the vortex core, respectively, then the dependence on $k$ in expressions (3.31) and (3.32) is of the form

$$k^{2/3}\,\sigma\,\epsilon^{1/3}\,\left(\frac{\Gamma}{\nu}\right)^{1/3}. \tag{3.33}$$

Thus the winding of the vorticity and the scalar has lead to an inertial timescale $k^{-2/3}\,\epsilon^{-1/3}$, although there is also a dependence on the vortex Reynolds number $\Gamma/\nu$. The viscosity enters expressions (3.31) and (3.32) only through our assumption about the strain-rate $a$, and as we mentioned before, there is no dependence on the scalar diffusivity in expression (3.32). Note that the preceding analysis is valid for large wavenumber, in the dissipation range as well as the inertial range.

### 3.2.3 Numerical evaluation

Expressions (3.19) and (3.20) were evaluated numerically for $\check{R}(k,\sigma)$ and $\check{R}^c(k,\sigma)$ using an implementation of adaptive Gauss-Konrod integration in the GNU Scientific Library [10]. This will be more accurate than the asymptotic approach of section (3.2.2), but specific choices have to be made, for example, the precise form of $\Omega(\rho)$ must be specified. We first define the non-dimensional parameters (indicated with an overbar), $r = \bar{r}\,r_0$, $\sigma = \bar{\sigma}/a$, $\omega_n = \bar{\omega}_n(\bar{r})\,\Gamma/r_0^2$, $\mathcal{C}_n = \bar{\mathcal{C}}_n(\bar{r})\,c_c$, $\Omega = \bar{\Omega}(\bar{r})\,\Gamma/r_0^2$, and $k = \bar{k}/r_0$. Here $r_0$ is the characteristic length scale, $\Gamma$ is the characteristic circulation of the vortex, and $c_c$ is a characteristic value of the scalar. We also define the Kolmogorov length scale $\eta = (\frac{\nu^3}{\epsilon})^{1/4}$ and estimate the strain rate as $a = (\frac{\epsilon}{15\,\nu})^{1/2}$, where $\epsilon$ is the energy dissipation. The Schmidt number was set to unity, and the following choices were made for the two remaining non-dimensional numbers

$$\frac{\Gamma}{\nu} = 10^7, \qquad \frac{r_0}{\eta} = 15^{1/4}\,\left(\frac{\Gamma}{\nu}\right)^{1/2}. \tag{3.34}$$

These values were chosen because they were found numerically to give a clear inertial range for the energy spectrum obtained from expression (3.13). The value for $\Gamma/\nu$ is much higher than is used in section 3.3.1, where the aim is to compare with simulation,

and in sections 2.2.3 and 2.5 where the primary aim is to compare with experiment. The initial conditions for the non-axisymmetric part of the vorticity and the scalar were chosen to be

$$\begin{aligned} \bar{\mathcal{C}}_1(\bar{r},0) = \bar{\omega}_1(\bar{r},0) &= A\,\exp(-\bar{r}^2), \\ \bar{\mathcal{C}}_n(\bar{r},0) = \bar{\omega}_n(\bar{r},0) &= 0,\ |n|>1, \end{aligned} \tag{3.35}$$

where $\check{R}(k,\sigma)$ and $\check{R}^c(k,\sigma)$ are independent of the non-dimensional constant $A$. The azimuthally averaged angular velocity was chosen to be $\bar{\Omega}(\bar{r}) = \bar{r}^{-1/2}\,\exp(-\bar{r}^2)$, ensuring that $\bar{\Lambda}(\bar{r})$ is monotonic (see later in this section). The viscous diffusion of the vortex core was neglected.

The resulting graphs for $\check{R}(k,\sigma)$ and $\check{R}^c(k,\sigma)$ are shown in Figures 3.1(a) and 3.1(b) at $\bar{k}=200$, and Figures 3.2(a) and 3.2(b) at $\bar{k}=3000$, compared with their asymptotic expressions (3.31) and (3.32).

Numerical evaluation of expression (3.13) for $E(k)$ (setting $\sigma=0$) indicates that $\bar{k}=200$ is representative of the inertial range, and that $\bar{k}=3000$ is representative of the dissipation range, see Figure 3.3. The agreement between the asymptotics and the numerical results is reasonable for $\bar{k}^{2/3}\bar{\sigma}^2$ small enough, with better agreement for the higher value of $\bar{k}$. However the main success of the asymptotic analysis is in capturing the $(\bar{k}^{2/3}\,\bar{\sigma})$ dependence.

Similar results were found for other choices of $\bar{\Omega}(\bar{r})$, $\bar{\omega}_n(\bar{r},0)$ and $\bar{c}_n(\bar{r},0)$, as long as $\bar{\Lambda}(\bar{r})$ was monotonic. If $\bar{\Lambda}(\bar{r})$ is not monotonic, for example, in the case of a Gaussian angular velocity $\bar{\Omega}(\bar{r}) = \exp(-\bar{r}^2)$, then there will be more than one point of stationary phase in the asymptotic analysis, and our results (3.31) and (3.32) are no longer valid. Numerically we find that for a Gaussian $\bar{\Omega}(\bar{r})$, the dependence on $k$ and $\sigma$ if of the form $(\bar{k}^{5/6}\,\bar{\sigma})$. Finally, it is noted that $\check{R}(k,\sigma)$ and $\check{R}^c(k,\sigma)$, calculated using the stretched-spiral vortex model, do not necessarily remain positive, unlike results from direct numerical simulation and experiment.

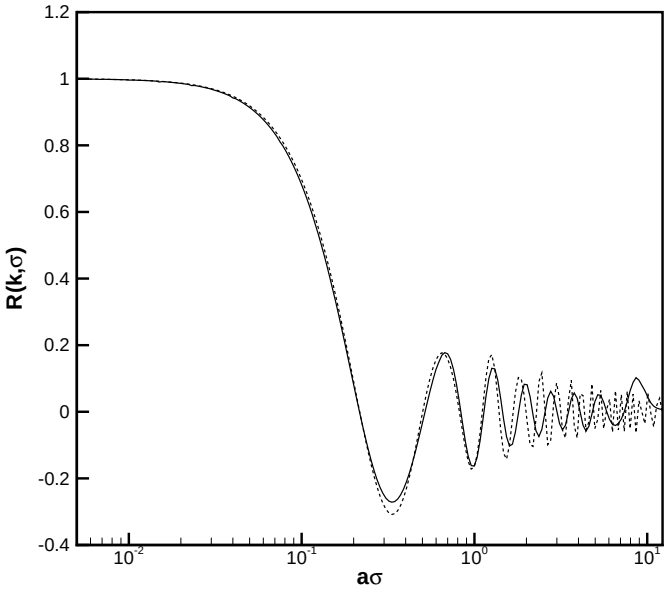


(a)

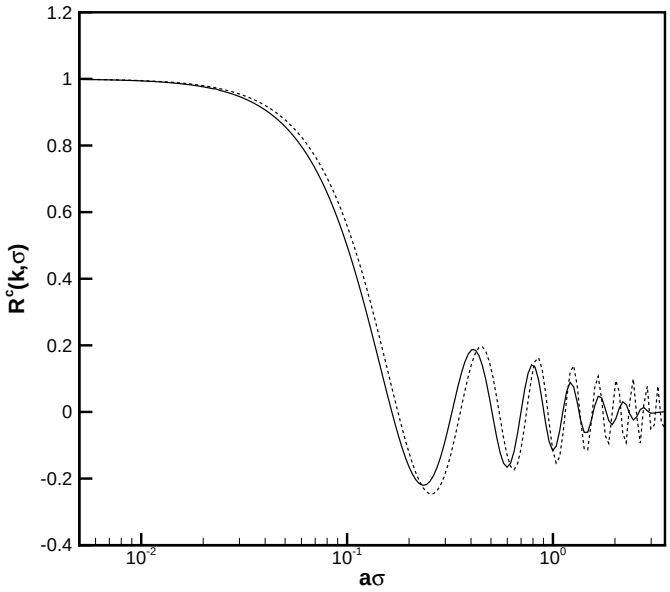


(b)

Figure 3.1: (a) $\check{R}(k,\sigma)$ and (b) $\check{R}^c(k,\sigma)$ for $\bar{k} = 200$ from the stretched-spiral vortex model with stationary vortex structure centers; numerical evaluation (full line), asymptotic evaluation (dashed line).

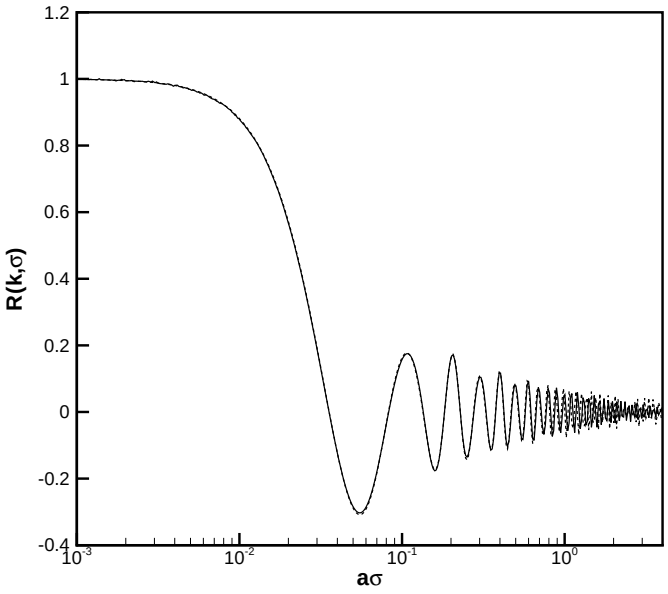


(a)

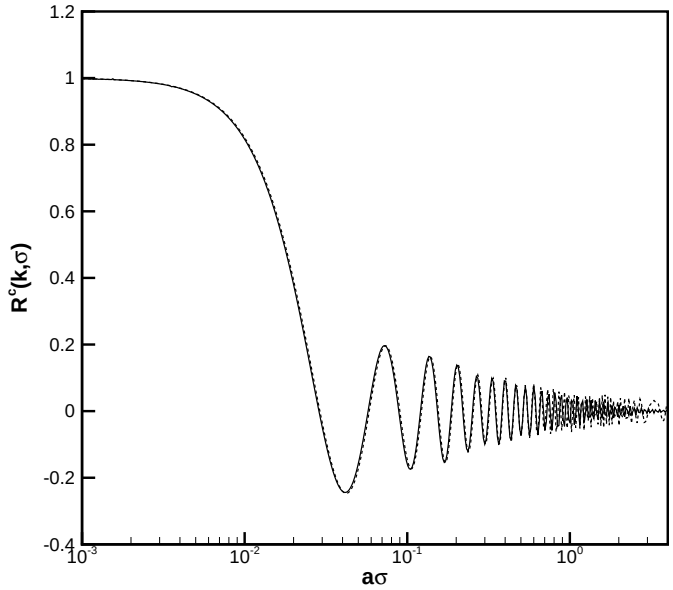


(b)

Figure 3.2: (a) $\check{R}(k,\sigma)$ and (b) $\check{R}^c(k,\sigma)$ for $\bar{k} = 3000$ from the stretched-spiral vortex model with stationary vortex structure centers; numerical evaluation (full line), asymptotic evaluation (dashed line).

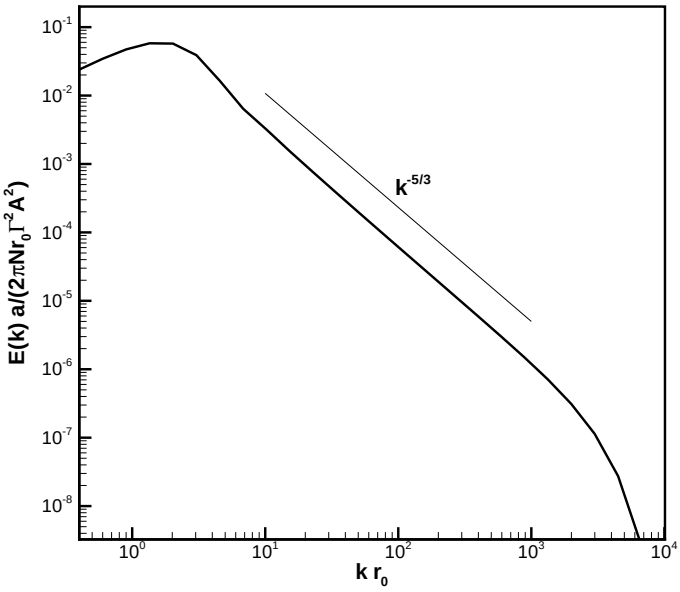


Figure 3.3: Energy spectrum from the non-axisymmetric vorticity for the stretched-spiral vortex model.

### 3.2.4 Vortex structures with moving centers

We are considering two-time statistics and the preceding analysis is valid only if the centers of the vortex structures remain stationary. We will now generalize to the case where the vortex structures are allowed to move with a constant velocity relative to the frame in which measurements are made. Each structure in the ensemble has its own velocity, $\mathbf{U}$, with the probability distribution for this velocity assumed isotropic and independent of all other parameters (e.g., vortex orientation). We denote the velocity in a frame moving with the vortex structure by $\check{\mathbf{u}}(\check{\mathbf{x}})$, where $\check{\mathbf{x}}$ are structure fixed coordinates. The velocity in the vortex structure is given by $\mathbf{u}(\mathbf{x},t) = \check{\mathbf{u}}(\mathbf{x}+\mathbf{U}\,t,t)+\mathbf{U}$. The numerator in the definition of $R(k,\sigma)$, equation (3.5), is then given by

$$\frac{1}{(2\pi)^3}\int_S\int_V\left(\int\langle\check{\mathbf{u}}_i(\mathbf{x}-\mathbf{U}t,t)\,\check{\mathbf{u}}_i(\mathbf{x}-\mathbf{U}(t+\sigma)+\mathbf{r},t+\sigma)\rangle p(\mathbf{U})\,d\mathbf{U}\right)e^{-i\mathbf{k}\cdot\mathbf{r}}d\mathbf{r}\,dS_k \tag{3.36}$$

where $\langle\cdot\rangle$ represents the averages over time, space and vortex orientation in the stretched-spiral vortex model. The $\int p(\mathbf{U})\,d\mathbf{U}$ integral implements an average over the gross velocities of the structures in the ensemble. The denominator in equation

(3.5) involves single time statistics that are not influenced by $\mathbf{U}$. Making the change of integration variables $\check{\mathbf{r}} = \mathbf{r} - \mathbf{U}\,\sigma$ and $\check{\mathbf{x}} = \mathbf{x} - \mathbf{U}\,t$, we find that

$$R(k,\sigma) = \left( \int p(\mathbf{U})\, e^{-i\mathbf{k}\cdot\mathbf{U}\,\sigma} d\mathbf{U} \right) \check{R}(k,\sigma), \tag{3.37}$$

where $\check{R}$ is the modal correlation function for vortex structures with stationary centers. We have used the fact that the $\mathbf{r}$ integration is over an infinite volume, while the $\mathbf{x}$ integral (representing a spatial average) is over an infinite interval in two directions perpendicular to the vortex axis, and the integrand is independent of the coordinate parallel to the vortex axis. The distribution of $\mathbf{U}$ is isotropic, so that we can write $p(\mathbf{U}) = P(\frac{|\mathbf{U}|}{u_{gross}})$ for a non-dimensional function $P$ and a characteristic velocity $u_{gross}$, and so $R(k,\sigma) = f(k\,u_{gross}\,\sigma)\,\check{R}(k,\sigma)$, for some function $f$. Thus, unsurprisingly, the constant motion of the structures has introduced a sweeping timescale $(k\,u_{gross})^{-1}$.

For example, if $p(\mathbf{U}) = (2\pi u_{rms}^2)^{-3/2} \exp(-|\mathbf{U}|^2/(2\,u_{rms}^2))$ where $u_{rms}$ is the rms turbulent velocity, then

$$R(k,\sigma) = \exp(-k^2\,u_{rms}^2\,\sigma^2/2)\,\check{R}(k,\sigma). \tag{3.38}$$

Note that the factor $\exp(-k^2\,u_{rms}^2\,\sigma^2/2)$ is the same as Kraichnan's linearized estimate for $R(k,\sigma)$ [25]. The analysis for the scalar modal correlation function is identical, and so

$$R^c(k,\sigma) = \exp(-k^2\,u_{rms}^2\,\sigma^2/2)\,\check{R}^c(k,\sigma), \tag{3.39}$$

where $\check{R}^c$ is the scalar modal correlation function for vortex structures with stationary centers.

## 3.3 Direct numerical simulation

The modal time correlation functions for both velocity and scalar fields were calculated in a DNS at $R_\lambda$ of 265. A basic description of the DNS is given in section 2.4.1 The modal time correlation functions were calculated for a set of $n_{shell}$ wavenumbers

$\{k^i\}$, and $n_{delay}$ time delays $\{\sigma^i\}$. They were calculated at several times $\{T_i\}$, and an average was then taken for the final results. The intervals between the $T_i$'s were greater than the maximum $\sigma^i$. For a given $T_j$, the velocity and scalar fields were needed at the $n_{delay}$ times $t = T_j - \sigma^i$. To minimize storage requirements the velocity and scalar fields were stored only in the wavenumber shells $\{k^i\}$ at these times. The $\{\sigma^i\}$ were chosen to be multiples of the simulation timestep. The above method requires the timestep to be fixed throughout the stationary period of the simulation, and so the Courant number must be chosen to be lower than for a simulation with a variable timestep.

Results from the $512^3$ simulation for the modal correlation function of the velocity are shown in Figure 3.4(a), and for the scalar in Figure 3.4(b). These are replotted using the sweeping time-scaling in Figures 3.5(a) and 3.5(b), and inertial time-scaling in Figures 3.6(a) and 3.6(b). The best collapse is for the sweeping timescale for both the velocity and the scalar. The collapse occurs for wavenumbers in the inertial-convective and dissipation ranges.

In Figure 3.7 we compare the modal time correlation functions for the velocity and the scalar. We see that, for sufficiently large wavenumber, the modal time correlation functions coincide. This is consistent with the picture of the primary decorrelation mechanism for the small scale structures (in both the velocity and the scalar) being convection by the large scale motions.

### 3.3.1 Comparison of DNS and the stretched-spiral vortex model

To compare with the predictions of the stretched-spiral vortex model for the modal time correlation functions, we needed to choose some parameters to characterize the vortex structures in the model. We used $u_{rms}$, $\epsilon$ and $\nu$ from the DNS with $a = (\frac{\epsilon}{15\,\nu})^{1/2}$, and let the characteristic length scale of the vortex structures, $r_0$, be the Taylor length scale. We set the vortex Reynolds number $\Gamma/\nu$ to 200, noting that it should at least be below the Taylor Reynolds number of 265. The initial vorticity and scalar profiles

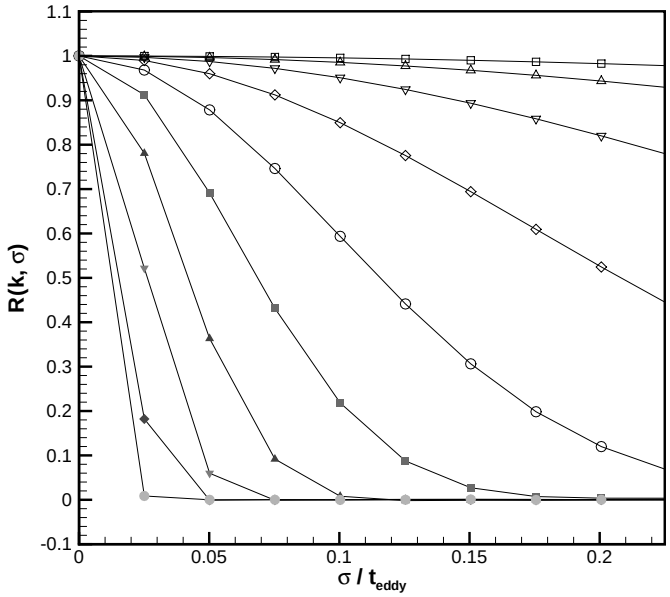


(a)

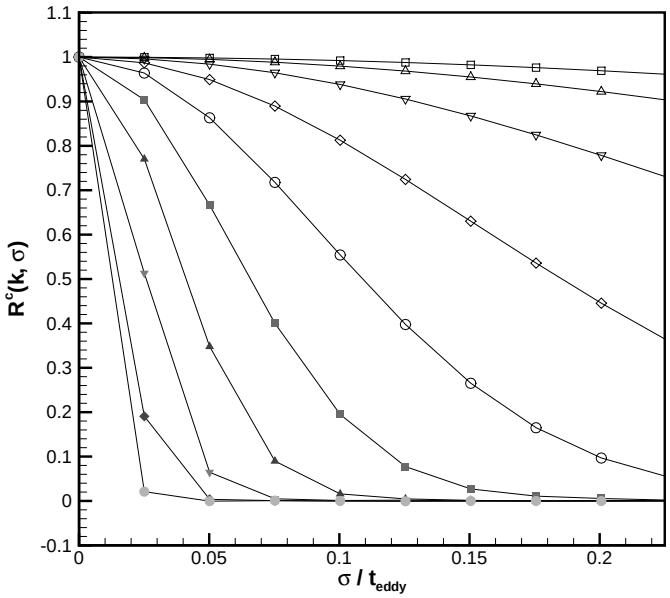


(b)

Figure 3.4: DNS results for the modal correlation function of (a) the velocity, and (b) the scalar: □ $k\eta = 0.0087$, △ $k\eta = 0.0137$, ▽ $k\eta = 0.0216$, ◇ $k\eta = 0.0341$, ○ $k\eta = 0.0538$, ■ $k\eta = 0.0848$, ▲ $k\eta = 0.134$, ▼ $k\eta = 0.211$, ♦ $k\eta = 0.332$, ● $k\eta = 0.524$.

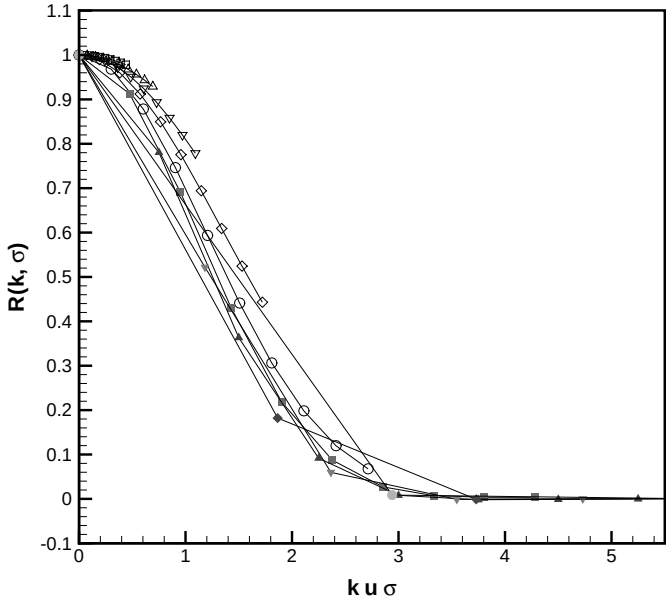


(a)

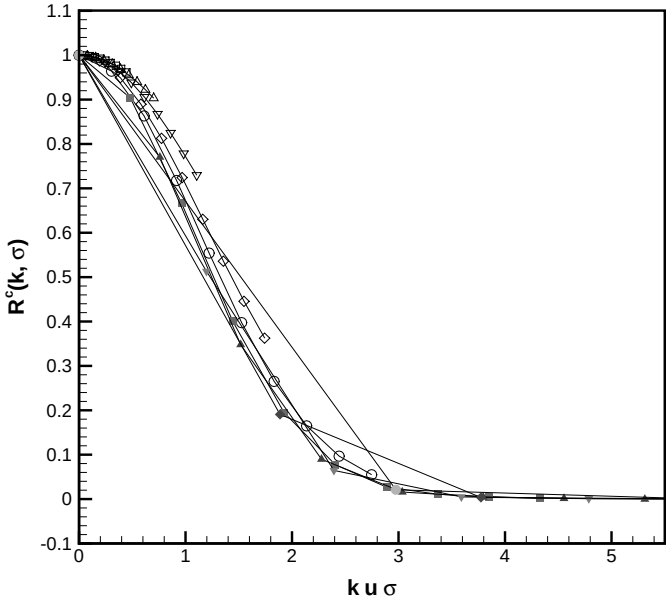


(b)

Figure 3.5: DNS results for the modal correlation function of (a) the velocity, and (b) the scalar using the sweeping time scaling. See Figure 6 for the key to the symbols used.

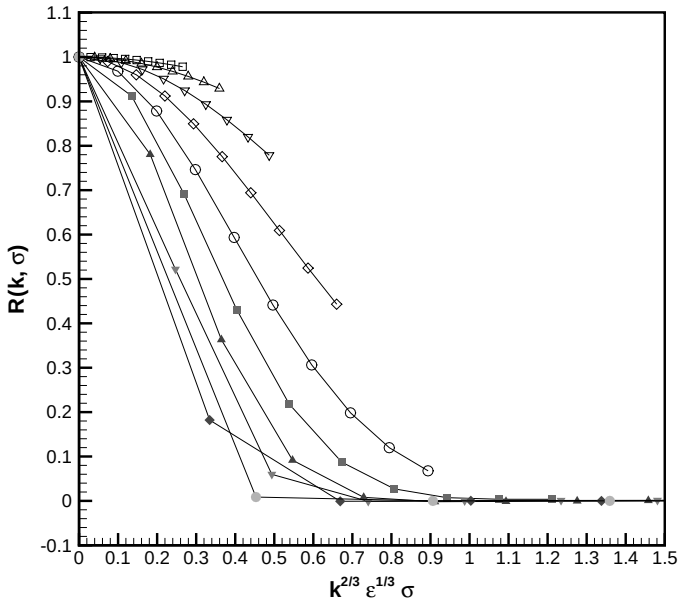


(a)

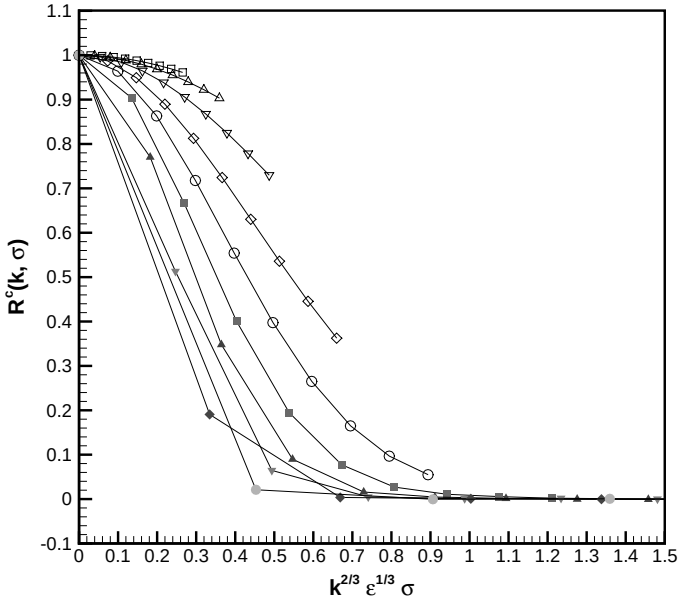


(b)

Figure 3.6: DNS results for the modal correlation function of (a) the velocity, and (b) the scalar using the inertial time scaling. See Figure 6 for the key to the symbols used.

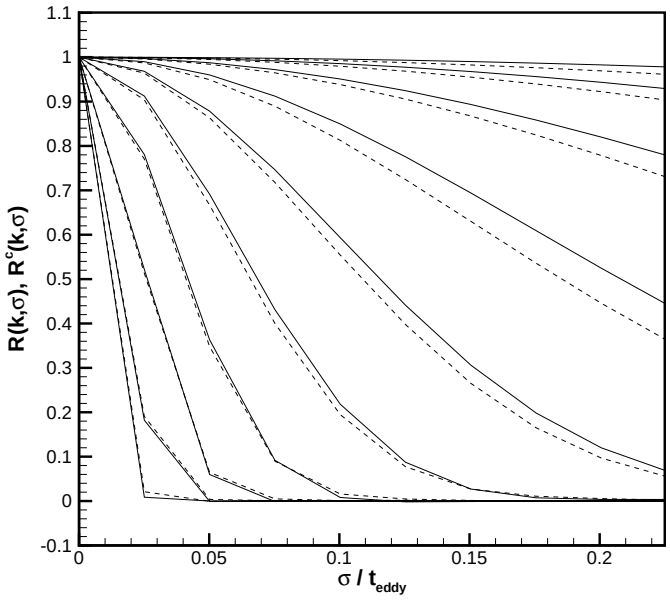


Figure 3.7: Comparison of DNS results for the modal time correlation function of the velocity (full line) and the scalar (dashed line) using the same wavenumbers as in Figure 6.

were the same as used in section (3.2.3). The results for the stretched-spiral vortex model were calculated using numerical evaluation of (3.19) and (3.20) for $\check{R}(k,\sigma)$ and $\check{R}^c(k,\sigma)$ in expressions (3.38) and (3.39), respectively.

In Figures 3.8 and 3.9 the DNS and stretched-spiral vortex model results are compared for representative wavenumbers $k\eta = 0.0848$ and $k\eta = 0.211$. These wavenumbers correspond to $kr_0 = 2.72$ and $kr_0 = 6.76$, respectively. We do not consider smaller values of $kr_0$ because the stretched-spiral vortex model is only considered appropriate for the fine scales within the vortex structures. Also shown are the convective part, $\exp(-k^2\, u_{rms}^2\, \sigma^2/2)$, and the winding parts $\check{R}(k,\sigma)$ and $\check{R}^c(k,\sigma)$, that make up the stretched-spiral vortex model results. Clearly for these wavenumbers the convective part is dominant. It is important to note that for other Reynolds numbers, and other values of the parameters (e.g., the vortex length scale $r_0$) the spiral winding may be more significant.

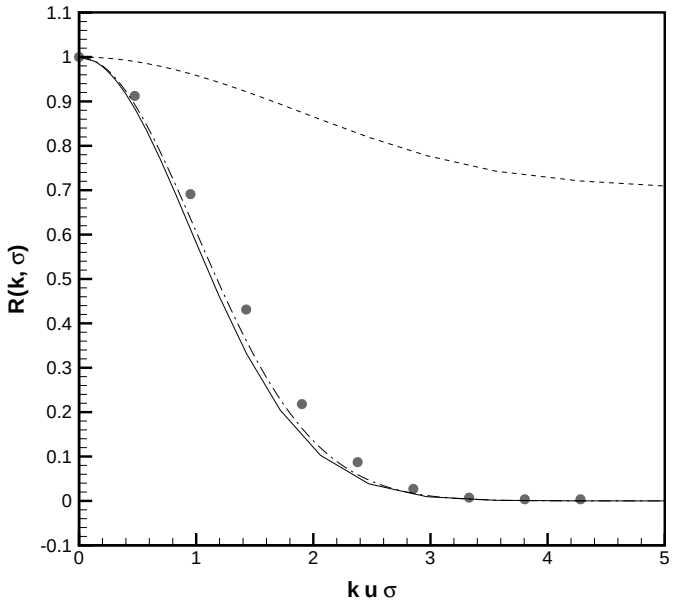


(a)

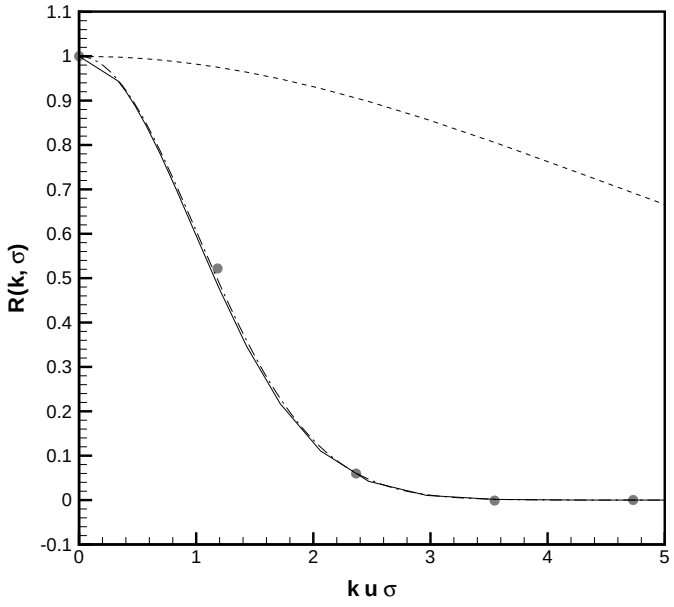


(b)

Figure 3.8: $R(k,\sigma)$ at (a) $k\eta = 0.0848$, and (b) $k\eta = 0.211$: DNS results ●, stretched-spiral vortex model (full line). Also shown are $\exp(-k^2\, u_{rms}^2\, \sigma^2/2)$ (dash-dotted line), and $\check{R}(k,\sigma)$ (dashed line).

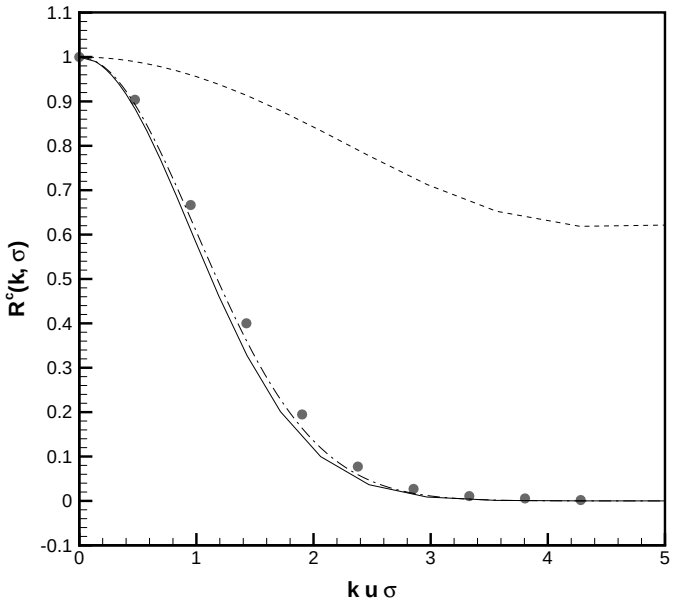


(a)

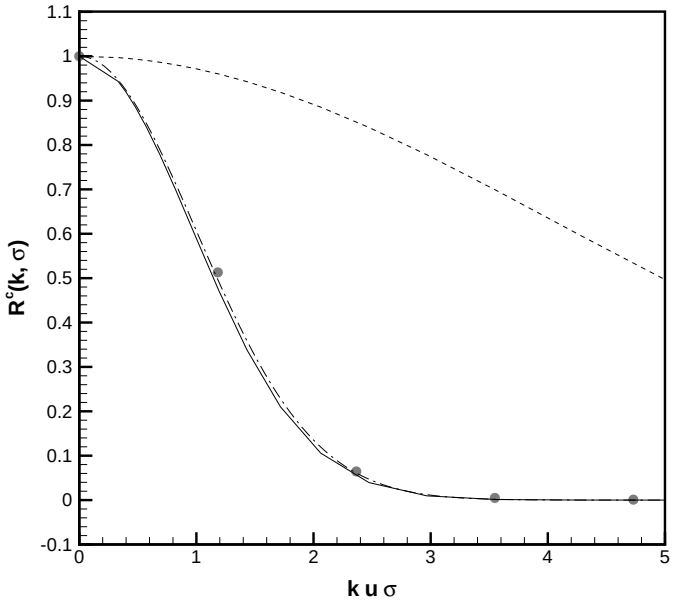


(b)

Figure 3.9: $R^c(k,\sigma)$ at (a) $k\eta = 0.0848$, and (b) $k\eta = 0.211$: DNS results ●, stretched-spiral vortex model (full line). Also shown are $\exp(-k^2\, u_{rms}^2\, \sigma^2/2)$ (dash-dotted line), and $\check{R}^c_{stat}(k,\sigma)$ (dashed line).

# Chapter 4 Conclusions and Future Work

The problem of passive-scalar mixing with a mean scalar gradient has been studied, with particular attention being paid to the distribution of the scalar flux across scales, and the characteristic timescales of the Fourier modes of the velocity and scalar fields.

Several properties of the velocity-scalar cospectrum were examined in this study. In the inertial-convective range the SDIP result for the cospectrum was shown to agree with the Lumley $\mu\,\epsilon^{1/3}\,k^{-7/3}$ scaling [28]. The result for the cospectrum from the stretched-spiral vortex model could be split into two additive components. An asymptotic form was found for the component contributed by the axial velocity field, with a $k^{-5/3}$ wavenumber dependence at leading order. The next-order term had a $k^{-7/3}$ range, and the sign of its coefficient depended on the initial conditions. The component of the cospectrum contributed by the velocity field in the plane of the vortex was also calculated, but its form was found to depend on the choice of vortex core. A new feature of the analysis was the use of a solution for the scalar in the stretched vortex, where the scalar could vary in the axial direction. This allowed the contribution of the axial velocity to the cospectrum be taken in to account, but restricted the calculation to Schmidt number unity. Results for the cospectrum from a direct numerical simulation at Schmidt number 0.7 were also presented. A comparison was made of the experimental data of Mydlarski and Warhaft [34] with the results from the SDIP, the stretched-spiral vortex model, and the DNS. The cospectral slopes at the beginning of the inertial-convective range were all found to be shallower than $k^{-7/3}$, where Mydlarski and Warhaft had found $k^{-2}$ at their largest $R_\lambda$. The decay of the cospectrum with wavenumber in the inertial-convective range was found to be faster than that of the scalar or the energy spectra, and this is consistent with the idea of an approach to isotropy at small scales.

The effect on the cospectrum of different Schmidt numbers was also investigated. An upper bound was derived for the magnitude of the cospectrum in terms of the shell-

summed energy and scalar spectra, with the implication that at high Schmidt number the cospectrum would decay exponentially with wavenumber in the viscous-convective range. This limits the possible contribution of sub-Kolmogorov lengthscales to the mean scalar flux, a result that may be important in subgrid modeling of the scalar flux. At low Schmidt number the argument of Batchelor, Howells, and Townsend [2] for the form of the scalar spectrum in the inertial-diffusive range was modified to include the effect of the mean scalar gradient. Using a similar argument, a new asymptotic form was found for the velocity-scalar cospectrum, with a $k^{-11/3}$ power law wavenumber dependence in the inertial-diffusive range. The inertial-diffusive results for the cospectrum and the scalar spectrum were confirmed using LES with no subgrid model for the scalar field, and are in principle subject to experimental verification, perhaps using a liquid metal. It is interesting to note that at least in this regime, the forcing of the scalar fluctuation by the mean scalar gradient is important at small wavenumber for both the scalar spectrum and the velocity-scalar cospectrum. Although the derivation of the SDIP equation for the cospectrum was rather complicated, one advantage is that it was then relatively inexpensive to investigate a wide range of Schmidt numbers. Using the SDIP equation, the asymptotic form of the cospectrum in the inertial-diffusive range was confirmed and extended to the viscous-diffusive range. At high Schmidt number the SDIP result for the cospectrum was indeed found to decay exponentially in the viscous-convective range, as was expected from the cospectrum inequality.

Moving now to the study of two-time statistics, the stretched-spiral vortex model has been shown to predict two characteristic timescales for the velocity and scalar modal time correlation functions. An inertial timescale arises from the winding of the vorticity and the scalar by the vortex cores, and a sweeping timescale arises from the movement of the centers of the vortex structures. Thus the model provides an integrated treatment of both these decorrelation mechanisms. Many studies have been performed on the modal time correlation function of the velocity field, but here we have also considered the modal time correlation function of a passive scalar. The stretched-spiral vortex model predicts a similar form for both functions, and this

is borne out by the results from the DNS. The DNS results for both the velocity and scalar modal time correlation functions were well collapsed using the sweeping timescale.

It is perhaps appropriate at this point to make a brief comparison of the two theories of turbulence used here, namely, the SDIP and the stretched-spiral vortex model. The stretched-spiral vortex model is a structure-based model, where turbulence is modeled as an ensemble of vortex structures, and then statistics such as spectra [29, 40], structure functions [43], or modal time correlations may be calculated numerically, and sometimes asymptotically. One disadvantage is that there are many unknown parameters such as the background strain rate, or the orientation probability density function of the vortex structures. In contrast, the SDIP has no free parameters. However the SDIP is formulated as a two-point closure theory in a Lagrangian framework, with corresponding limitations on the statistics that it can be used to calculate. For example, in the context of the work described here, the SDIP gives a result for the Lagrangian two-point, two-time velocity and scalar correlations, but not the Eulerian two-point, two-time correlations discussed in Chapter 3.

Possibilities for future work include the use of the cospectrum results to help build subgrid models for the scalar flux. Pullin and Saffman [42] were able to relate subgrid stress terms to the energy spectrum and orientation pdf of subgrid vortex structures, and this result together with the stretched-spiral vortex model was used by Misra and Pullin [32] to perform successful large-eddy simulations. It may be possible to do something similar for the subgrid terms in the passive scalar equation using the velocity-scalar cospectrum, although this is made difficult by the nature of the stretched-spiral vortex model result for the cospectrum, for example, the dependence of the planar contribution on the choice of vortex core. A comparison with the vortex-based subgrid scalar flux model of Pullin [38] would also be useful.

Another interesting possibility for future work is the calculation of the scalar spectrum using the SDIP in the case of a mean scalar gradient. Goto and Kida [14] considered the case of the scalar spectrum for a statistically isotropic scalar field. Here we have considered the case of a statistically non-isotropic scalar field, but the

cospectrum was nonetheless describable using a single isotropic function because of the condition of incompressibility. The SDIP calculation of the scalar spectrum in the axisymmetric case would be more difficult, but it would be interesting to see, for example, the effect of the mean scalar gradient on the Obukhov-Corrsin constant. Also, because the SDIP equation for the passive scalar spectrum would then involve the velocity-scalar cospectrum, in a sense some of the work has already been done.

# Appendix A Properties of the velocity-scalar cross spectrum

The velocity field is assumed to be statistically isotropic and homogeneous. The scalar fluctuation is statistically homogeneous, with the mean scalar gradient given by the vector $\mu_i$. We define $\mathcal{F}_{u_ic}(\mathbf{k})$ to be the Fourier transform of $\mathcal{R}_{u_ic}(\mathbf{r})$,

$$\mathcal{F}_{u_ic}(\mathbf{k}) = \frac{1}{(2\pi)^3} \int \mathcal{R}_{u_ic}(\mathbf{r}) e^{-i\,\mathbf{k}\cdot\mathbf{r}} d\mathbf{r}. \tag{A.1}$$

Then $\mathcal{F}_{u_ic}$ is a first-order tensor that is axisymmetric about $\mu_i$, and so must have the following form

$$\mathcal{F}_{u_ic}(\mathbf{k}) = A_1\, k_i + A_2\, \mu_i, \tag{A.2}$$

where $A_1$ and $A_2$ are functions of $k_i\mu_i$, $k$ and $\mu$. Using the incompressibility of the velocity field we have that

$$k_i\, \mathcal{F}_{u_ic} = A_1\, k^2 + A_2\, \mu_i\, k_i = 0. \tag{A.3}$$

Using this relation, and defining $A_3 = -A_1\, k^2/(\mu_j k_j)$, we find that

$$\mathcal{F}_{u_ic}(\mathbf{k}) = A_3(k, \mu, k_j\mu_j) \left( \mu_i - \frac{k_j\mu_j}{k^2}\, k_i \right). \tag{A.4}$$

We will now use the fact that the equation governing the scalar is linear. If the spectrum is measured after a sufficiently long time, the effect of initial fluctuations about the mean gradient will have decayed to zero, and the scalar fluctuation must have a linear dependence on the vector $\mu_i$. Also $\mathcal{F}_{u_ic}(\mathbf{k})$ depends linearly on the scalar, and so must also depend linearly on $\mu_i$. Therefore $A_3 = A_3(k)$ is a function of $k$, and has no dependence on $k_i\mu_i$ or $\mu$. A similar analysis to the above is given in

Herr, Wang and Collins [17].

We will now use this simplified form for $\mathcal{F}_{u_ic}(\mathbf{k})$ to relate the shell-summed cospectrum and one-dimensional cross spectrum. We specialize to the case where $\mu_1 = \mu$ and $\mu_2 = \mu_3 = 0$, and consider the one-dimensional cross spectrum in the $k_3$ direction. Then it is easy to show that

$$F^{1D}_{u_ic}(k_3) = \int_{-\infty}^{\infty}\int_{-\infty}^{\infty} \mathcal{F}_{u_ic}(\mathbf{k})\, dk_1\, dk_2. \tag{A.5}$$

Changing to polar coordinates $k_1 = k^{2d}\cos\theta$ and $k_2 = k^{2d}\sin\theta$, and performing the $\theta$ integral gives $F^{1D}_{u_2c}(k_3) = F^{1D}_{u_3c}(k_3) = 0$. Making a further change of integration variables from $k^{2d}$ to $k$ gives

$$F^{1D}_{u_ic}(k_3) = \mu\,\pi \int_{k_3}^{\infty} A_3(k)\, \left(k + \frac{k_3^2}{k}\right)\, dk. \tag{A.6}$$

We can also find the shell-summed cospectrum in terms of $A_3(k)$ as follows,

$$C_{u_ic}(k) = \int_S \mathcal{F}_{u_ic}(\mathbf{k})\, dS_k. \tag{A.7}$$

Using spherical polar coordinates we find that $C_{u_2c}(k) = C_{u_3c}(k) = 0$, and

$$C_{u_1c}(k) = \frac{8\pi}{3}\, k^2\, A_3(k)\, \mu. \tag{A.8}$$

Then comparing (A.6) and (A.8) we have that

$$F^{1D}_{u_1c}(k_3) = \frac{3}{8} \int_{k_3}^{\infty} \frac{k^2 + k_3^2}{k^3}\, C_{u_1c}(k)\, dk. \tag{A.9}$$

Finally we can easily show that the quadrature spectrum, $Q^{1D}_{u_1c}(k_3)$, must be zero. Noting that $\mathcal{F}_{u_ic}(\mathbf{k})$ is the Fourier transform of a real function gives $\mathcal{F}_{u_ic}(-\mathbf{k}) = \mathcal{F}^*_{u_ic}(\mathbf{k})$. Also equation (A.4) implies that $\mathcal{F}_{u_ic}(-\mathbf{k}) = \mathcal{F}_{u_ic}(\mathbf{k})$, and so $A_3(k)$ is real, and the quadrature spectrum must be zero.

# Appendix B Effect on the scalar spectrum of axial scalar variation

In their calculation of the scalar spectrum PL assumed that the scalar had no $x_3$ dependence. We will now consider the effect of an $x_3$ dependence in the particular case when the scalar initial condition is given by a gradient in the lab frame. An expression for the scalar spectrum is given by replacing $M_{ji}\, v_j(\mathbf{x},t)$ with $c^t(\mathbf{x},t)$ in equation (2.70),

$$E_c(k) = \frac{N^c}{(2\pi)^3} < \langle \int_S \int_V \int_0^{t_c} \int_V c^t(\mathbf{x},t)\, c^t(\mathbf{x}+\mathbf{r},t)\, e^{-i\,\mathbf{k}\cdot\mathbf{r}}\, d\mathbf{x}\, dt\, d\mathbf{r}\, dS_k \rangle >, \quad \text{(B.1)}$$

where we are working in vortex fixed coordinates. We decompose $c(\mathbf{x},t)$ using equation (2.50), and assume the initial conditions (2.51). We set $c'(\mathbf{x},0) = 0$, because our solution (2.54) for $c_3$ is only valid for a linear initial condition. This approximation was not necessary in the case of the cross spectrum, where we were able to eliminate the $c'$ contribution by making an assumption about the statistical distribution of initial conditions. The orientation average may be performed immediately using the integrals (2.72) to give

$$E_c(k) = \frac{N^c}{3\,(2\pi)^3} \langle \int_S \int_V \int_0^{t_c} \int_V \sum_{j=1}^{3} c_j(\mathbf{x},t)\, c_j(\mathbf{x}+\mathbf{r},t)\, e^{-i\,\mathbf{k}\cdot\mathbf{r}}\, d\mathbf{x}\, dt\, d\mathbf{r}\, dS_k \rangle. \quad \text{(B.2)}$$

The terms in the integrand involving $c_1$ and $c_2$ have no $x_3$ dependence and so were dealt with in PL. We will consider $E_{c_3}$,the contribution from $c_3$. We assume $\nu = D$

and use solution (2.54) for $c_3$. Then we have that

$$\begin{aligned} c_3(\mathbf{x},t)\, c_3(\mathbf{x}+\mathbf{r},t) &= \mu^2\, \exp(-2\,at)\, (x_3\, r_3 + x_3^2) \\ &- \mu^2\, a^{-1} \exp(-at)\, \sinh(at)\, (x_3\, v_3(\mathbf{x}+\mathbf{r},t) + x_3\, v_3(\mathbf{x},t) + r_3\, v_3(\mathbf{x},t)) \\ &+ \mu^2\, a^{-2}\, \sinh^2(at)\, v_3(\mathbf{x},t)\, v_3(\mathbf{x}+\mathbf{r},t) \end{aligned} \tag{B.3}$$

We will now show that the first term in (2.54) does not contribute to the scalar spectrum. Noting that $v_3(\mathbf{x})$ has no $x_3$ dependence, terms in (B.3) that are linear in $x_3$ will be eliminated upon integration over $x_3$. Also terms that are linear in $v_3$ will be eliminated by performing the average over initial conditions. The term involving $x_3^2$ will not contribute to the high wavenumber spectrum. Therefore the only contribution comes from the second term of (2.54). We again simplify by replacing the average over initial conditions with one particular initial condition.

Changing to Fourier space using (2.74), and after some algebra, we find

$$E_{c_3}(k) = \frac{N(2\pi)^2}{3} \int_0^{t_c} \int_0^{2\pi} \mu^2\, a^{-2}\, \sinh^2(at)\, \hat{u}_3\, \hat{v_3}^*\, k\, d\theta_k\, S(t)\, dt. \tag{B.4}$$

This is very similar to expression (2.77) for the axial contribution to the cross spectrum, except for a factor in the integrand of $-\mu/a\, \sinh(at)$. Following a similar analysis to sections 2.2.2 and 2.2.2, and keeping terms in the integrand of $O(\tau^{-1})$, we find

$$\begin{aligned} E_{c_3}(k) &= \frac{2\pi\mu^2 N}{9}\, k^{-1}\, a^{-3}\, \exp\left(-\frac{2\,\nu\,k^2}{3\,a}\right) \sum_{n=1}^{\infty} \int_0^{\infty} \rho\, |\check{\mathcal{U}}_n^{(0)}(\rho)|^2\, d\rho \\ &+ \frac{4\pi\mu^2 N}{9}\, k^{-5/3}\, a^{-8/3}\, \exp\left(-\frac{\nu\,k^2}{3\,a}\right) \sum_{n=1}^{\infty} n^{2/3} \int_0^{\infty} |\Lambda(\rho)|^{2/3}\, Re\left(\check{\mathcal{U}}_n^{(0)}(\rho)\Pi_n^*\right)\, d\rho. \end{aligned} \tag{B.5}$$

Thus the new contribution to $E_c$ is a combination of $k^{-1}$ and $k^{-5/3}$ power laws in a certain range. The wavenumber dependence is the same as was found in PL, equations (81-85), for scalar initial conditions with no $x_3$ dependence, and so the new contribution does not alter the nature of the spectrum.

# Appendix C SDIP evolution equations for $\tilde{W}_i(\mathbf{k},t,t)$ and $\tilde{W}_i(\mathbf{k},t,t')$

Here we will give the derivations of equations (2.162) and (2.164). Our starting point is the exact equation (2.143) for the evolution of $\tilde{W}_i(\mathbf{k},t,t)$. Decomposing the velocity and scalar fields, and making use of assumption (ii), the two triple correlations in equation (2.143) may be written as

$$-i\,k_j\left(\frac{2\pi}{L}\right)^6 \sum_{\substack{\mathbf{p}\\(\mathbf{k}+\mathbf{p}+\mathbf{q}=0)}}\sum_{\mathbf{q}} \Big[\ \overline{\tilde{u}_j^{(1)}(-\mathbf{p},t\|\mathbf{k},\mathbf{p},\mathbf{q})\,\tilde{c}^{(0)}(-\mathbf{q},t\|\mathbf{k},\mathbf{p},\mathbf{q})\,\tilde{u}_i^{(0)}(-\mathbf{k},t\|\mathbf{k},\mathbf{p},\mathbf{q})} + \overline{\tilde{u}_j^{(0)}(-\mathbf{p},t\|\mathbf{k},\mathbf{p},\mathbf{q})\,\tilde{c}^{(1)}(-\mathbf{q},t\|\mathbf{k},\mathbf{p},\mathbf{q})\,\tilde{u}_i^{(0)}(-\mathbf{k},t\|\mathbf{k},\mathbf{p},\mathbf{q})} + \overline{\tilde{u}_j^{(0)}(-\mathbf{p},t\|\mathbf{k},\mathbf{p},\mathbf{q})\,\tilde{c}^{(0)}(-\mathbf{q},t\|\mathbf{k},\mathbf{p},\mathbf{q})\,\tilde{u}_i^{(1)}(-\mathbf{k},t\|\mathbf{k},\mathbf{p},\mathbf{q})}\Big] \tag{C.1}$$

$$+\frac{i}{2}\left(\frac{2\pi}{L}\right)^6 \tilde{P}_{ijm}(\mathbf{k}) \sum_{\substack{\mathbf{p}\\(\mathbf{k}+\mathbf{p}+\mathbf{q}=0)}}\sum_{\mathbf{q}} \Big[\ \overline{\tilde{u}_j^{(1)}(\mathbf{p},t\|\mathbf{k},\mathbf{p},\mathbf{q})\,\tilde{u}_m^{(0)}(\mathbf{q},t\|\mathbf{k},\mathbf{p},\mathbf{q})\,\tilde{c}^{(0)}(\mathbf{k},t\|\mathbf{k},\mathbf{p},\mathbf{q})} + \overline{\tilde{u}_j^{(0)}(\mathbf{p},t\|\mathbf{k},\mathbf{p},\mathbf{q})\,\tilde{u}_m^{(1)}(\mathbf{q},t\|\mathbf{k},\mathbf{p},\mathbf{q})\,\tilde{c}^{(0)}(\mathbf{k},t\|\mathbf{k},\mathbf{p},\mathbf{q})} + \overline{\tilde{u}_j^{(0)}(\mathbf{p},t\|\mathbf{k},\mathbf{p},\mathbf{q})\,\tilde{u}_m^{(0)}(\mathbf{q},t\|\mathbf{k},\mathbf{p},\mathbf{q})\,\tilde{c}^{(1)}(\mathbf{k},t\|\mathbf{k},\mathbf{p},\mathbf{q})}\Big] \tag{C.2}$$

Note that we choose $\mathbf{k}$, $\mathbf{p}$, and $\mathbf{q}$ as the triad of non-interacting wavenumbers for each term in the double summation. Consider the first term of (C.1). We can substitute

for the velocity deviation field using the following expression derived in [24],

$$\begin{aligned}\tilde{u}_i^{(1)}(\mathbf{k},t\|\mathbf{k}_0,\mathbf{p}_0,\mathbf{q}_0) &= i\,\frac{(2\pi)^9}{L^6}\,\tilde{P}_{abc}(\mathbf{k})\int_{t_0}^{t} dt'\,\tilde{G}_{ia}^{(E0)}(\mathbf{k},t|-\mathbf{k},t'\|\mathbf{k}_0,\mathbf{p}_0,\mathbf{q}_0)\\ &\times\ [\,-\delta^3_{\mathbf{k}-\mathbf{k}_0}\,\tilde{u}_b^{(0)}(-\mathbf{p}_0,t'\|\mathbf{k}_0,\mathbf{p}_0,\mathbf{q}_0)\,\tilde{u}_c^{(0)}(-\mathbf{q}_0,t'\|\mathbf{k}_0,\mathbf{p}_0,\mathbf{q}_0)\\ &-\ \delta^3_{\mathbf{k}+\mathbf{k}_0}\,\tilde{u}_b^{(0)}(\mathbf{p}_0,t'\|\mathbf{k}_0,\mathbf{p}_0,\mathbf{q}_0)\,\tilde{u}_c^{(0)}(\mathbf{q}_0,t'\|\mathbf{k}_0,\mathbf{p}_0,\mathbf{q}_0)\\ &+\ (\mathbf{k}_0\to\mathbf{p}_0\to\mathbf{q}_0\to\mathbf{k}_0)\,]\,, \end{aligned} \tag{C.3}$$

so that

$$\begin{aligned}&[\text{first term of (C.1)}] =\\ &k_j\,\frac{(2\pi)^{15}}{L^{12}}\sum_{\substack{\mathbf{p}\\(\mathbf{k}+\mathbf{p}+\mathbf{q}=0)}}\sum_{\mathbf{q}}\tilde{P}_{abc}(\mathbf{p})\int_{t_0}^{t}dt'\,\overline{\tilde{G}_{ja}^{(E0)}(-\mathbf{p},t|\mathbf{p},t'\|\mathbf{k},\mathbf{p},\mathbf{q})}\\ &\overline{\times\,\tilde{u}_b^{(0)}(\mathbf{k},t'\|\mathbf{k},\mathbf{p},\mathbf{q})\,\tilde{u}_c^{(0)}(\mathbf{q},t'\|\mathbf{k},\mathbf{p},\mathbf{q})\,\tilde{c}^{(0)}(-\mathbf{q},t\|\mathbf{k},\mathbf{p},\mathbf{q})\,\tilde{u}_i^{(0)}(-\mathbf{k},t\|\mathbf{k},\mathbf{p},\mathbf{q})}. \end{aligned} \tag{C.4}$$

This is rewritten using assumption (ii) as

$$\begin{aligned}&[\text{first term of (C.1)}] =\\ &=k_j\,\frac{(2\pi)^{15}}{L^{12}}\sum_{\substack{\mathbf{p}\\(\mathbf{k}+\mathbf{p}+\mathbf{q}=0)}}\sum_{\mathbf{q}}\tilde{P}_{abc}(\mathbf{p})\int_{t_0}^{t}dt'\,\overline{\tilde{G}_{ja}^{(E0)}(-\mathbf{p},t|\mathbf{p},t'\|\mathbf{k},\mathbf{p},\mathbf{q})}\\ &\times\overline{\tilde{u}_b^{(0)}(\mathbf{k},t'\|\mathbf{k},\mathbf{p},\mathbf{q})\,\tilde{u}_i^{(0)}(-\mathbf{k},t\|\mathbf{k},\mathbf{p},\mathbf{q})}\;\overline{\tilde{u}_c^{(0)}(\mathbf{q},t'\|\mathbf{k},\mathbf{p},\mathbf{q})\,\tilde{c}^{(0)}(-\mathbf{q},t\|\mathbf{k},\mathbf{p},\mathbf{q})}. \end{aligned} \tag{C.5}$$

Next we make use of results derived in Appendix E,

$$\tilde{W}_i(\mathbf{k},t,t') = \left(\frac{2\pi}{L}\right)^3\overline{\tilde{c}^{(0)}(\mathbf{k},t\|\mathbf{k}_0,\mathbf{p}_0,\mathbf{q}_0)\,\tilde{u}_i^{(0)}(-\mathbf{k},t'\|\mathbf{k}_0,\mathbf{p}_0,\mathbf{q}_0)}. \tag{C.6}$$

and in [24],

$$\tilde{Q}_{ij}(\mathbf{k},t,t') = \left(\frac{2\pi}{L}\right)^3\overline{\tilde{u}_i^{(0)}(\mathbf{k},t\|\mathbf{k}_0,\mathbf{p}_0,\mathbf{q}_0)\,\tilde{u}_j^{(0)}(-\mathbf{k},t'\|\mathbf{k}_0,\mathbf{p}_0,\mathbf{q}_0)}, \tag{C.7}$$

$$\overline{\tilde{G}_{ij}^{(E0)}(\mathbf{k},t|\mathbf{k}',t'\|\mathbf{k}_0,\mathbf{p}_0,\mathbf{q}_0)} = \overline{\tilde{G}_{ij}^{(L0)}(t|\mathbf{k},\mathbf{k}',t'\|\mathbf{k}_0,\mathbf{p}_0,\mathbf{q}_0)}, \tag{C.8}$$

$$\frac{(2\pi)^6}{L^3}\,\overline{\tilde{G}^{(L0)}_{im}(t|\mathbf{k},-\mathbf{k},t'\|\mathbf{k}_0,\mathbf{p}_0,\mathbf{q}_0)}\,\tilde{P}_{mj}(\mathbf{k})=\tilde{G}_{ij}(\mathbf{k},t,t'), \tag{C.9}$$

to find

$$\begin{aligned}[\text{first term of (C.1)}] &= k_j\left(\frac{2\pi}{L}\right)^3\sum_{\substack{\mathbf{p}\\(\mathbf{k}+\mathbf{p}+\mathbf{q}=0)}}\sum_{\mathbf{q}}\int_{t_0}^{t}dt'\,\tilde{Q}_{ib}(-\mathbf{k},t,t')\,\tilde{W}_c(-\mathbf{q},t,t')\\ &\times\ \Big[p_c\,\tilde{G}_{jb}(-\mathbf{p},t,t')+p_b\,\tilde{G}_{jc}(-\mathbf{p},t,t')\Big]. \end{aligned}\tag{C.10}$$

Turning now to the second term of (C.1), we perform a similar procedure, and begin by substituting for $\tilde{c}^{(1)}(-\mathbf{q},t\|\mathbf{k},\mathbf{p},\mathbf{q})$ according to equation (2.161). We use assumption (i) to change $\tilde{u}_j$ to $\tilde{u}^{(0)}_j$, and also make use of assumption (ii) to find

$$\begin{aligned}&[\text{second term of (C.1)}]\\ &= k_j\,\frac{(2\pi)^{15}}{L^{12}}\sum_{\substack{\mathbf{p}\\(\mathbf{k}+\mathbf{p}+\mathbf{q}=0)}}\sum_{\mathbf{q}}q_l\int_{t_0}^{t}dt'\,\overline{\tilde{G}^{E(0)}(-\mathbf{q},t|\mathbf{q},t'\|\mathbf{k},\mathbf{p},\mathbf{q})}\\ &\times\Big[\overline{\tilde{u}^{(0)}_j(-\mathbf{p},t\|\mathbf{k},\mathbf{p},\mathbf{q})\,\tilde{u}^{(0)}_l(\mathbf{p},t'\|\mathbf{k},\mathbf{p},\mathbf{q})}\;\overline{\tilde{c}^{(0)}(k,t'\|\mathbf{k},\mathbf{p},\mathbf{q})\,\tilde{u}^{(0)}_i(-\mathbf{k},t\|\mathbf{k},\mathbf{p},\mathbf{q})}\\ &\quad+\overline{\tilde{u}^{(0)}_l(\mathbf{k},t'\|\mathbf{k},\mathbf{p},\mathbf{q})\,\tilde{u}^{(0)}_i(-\mathbf{k},t\|\mathbf{k},\mathbf{p},\mathbf{q})}\;\overline{\tilde{c}^{(0)}(p,t'\|\mathbf{k},\mathbf{p},\mathbf{q})\,\tilde{u}^{(0)}_j(-\mathbf{p},t\|\mathbf{k},\mathbf{p},\mathbf{q})}\Big]. \end{aligned}\tag{C.11}$$

It is shown in Appendix E that

$$\tilde{X}_i(\mathbf{k},t,t')=\left(\frac{2\pi}{L}\right)^3\overline{\tilde{u}^{(0)}_i(\mathbf{k},t\|\mathbf{k}_0,\mathbf{p}_0,\mathbf{q}_0)\,\tilde{c}^{(0)}(-\mathbf{k},t'\|\mathbf{k}_0,\mathbf{p}_0,\mathbf{q}_0)}, \tag{C.12}$$

and in [14] that

$$\overline{\tilde{G}^{E(0)}(\mathbf{k},t|-\mathbf{k},t'\|\mathbf{k}_0,\mathbf{p}_0,\mathbf{q}_0)}=\overline{\tilde{G}^{(L)}(t|\mathbf{k},-\mathbf{k},t')}, \tag{C.13}$$

so that

$$\begin{aligned}[\text{second term of (C.1)}] &= k_j \frac{(2\pi)^9}{L^6} \sum_{\substack{\mathbf{p} \\ (\mathbf{k}+\mathbf{p}+\mathbf{q}=0)}} \sum_{\mathbf{q}} q_l \int_{t_0}^{t} dt' \, \overline{\tilde{G}^{(L)}(t|-\mathbf{q},\mathbf{q},t')} \\ &\times \Big[\tilde{Q}_{jl}(-\mathbf{p},t,t')\,\tilde{X}_i(-\mathbf{k},t,t') + \tilde{Q}_{il}(-\mathbf{k},t,t')\,\tilde{X}_j(-\mathbf{p},t,t')\Big]. \end{aligned} \tag{C.14}$$

It remains to find a more useful expression for $\overline{\tilde{G}^{(L)}(t|\mathbf{k},-\mathbf{k},t')}$. From equation (2.149) we can write

$$\begin{aligned} \frac{\partial}{\partial t}\overline{\tilde{G}^{(L)}(t|\mathbf{k},-\mathbf{k},t')} &= -D\,\frac{(2\pi)^6}{L^3} \sum_{\mathbf{p}} p^2\, \overline{\tilde{G}^{(E)}(\mathbf{p},t|-\mathbf{k},t')\,\tilde{\phi}(-\mathbf{p},t|\mathbf{k},t')} \\ &= -D\,\frac{(2\pi)^6}{L^3} \sum_{\mathbf{p}} p^2\, \overline{\tilde{G}^{E(0)}(\mathbf{p},t|-\mathbf{k},t'\|\mathbf{k}_0,\mathbf{p}_0,\mathbf{q}_0)\,\tilde{\phi}^{(0)}(-\mathbf{p},t|\mathbf{k},t'\|\mathbf{k}_0,\mathbf{p}_0,\mathbf{q}_0)} \\ &= -D\,k^2\,\overline{\tilde{G}^{E(0)}(\mathbf{k},t|-\mathbf{k},t'\|\mathbf{k}_0,\mathbf{p}_0,\mathbf{q}_0)} \\ &= -D\,k^2\,\overline{\tilde{G}^{(L)}(t|\mathbf{k},-\mathbf{k},t')}, \end{aligned} \tag{C.15}$$

where we have used assumptions (i) and (iii), and (E.2) and (C.13). This can be solved with initial condition (2.150) to give

$$\tilde{G}^{(L)}(t|\mathbf{k},-\mathbf{k},t') = \frac{L^3}{(2\pi)^6}\,\exp[-D\,k^2\,(t-t')]. \tag{C.16}$$

Therefore,

$$\begin{aligned}[\text{second term of (C.1)}] &= k_j \frac{(2\pi)^9}{L^6} \sum_{\substack{\mathbf{p} \\ (\mathbf{k}+\mathbf{p}+\mathbf{q}=0)}} \sum_{\mathbf{q}} q_l \int_{t_0}^{t} dt' \, \exp[-D\,q^2\,(t-t')] \\ &\times \Big[\tilde{Q}_{jl}(-\mathbf{p},t,t')\,\tilde{X}_i(-\mathbf{k},t,t') + \tilde{Q}_{il}(-\mathbf{k},t,t')\,\tilde{X}_j(-\mathbf{p},t,t')\Big]. \end{aligned} \tag{C.17}$$

Performing a similar procedure on the remaining terms in (C.1) and (C.2) results in equation (2.162).

Turning now to the evolution of the two-time correlation $\tilde{W}_i(\mathbf{k}, t, t')$, we can approximate the diffusive term in (2.144) as

$$
\begin{aligned}
&- D\,\frac{(2\pi)^9}{L^6}\sum_{\mathbf{p}} p^2\,\overline{\tilde{c}(\mathbf{p},t)\,\tilde{\phi}(-\mathbf{p},t|\mathbf{k},t')\,\tilde{u}_i(-\mathbf{k},t')} \\
&= -D\,\frac{(2\pi)^9}{L^6}\sum_{\mathbf{p}} p^2\,\overline{\tilde{c}^{(0)}(\mathbf{p},t\|\mathbf{k}_0,\mathbf{p}_0,\mathbf{q}_0)\,\tilde{\phi}^{(0)}(-\mathbf{p},t|\mathbf{k},t'\|\mathbf{k}_0,\mathbf{p}_0,\mathbf{q}_0)\,\tilde{u}_i^{(0)}(-\mathbf{k},t'\|\mathbf{k}_0,\mathbf{p}_0,\mathbf{q}_0)} \\
&= -D\,\left(\frac{2\pi}{L}\right)^3 k^2\,\overline{\tilde{c}^{(0)}(\mathbf{k},t\|\mathbf{k}_0,\mathbf{p}_0,\mathbf{q}_0)\,\tilde{u}_i^{(0)}(-\mathbf{k},t'\|\mathbf{k}_0,\mathbf{p}_0,\mathbf{q}_0)} \\
&= -D\,k^2\,\tilde{W}_i(\mathbf{k},t,t'),
\end{aligned}
\tag{C.18}
$$

where we have used assumptions (i) and (iii), and equations (E.2) and (E.3). Substituting into equation (2.144) leads to (2.164).

# Appendix D SDIP evolution equation for $\tilde{X}_i(\mathbf{k}, t, t')$

Here we will outline the derivation of equation (2.165). We begin with the evolution equation (2.145) for $\tilde{Y}_i(\mathbf{k}, t, t')$. Making the DIA decompositions for the velocity, position function, and scalar fields, the viscous term becomes

$$
\begin{aligned}
&-\nu \frac{(2\pi)^9}{L^6} \sum_{\mathbf{p}} p^2 \, \overline{\tilde{c}(-\mathbf{k}, t') \, \tilde{u}_i(\mathbf{p}, t) \, \tilde{\phi}(-\mathbf{p}, t|\mathbf{k}, t')} \\
&= -\nu \frac{(2\pi)^9}{L^6} \sum_{\mathbf{p}} p^2 \, \overline{\tilde{c}^{(0)}(-\mathbf{k}, t'\|\mathbf{k}_0, \mathbf{p}_0, \mathbf{q}_0) \, \tilde{u}_i^{(0)}(\mathbf{p}, t\|\mathbf{k}_0, \mathbf{p}_0, \mathbf{q}_0) \, \tilde{\phi}^{(0)}(-\mathbf{p}, t|\mathbf{k}, t'\|\mathbf{k}_0, \mathbf{p}_0, \mathbf{q}_0)} \\
&= -\nu \left(\frac{2\pi}{L}\right)^3 k^2 \, \overline{\tilde{c}^{(0)}(-\mathbf{k}, t'\|\mathbf{k}_0, \mathbf{p}_0, \mathbf{q}_0) \, \tilde{u}_i^{(0)}(\mathbf{k}, t\|\mathbf{k}_0, \mathbf{p}_0, \mathbf{q}_0)} \\
&= -\nu \, k^2 \, \tilde{X}_i(\mathbf{k}, t, t'),
\end{aligned}
\tag{D.1}
$$

where we have used assumptions (i) and (iii), and equations (E.2) and (E.4). Again using assumptions (i), (iii), and (E.2) we see that the quadruple correlation in (2.145) leads to three terms proportional to $k_i$ (containing a deviation field $\tilde{u}_m^{(1)}(\mathbf{p}, t)$, $\tilde{u}_n^{(1)}(\mathbf{q}, t)$, and $\tilde{c}^{(1)}(-\mathbf{k}, t')$ , respectively), a term with no deviation field that is zero by assumption (ii), and the following term,

$$
\begin{aligned}
&-i \frac{(2\pi)^{12}}{L^9} \sum_{\substack{\mathbf{p} \\ (\mathbf{p}+\mathbf{q}+\mathbf{r}=0)}} \sum_{\mathbf{q}} \sum_{\mathbf{r}} \frac{r_i \, r_m \, r_n}{r^2} \\
&\times \overline{\tilde{c}^{(0)}(-\mathbf{k}, t'\|\mathbf{r}, \mathbf{p}, \mathbf{q}) \, \tilde{u}_m^{(0)}(\mathbf{p}, t\|\mathbf{r}, \mathbf{p}, \mathbf{q}) \, \tilde{u}_n^{(0)}(\mathbf{q}, t\|\mathbf{r}, \mathbf{p}, \mathbf{q}) \, \tilde{\phi}^{(1)}(\mathbf{r}, t|\mathbf{k}, t'\|\mathbf{r}, \mathbf{p}, \mathbf{q})}
\end{aligned}
\tag{D.2}
$$

We now substitute for $\tilde{\phi}^{(1)}(r,t|\mathbf{k},t'\|\mathbf{r},\mathbf{p},\mathbf{q})$ with the following equation derived in Ref. [24],

$$\begin{aligned}\tilde{\phi}^{(1)}(\mathbf{k},t|\mathbf{k}',t'\|\mathbf{k}_0,\mathbf{p}_0,\mathbf{q}_0) = -i\,k_j\,\frac{(2\pi)^9}{L^6}\int_{t'}^{t} dt''\,\tilde{\phi}^{(0)}(\mathbf{k},t|-\mathbf{k},t''\|\mathbf{k}_0,\mathbf{p}_0,\mathbf{q}_0)\\ \times\,[\,\delta^3_{\mathbf{k}-\mathbf{k}_0}\,\tilde{u}^{(0)}_j(-\mathbf{p}_0,t''\|\mathbf{k}_0,\mathbf{p}_0,\mathbf{q}_0)\,\tilde{\phi}^{(0)}(-\mathbf{q}_0,t''|\mathbf{k}',t'\|\mathbf{k}_0,\mathbf{p}_0,\mathbf{q}_0)\\ +\,\delta^3_{\mathbf{k}-\mathbf{k}_0}\,\tilde{u}^{(0)}_j(-\mathbf{q}_0,t''\|\mathbf{k}_0,\mathbf{p}_0,\mathbf{q}_0)\,\tilde{\phi}^{(0)}(-\mathbf{p}_0,t''|\mathbf{k}',t'\|\mathbf{k}_0,\mathbf{p}_0,\mathbf{q}_0)\\ +\,\delta^3_{\mathbf{k}+\mathbf{k}_0}\,\tilde{u}^{(0)}_j(\mathbf{p}_0,t''\|\mathbf{k}_0,\mathbf{p}_0,\mathbf{q}_0)\,\tilde{\phi}^{(0)}(\mathbf{q}_0,t''|\mathbf{k}',t'\|\mathbf{k}_0,\mathbf{p}_0,\mathbf{q}_0)\\ +\,\delta^3_{\mathbf{k}+\mathbf{k}_0}\,\tilde{u}^{(0)}_j(\mathbf{q}_0,t''\|\mathbf{k}_0,\mathbf{p}_0,\mathbf{q}_0)\,\tilde{\phi}^{(0)}(\mathbf{p}_0,t''|\mathbf{k}',t'\|\mathbf{k}_0,\mathbf{p}_0,\mathbf{q}_0)\\ +\,(\mathbf{k}_0\to\mathbf{p}_0\to\mathbf{q}_0\to\mathbf{k}_0)\,]\,.\end{aligned} \tag{D.3}$$

Using assumption (iii) and equation (E.2), and after some algebra, expression (D.2) becomes

$$\begin{aligned}-2\,\frac{(2\pi)^9}{L^9}\sum_{\substack{\mathbf{p}\\(\mathbf{k}+\mathbf{p}+\mathbf{q}=0)}}\sum_{\mathbf{q}}\frac{q_i\,q_m\,q_n\,q_j}{q^2}\int_{t'}^{t}dt''\\ \times\,\overline{\tilde{c}^{(0)}(-\mathbf{k},t'\|\mathbf{k},\mathbf{p},\mathbf{q})\,\tilde{u}^{(0)}_n(\mathbf{k},t\|\mathbf{k},\mathbf{p},\mathbf{q})}\;\overline{\tilde{u}^{(0)}_m(\mathbf{p},t\|\mathbf{k},\mathbf{p},\mathbf{q})\,\tilde{u}^{(0)}_j(-\mathbf{p},t''\|\mathbf{k},\mathbf{p},\mathbf{q})}.\end{aligned} \tag{D.4}$$

It is convenient to take the incompressible projection of equation (2.145), so that terms proportional to $k_i$ drop out, and use of (C.7) and (E.4) results in equation (2.165).

# Appendix E SDIP expressions for $\tilde{W}_i(\mathbf{k},t,t')$ and $\tilde{X}_i(\mathbf{k},t,t')$

Here we will relate $\tilde{W}_i(\mathbf{k},t,t')$ and $\tilde{X}_i(\mathbf{k},t,t')$ to $\tilde{c}^{(0)}(\mathbf{k},t\|\mathbf{k}_0,\mathbf{p}_0,\mathbf{q}_0)$ and $\tilde{u}_i^{(0)}(\mathbf{k},t\|\mathbf{k}_0,\mathbf{p}_0,\mathbf{q}_0)$. Starting with the definition (2.141) of $\tilde{W}_i(\mathbf{k},t,t')$, and using (2.138) and assumption (i), we can write

$$\begin{aligned}\tilde{W}_i(\mathbf{k},t,t') &= \frac{(2\pi)^9}{L^6}\sum_{\mathbf{k}'}\overline{\tilde{c}(\mathbf{k}',t)\,\tilde{\phi}(-\mathbf{k}',t|\mathbf{k},t')\,\tilde{u}_i(-\mathbf{k},t')} \\ &= \frac{(2\pi)^9}{L^6}\sum_{\mathbf{k}'}\overline{\tilde{c}^{(0)}(\mathbf{k}',t\|\mathbf{k}_0,\mathbf{p}_0,\mathbf{q}_0)\,\tilde{\phi}^{(0)}(-\mathbf{k}',t|\mathbf{k},t'\|\mathbf{k}_0,\mathbf{p}_0,\mathbf{q}_0)} \\ &\quad \overline{\times\tilde{u}_i^{(0)}(-\mathbf{k},t'\|\mathbf{k}_0,\mathbf{p}_0,\mathbf{q}_0)}. \end{aligned} \tag{E.1}$$

Then, using assumption (iii) and a result from [24],

$$\overline{\tilde{\phi}^{(0)}(\mathbf{k},t|\mathbf{k}',t'\|\mathbf{k}_0,\mathbf{p}_0,\mathbf{q}_0)} = \frac{L^3}{(2\pi)^6}\,\delta^3_{\mathbf{k}+\mathbf{k}'}, \tag{E.2}$$

gives

$$\tilde{W}_i(\mathbf{k},t,t') = \left(\frac{2\pi}{L}\right)^3\overline{\tilde{c}^{(0)}(\mathbf{k},t\|\mathbf{k}_0,\mathbf{p}_0,\mathbf{q}_0)\,\tilde{u}_i^{(0)}(-\mathbf{k},t'\|\mathbf{k}_0,\mathbf{p}_0,\mathbf{q}_0)}. \tag{E.3}$$

Similarly for $\tilde{X}_i(\mathbf{k},t,t')$ defined by (2.156),

$$\begin{aligned}\tilde{X}_i(\mathbf{k},t,t') &= \frac{(2\pi)^9}{L^6}\,\tilde{P}_{ia}(\mathbf{k})\sum_{\mathbf{k}'}\overline{\tilde{u}_a(\mathbf{k}',t)\,\tilde{\phi}(-\mathbf{k}',t|\mathbf{k},t')\,\tilde{c}(-\mathbf{k},t')} \\ &= \frac{(2\pi)^9}{L^6}\sum_{\mathbf{k}'}\overline{\tilde{u}_a^{(0)}(\mathbf{k}',t\|\mathbf{k}_0,\mathbf{p}_0,\mathbf{q}_0)\,\tilde{\phi}^{(0)}(-\mathbf{k}',t|\mathbf{k},t'\|\mathbf{k}_0,\mathbf{p}_0,\mathbf{q}_0)} \\ &\quad \overline{\times\tilde{c}^{(0)}(-\mathbf{k},t'\|\mathbf{k}_0,\mathbf{p}_0,\mathbf{q}_0)} \\ &= \left(\frac{2\pi}{L}\right)^3\overline{\tilde{u}_i^{(0)}(\mathbf{k},t\|\mathbf{k}_0,\mathbf{p}_0,\mathbf{q}_0)\,\tilde{c}^{(0)}(-\mathbf{k},t'\|\mathbf{k}_0,\mathbf{p}_0,\mathbf{q}_0)}. \end{aligned} \tag{E.4}$$

Note that we consistently have $t \geq t'$, and so equations (E.3) and (E.4) do not mean that $\tilde{W}_i(\mathbf{k}, t, t')$ and $\tilde{X}_i(\mathbf{k}, t, t')$ are equivalent in this approximation.

# Appendix F Behavior of the modal time correlation function at zero delay time

Consider the derivative of $\mathcal{R}_{jj}(\mathbf{r},t,\sigma)$ with respect to $\sigma$ evaluated at $\sigma = 0$,

$$\begin{aligned} \frac{\partial}{\partial\,\sigma}\,\mathcal{R}_{jj}(\mathbf{r},t,\sigma)\,\Big|_{\sigma=0} &= \overline{u_j(\mathbf{x},t)\,\frac{\partial}{\partial\,\sigma}\,u_j(\mathbf{x}+\mathbf{r},t+\sigma)\Big|_{\sigma=0}} \\ &= \overline{u_j(\mathbf{x},t)\,\frac{\partial}{\partial\,t}\,u_j(\mathbf{x}+\mathbf{r},t)}. \end{aligned} \tag{F.1}$$

The assumption of homogeneity then gives

$$\begin{aligned} \frac{\partial}{\partial\,\sigma}\,\mathcal{R}_{jj}(-\mathbf{r},t,\sigma)\,\Big|_{\sigma=0} &= \overline{u_j(\mathbf{x},t)\,\frac{\partial}{\partial\,t}\,u_j(\mathbf{x}-\mathbf{r},t)} \\ &= \overline{u_j(\mathbf{x}+\mathbf{r},t)\,\frac{\partial}{\partial\,t}\,u_j(\mathbf{x},t)}, \end{aligned} \tag{F.2}$$

so that

$$\frac{\partial}{\partial\,\sigma}\,\mathcal{R}_{jj}(\mathbf{r},t,\sigma)\,\Big|_{\sigma=0} + \frac{\partial}{\partial\,\sigma}\,\mathcal{R}_{jj}(-\mathbf{r},t,\sigma)\,\Big|_{\sigma=0} = \frac{\partial}{\partial\,t}\,\mathcal{R}_{jj}(\mathbf{r},t,0). \tag{F.3}$$

Then we have that

$$\begin{aligned} &\frac{\partial}{\partial\,\sigma}\,\mathcal{F}_{jj}(k,t,\sigma)\,\Big|_{\sigma=0} \\ &= \frac{1}{(2\pi)^3}\int_S\int_V \left(-\frac{\partial}{\partial\,\sigma}\,\mathcal{R}_{jj}(-\mathbf{r},t,\sigma)\,\Big|_{\sigma=0} + \frac{\partial}{\partial\,t}\,\mathcal{R}_{jj}(\mathbf{r},t,0)\right) e^{-i\mathbf{k}\cdot\mathbf{r}}d\mathbf{r}\,dS_k \\ &= -\frac{1}{(2\pi)^3}\int_S\int_V \frac{\partial}{\partial\,\sigma}\,\mathcal{R}_{jj}(\mathbf{r},t,\sigma)\,\Big|_{\sigma=0} e^{-i\mathbf{k}\cdot\mathbf{r}}d\mathbf{r}\,dS_k + 2\,\frac{\partial}{\partial t}\,E(k,t) \\ &= -\frac{\partial}{\partial\,\sigma}\,\mathcal{F}_{jj}(k,t,\sigma)\,\Big|_{\sigma=0} + 2\,\frac{\partial}{\partial t}\,E(k,t), \end{aligned} \tag{F.4}$$

where we have made a change of integration variables from $\mathbf{r}$ to $-\mathbf{r}$, and from $\mathbf{k}$ to $-\mathbf{k}$. Thus we have the result

$$\begin{aligned} \frac{\partial}{\partial \sigma} R(k,t,\sigma)\bigg|_{\sigma=0} &= \frac{\frac{\partial}{\partial \sigma}\mathcal{F}_{jj}(k,t,\sigma)\big|_{\sigma=0}}{2\,E(k,t)} - \frac{\mathcal{F}_{jj}(k,0,t)}{4\,E(k,t)^2}\frac{\partial}{\partial t}E(k,t) \\ &= 0. \end{aligned} \tag{F.5}$$

# Appendix G Asymptotic evaluation of $w_n(\rho'_s) - w_n(\rho_s)$

We wish to find $w_n(\rho'_s) - w_n(\rho_s)$ to leading order in the small parameters $\epsilon_1 = a\sigma$ and $\epsilon_2 = 1/(a\tau)$. Using equation (3.27) to relate $\tau'$ to $\tau$, we find that

$$a\tau' = a\tau + (a\sigma)(a\tau) + O(\epsilon_1) + O(\epsilon_1^2/\epsilon_2). \tag{G.1}$$

To relate $\rho'_s$ to $\rho_s$, we start with the exact relation $\Lambda(\rho'_s)\, a\tau'\, (1+a\tau')^{1/2} = \Lambda(\rho_s)\, a\tau\, (1+a\tau)^{1/2}$. Substituting for $(a\tau')$ from equation (G.1) we find

$$\Lambda(\rho'_s) = \Lambda(\rho_s)\, \left(1 - \frac{3}{2}\, a\sigma\right) + O(\epsilon_1^2) + O(\epsilon_1\ \epsilon_2). \tag{G.2}$$

Taylor expanding $\Lambda(\rho'_s)$ about $\rho_s$, and comparing with equation (G.2) we find

$$\rho'_s = \rho_s - \frac{3}{2}\, (a\sigma)\, \frac{\Lambda(\rho_s)}{\Delta(\rho_s)} + O(\epsilon_1^2) + O(\epsilon_1\ \epsilon_2). \tag{G.3}$$

Finally, Taylor expanding $\Omega(\rho'_s)$ about $\rho_s$, and using equation (G.3) gives

$$\Omega(\rho'_s) = \Omega(\rho_s) - \frac{3}{2}\, (a\sigma)\, \frac{\Lambda(\rho_s)^2}{\Delta(\rho_s)} + O(\epsilon_1^2) + O(\epsilon_1\ \epsilon_2). \tag{G.4}$$

Substituting for $\tau'$, $\rho'_s$ and $\Omega(\rho'_s)$ in the definition of $w_n(\rho'_s)$ gives

$$\begin{aligned} w_n(\rho'_s) - w_n(\rho_s) &= a\sigma\, \left(-n\, \Omega(\rho_s)\, \tau + \frac{3\, n\, \tau\, \Lambda(\rho_s)^2}{2\, \Delta(\rho_s)} + \frac{k}{(a\tau)^{1/2}}\, \left(\frac{3\, \Lambda(\rho_s)}{2\, \Delta(\rho_s)} + \frac{\rho_s}{2}\right)\right) \\ &+ O(\epsilon_1) + O(\epsilon_1^2/\epsilon_2), \end{aligned} \tag{G.5}$$

where we have used that $(k\,r_0)$ is $O(\epsilon_2^{-3/2})$ from equation (3.26). Then substituting for $\tau$ using equation (3.26), and after some algebra we find

$$w_n(\rho_s') - w_n(\rho_s) = k^{2/3}\,\sigma\,n^{1/3}\,a^{2/3}\,e(\rho_s) + O((k\,r_0)^{2/3}\,(a\,\sigma)^2) + O(a\sigma), \tag{G.6}$$

where

$$e(\rho_s) = \left(\frac{|\Lambda(\rho_s)|^{1/3}\rho_s}{2} - \frac{\Omega(\rho)}{|\Lambda(\rho_s)|^{2/3}}\right), \tag{G.7}$$

and we have assumed $\Lambda(\rho) = -|\Lambda(\rho)|$.

# Appendix H Nomenclature

## Roman letters

| | |
|---|---|
| $a_i$, $a$ | Background strain-rate in a stretched vortex |
| $c$ | Scalar fluctuation |
| $c'$ | Difference between the scalar, and a scalar with an initial condition of the scalar gradient, in a stretched vortex |
| $c_i$ | Scalar with initial condition of a gradient in the 'i' direction |
| $c^t$ | Scalar field including the uniform gradient |
| $c^L$ | Lagrangian scalar |
| $c_c$ | Characteristic value of the scalar |
| $C$ | Courant number |
| $C_{u_ic}$ | Shell-summed velocity-scalar cospectrum |
| $C^{(a)}_{u_ic}$, $C^{(p)}_{u_ic}$ | Shell-summed velocity-scalar cospectrum (axial/planar velocity contribution) |
| $C^{1D}_{u_ic}$ | 1D velocity-scalar cospectrum |
| $\mathcal{C}_n$ | Scalar polar harmonic |
| $D$ | Diffusivity |
| $E$ | Energy spectrum |
| $E_c$ | Scalar spectrum |
| $F^{1D}_{u_ic}$ | 1D velocity-scalar cross-spectrum |
| $\mathcal{F}_c$ | Fourier transform of the two-time, two-point scalar correlation |
| $\mathcal{F}_{ij}$ | Fourier transform of the two-time, two-point velocity correlation |
| $\mathcal{F}_{u_ic}$ | Fourier transform of the two-point velocity-scalar correlation |
| $\tilde{G}^{(E)}_{ij}$ | Eulerian velocity response function |
| $\tilde{G}_{ij}$ | Incompressible projection of $\tilde{G}^{(L)}_{ij}$ |

| | |
|---|---|
| $\tilde{G}_{ij}^{(L)}$ | Lagrangian velocity response function |
| $\tilde{G}^{(L)}$ | Lagrangian scalar response function |
| $\tilde{G}^{(E)}$ | Eulerian scalar response function |
| $G^{\dagger}$ | Isotropic form of the Eulerian velocity response function |
| $H$ | Definite time integral of $Q$ |
| $I_0$ | Modified Bessel function |
| $J_n$ | Bessel function |
| $k$ | Wavenumber |
| $k_K$ | Kolmogorov wavenumber |
| $k_B$ | Batchelor wavenumber |
| $k_C$ | Obukhov-Corrsin wavenumber |
| $k_P$ | Spectral peak wavenumber |
| $K$ | Kolmogorov constant |
| $l$ | Turbulent integral length scale |
| $l_\epsilon$ | Dissipation length scale |
| $L$ | Size of box |
| $M_{ij}$ | Rotation matrix |
| $n_k$ | Number of modes in the DNS in one direction |
| $N^c$ | Rate of creation of vortex structures per unit time and volume |
| $N$ | Rate of creation of length of vortex structures per unit time and volume |
| $p(U)$ | Pdf of the gross velocities of the vortex structures |
| $P(\alpha, \beta, \gamma)$ | Pdf for orientation of vortex structures |
| $P_{ijk}$,$P_{ij}$ | Incompressible projection operators |
| $Q$ | Non-dimensional form of $Q^{\dagger}$ |
| $Q^{\dagger}$ | Isotropic form of $\tilde{Q}_{ij}$ |
| $\tilde{Q}_{ij}$ | Incompressible projection of $\tilde{V}_{ij}$ |
| $Q_{u_ic}^{1D}$ | 1D velocity-scalar quadrature spectrum |
| $r_0$ | Characteristic vortex radius |

| | |
|---|---|
| $R$ | Velocity modal time correlation function |
| $R^c$ | Scalar modal time correlation function |
| $R_l$ | Reynolds number based on the integral length scale |
| $R_\lambda$ | Taylor Reynolds number |
| $\check{R}^c$ | As $R^c$ but for vortex structures with stationary centers |
| $\check{R}$ | As $R$ but for vortex structures with stationary centers |
| $\mathcal{R}^c$ | Two-time, two-point scalar correlation |
| $\mathcal{R}_{ij}$ | Two-time, two-point velocity correlation |
| $\mathcal{R}_{u_ic}$ | Two-point velocity-scalar correlation |
| $S$ | Stretching factor for vortex structures |
| $Sc$ | Schmidt number |
| $t_c$ | Vortex structure lifetime |
| $T_i$ | Times for collection of two-time statistics in the DNS |
| $T_{stat}$ | Time over which statistics were collected in the DNS |
| $T_{eddy}$ | Eddy turnover time in the DNS |
| $u_i$ | Velocity |
| $\check{u}_i$ | Velocity relative to frame moving with the vortex structure |
| $u_{gross}$ | Characteristic gross velocity of the vortex structures |
| $u_i^L$ | Lagrangian velocity |
| $u_{rms}$ | Root-mean-square turbulent velocity |
| $U$ | Gross velocity of a vortex structure |
| $\mathcal{U}$ | Unstretched axial velocity |
| $v_{3,n}$ | Polar harmonic of the axial velocity |
| $v_i$ | Velocity minus the background linear velocity field in a stretched vortex |
| $V^\dagger$ | Isotropic form of $\tilde{V}_{ij}$ |
| $V_{ij}$ | Lagrangian two-time, two-point velocity autocorrelation |
| $W$ | Non-dimensional form of $W^\dagger$ |

| | |
|---|---|
| $W_s$ | Rescaling of $W$ using the Schmidt number |
| $W^\dagger$ | Isotropic form of $\tilde{W}_i$ |
| $W_i$ | Two-point, two-time, cross correlation of the Lagrangian scalar and the velocity |
| $\mathcal{W}$ | Unstretched axial vorticity |
| $\mathcal{W}_0$ | Azimuthal average of unstretched axial vorticity |
| $X^\dagger$ | Isotropic form of $\tilde{X}_i$ |
| $\tilde{X}_i$ | Incompressible projection of $\tilde{Y}_i$ |
| $Y_i$ | Two-point, two-time, cross correlation of the Lagrangian velocity and the scalar |
| $Z_{ij}$ | Lagrangian two-time, two-point scalar autocorrelation |

# Greek letters

| | |
|---|---|
| $\alpha$ | Euler angle |
| $\alpha$ | Rescaling exponent in subsection 2.3.7 |
| $\beta$ | Euler angle |
| $\beta$ | Rescaling exponent in subsection 2.3.7 |
| $\chi_i$ | Lagrangian position |
| $\delta$ | Offset angle |
| $\Delta$ | Derivative of $\Lambda$ |
| $\epsilon$ | Energy dissipation |
| $\epsilon_c$ | Scalar dissipation |
| $\phi$ | Lagrangian position function |
| $\Phi$ | Unstretched scalar |
| $\gamma$ | Euler angle |
| $\Gamma$ | Circulation |
| $\eta$ | Kolmogorov length scale |
| $\kappa$ | Wavenumber scaled with the Kolmogorov wavenumber |
| $\kappa_s$ | Rescaling of $\kappa$ using the Schmidt number |
| $\Lambda$ | Derivative of $\Omega$ |

| | |
|---|---|
| $\mu$, $\mu_i$ | Scalar gradient magnitude and vector |
| $\nu$ | Viscosity |
| $\pi$ | Pressure-density ratio |
| $\pi^*$ | Reduced pressure |
| $\theta_k$ | Angle in wavenumber space |
| $\theta_n$ | Offset angle |
| $\rho$ | Stretched radial coordinate |
| $\rho_s$ | $\rho$ at point of stationary phase |
| $\sigma$ | Delay time for modal time correlations |
| $\tau$ | Stretched time coordinate |
| $\tau_s$ | $\tau$ at point of stationary phase |
| $\tau_k$ | Inertial time variable |
| $\tau_c$ | Characteristic timescale |
| $\omega_i(x_1, x_2, t)$ | Vorticity |
| $\omega_n(\rho, \tau)$ | Vorticity polar harmonic |
| $\Omega$ | Azimuthally averaged angular velocity |
| $\psi_i(x_1, x_2, t)$ | Vector potential (stream function) |
| $\psi_n(\rho, \tau)$ | Streamfunction polar harmonic |
| $\Psi$ | Unstretched stream function |
| $\zeta$ | Constant in inertial-convective form of the shell-summed velocity-scalar cospectrum |

# Other symbols

| | |
|---|---|
| $u_i', x_i', r_i', k_i'$ | Laboratory frame quantities when the distinction is necessary |
| $\hat{\cdot}$ | 2d Fourier transform |
| $\tilde{\cdot}$ | 3d Fourier transform |
| $\bar{\cdot}$ | Ensemble average |
| $\bar{\cdot}$ | Non-dimensional variables in subsection 3.2.3 |

# Bibliography

[1] G. K. Batchelor. Small-scale variation of convected quantities like temperature in turbulent fluid. Part I. General discussion and the case of small conductivity. *J. Fluid Mech*, 5:113–133, 1959.

[2] G. K. Batchelor, I. D. Howells, and A. A. Townsend. Small-scale variation of convected quantities like temperature in turbulent fluid. Part II. the case of large conductivity. *J. Fluid Mech*, 5:134–139, 1959.

[3] J. Bendat and A. Piersol. *Random data — analysis and measurement procedures, 2nd ed.* Wiley, 1986.

[4] G. Brethouwer, J. C. R. Hunt, and F. T. M. Nieuwstadt. Micro-structure and Lagrangian statistics of the scalar field with a mean gradient in isotropic turbulence. *J. Fluid Mech.*, 474:193–225, 2003.

[5] J. R. Chasnov. Simulation of the inertial-conductive subrange. *Phys. Fluids A*, 3:1164–1168, 1991.

[6] G. Comte-Bellot and S. Corrsin. Simple Eulerian time correlation of full- and narrow-band velocity signals in grid-generated, 'isotropic' turbulence. *J. Fluid Mech.*, 48:273–337, 1971.

[7] P. E. Dimotakis. Turbulent free shear layer mixing and combustion. In S. N. B. Murthy and E. T. Curran, editors, *High-speed flight propulsion systems*, volume 137 of *Progress in Astronautics and Aeronautics*, pages 265–340. AIAA, 1991.

[8] P. E. Dimotakis and P. L. Miller. Some consequences of the boundedness of scalar fluctuations. *Phys. Fluids A*, 2:1919–1920, 1990.

[9] W. H. Press et al. *Numerical recipes in C - 2nd ed.* Cambridge University Press, 1992.

[10] M. Galassi, J. Davies, J. Theiler, B. Gough, G. Jungman, M. Booth, and F. Rossi. *GNU Scientific Library Reference Manual - 2nd ed.* Network Theory Ltd, 2001.

[11] C. H. Gibson. Fine structure of scalar fields mixed by turbulence II. Spectral theory. *Phys. Fluids*, 11:2316–2327, 1968.

[12] J. P. Gleeson. A closure method for random advection of a passive scalar. *Phys. Fluids*, 12:1472–1484, 2000.

[13] S. Goto and S. Kida. Direct-interaction approximation and Reynolds-number reversed expansion for a dynamical system. *Physica D*, 117:191–214, 1998.

[14] S. Goto and S. Kida. Pasive scalar spectrum in isotropic turbulence: Prediction by the Lagrangian direct-interaction approximation. *Phys. Fluids*, 11:1936–1952, 1999.

[15] S. Goto and S. Kida. Sparseness of nonlinear coupling: importance in sparse direct-interaction perturbation. *Nonlinearity*, 15:1499–1520, 2002.

[16] T. Gotoh, R. S. Rogallo, J. R. Herring, and R. H. Kraichnan. Lagrangian velocity correlations in homogeneous isotropic turbulence. *Phys. Fluids A*, 5:2846–2864, 1993.

[17] S. Herr, L. Wang, and L. R. Collins. EDQNM model of a passive scalar with a uniform mean gradient. *Phys. Fluids*, 8:1588–1608, 1996.

[18] Mei-Jiau Huang. *Theoretical and computational studies of isotropic turbulence.* PhD thesis, Caltech, 1994.

[19] J. Jimenez, A. A. Wray, P. G. Saffman, and R. S. Rogallo. The structure of intense vorticity in isotropic turbulence. *J. Fluid Mech.*, 255:65–90, 1993.

[20] J. C. Kaimal, J. C. Wyndgaard, Y. Izumi, and O. R. Coté. Spectral characteristics of surface-layer turbulence. *Quart. J. R. Met. Soc.*, 98:563–589, 1972.

[21] Y. Kaneda. Renormalized expansions in the theory of turbulence with the use of the Lagrangian position function. *J. Fluid Mech.*, 107:131–145, 1981.

[22] Y. Kaneda, T. Ishihara, and K. Gotoh. Taylor expansions in powers of time of Lagrangian and Eulerian two-point two-time velocity correlations in turbulence. *Phys. Fluids*, 11:2154–2166, 1999.

[23] Y. Kaneda, T. Ishihara, M. Yokokawa, K. Itakura, and A. Uno. Energy dissipation rate and energy spectrum in high-resolution direct numerical simulations of turbulence in a periodic box. *Phys. Fluids*, 15:L21–L24, 2003.

[24] S. Kida and S. Goto. A Lagrangian direct-interaction approximation for homogeneous isotropic turbulence. *J. Fluid Mech.*, 345:307–345, 1997.

[25] R. H. Kraichnan. The structure of isotropic turbulence at very high Reynolds number. *J. Fluid Mech.*, 5:497–543, 1959.

[26] R. H. Kraichnan. Lagrangian-history closure approximation for turbulence. *Phys. Fluids*, 8:575–598, 1965.

[27] D. Leslie. *Developments in the theory of turbulence*. Oxford, 1973.

[28] J. L. Lumley. Similarity and the turbulent energy spectrum. *Phys. Fluids*, 10:855–858, 1967.

[29] T. S. Lundgren. Strained spiral vortex model for turbulent fine structure. *Phys. Fluids*, 25:2193–2203, 1982.

[30] W. D. McComb, V. Shanmugasundaram, and P. Hutchinson. Velocity-derivative skewness and two-time velocity correlations of isotropic turbulence as predicted by the LET theory. *J. Fluid Mech.*, 208:91–114, 1989.

[31] P. L. Miller and P. E. Dimotakis. Measurements of scalar power spectra in high Schmidt number turbulent jets. *J. Fluid Mech*, 308:129–146, 1996.

[32] A. Misra and D. I. Pullin. A vortex-based subgrid stress model for large-eddy simulation. *Phys. Fluids*, 9:2443–2454, 1997.

[33] L. Mydlarski. Mixed velocity-passive scalar statistics in high-Reynolds-number turbulence. *J. Fluid Mech.*, 475:173–203, 2003.

[34] L. Mydlarski and Z. Warhaft. Passive scalar statistics in high-Péclet-number grid turbulence. *J. Fluid Mech.*, 358:135–175, 1998.

[35] T. Ooura and M. Mori. The double exponential formula for oscillatory functions over the half infinite interval. *Journal of Computational and Applied Mathematics*, 38:353–360, 1991.

[36] S. A. Orszag and G. S. Patterson. Numerical simulation of three-dimensional homogeneous isotropic turbulence. *Phys. Rev. Lett.*, 28:76–79, 1992.

[37] M. R. Overholt and S. B. Pope. Direct numerical simulation of a passive scalar with imposed mean gradient in isotropic turbulence. *Phys. Fluids*, 8:3128–3148, 1996.

[38] D. I. Pullin. A vortex-based model for the subgrid flux of a passive scalar. *Phys. Fluids*, 12:2311–2319, 2000.

[39] D. I. Pullin, J. D. Buntine, and P. G. Saffman. On the spectrum of a stretched spiral vortex. *Phys. Fluids*, 6:3010–3027, 1994.

[40] D. I. Pullin and T. S. Lundgren. Axial motion and scalar transport in stretched spiral vortices. *Phys. Fluids*, 13:2553–2563, 2001.

[41] D. I. Pullin and P. G. Saffman. On the Lundgren-Townsend model of turbulent fine scales. *Phys. Fluids A*, 5:126–145, 1993.

[42] D. I. Pullin and P. G. Saffman. Reynolds stresses and one-dimensional spectra for a vortex model of homogeneous anisotropic turbulence. *Phys. Fluids*, 6:1787–1796, 1994.

[43] P. G. Saffman and D. I. Pullin. Calculation of velocity structure functions for vortex models of isotropic turbulence. *Phys. Fluids*, 8:3072–3084, 1996.

[44] P.G. Saffman. Lectures on homogeneous turbulence. In N. J. Zabusky, editor, *Topics in nonlinear physics*, pages 485–614. Springer, 1968.

[45] T. Sanada and V. Shanmugasundaram. Random sweeping effect in isotropic numerical turbulence. *Phys. Fluids A*, 4:1245–1250, 1992.

[46] H. Tennekes and J. L. Lumley. *A first course in turbulence.* The MIT Press, 1974.

[47] T. Voelkl, D. I. Pullin, and D. C. Chan. A physical-space version of the stretched-vortex subgrid-stress model for large-eddy simulation. *Phys. Fluids*, 12:1810–1825, 2000.

[48] Z. Warhaft. Passive scalars in turbulent flows. *Ann. Rev. Fluid Mech.*, 32:203–240, 2000.

[49] J. C. Wyngaard and O. R. Coté. Cospectral similarity in the atmospheric surface layer. *Quart. J. R. Met. Soc.*, 98:590–603, 1972.

[50] P. K. Yeung, Shuyi Xu, and K. R. Sreenivasan. Schmidt number effects on turbulent transport with uniform mean scalar gradient. *Phys. Fluids*, 14:4178–4191, 2002.